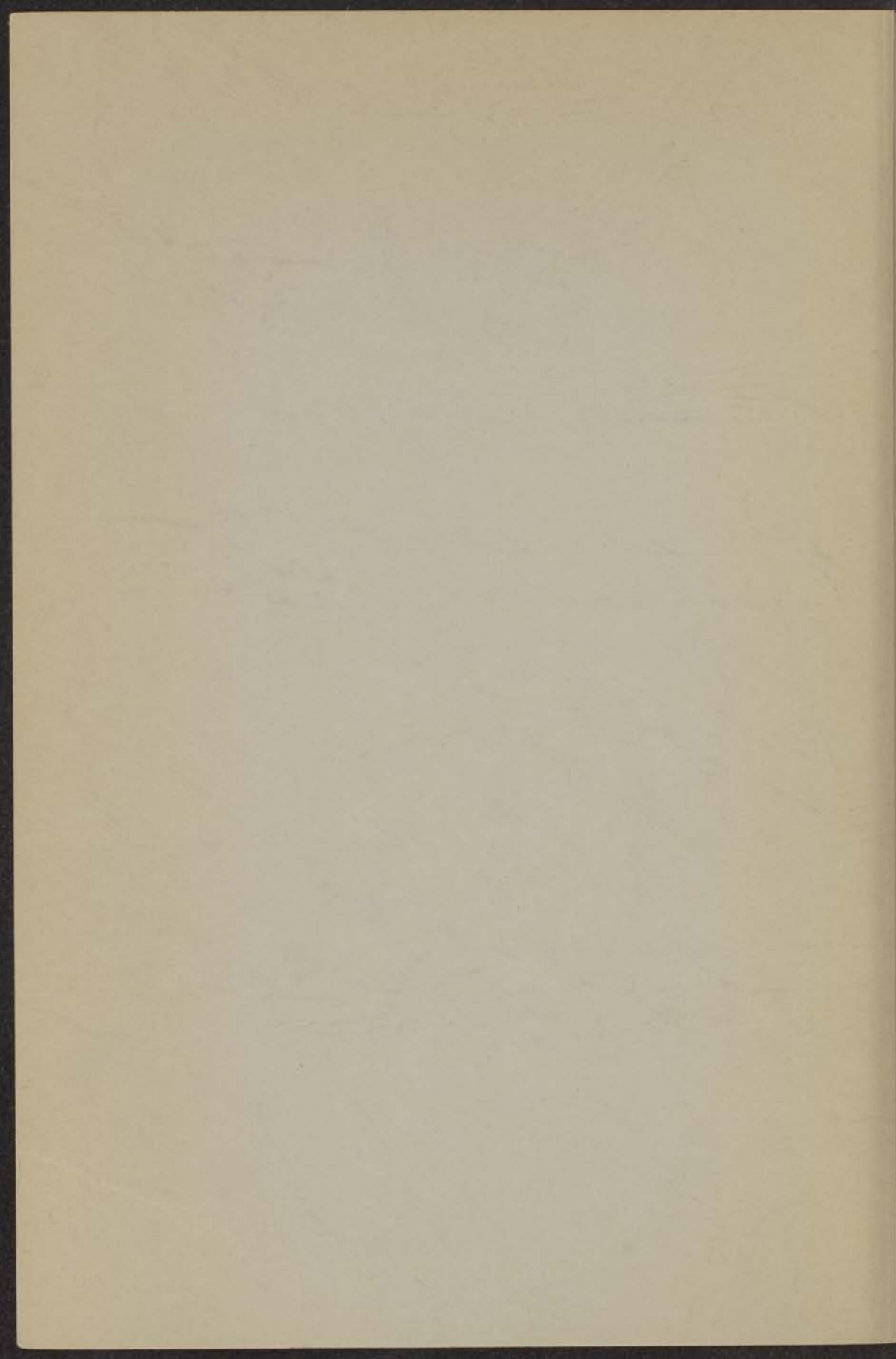


A STUDY OF  
THE DYNAMIC POLARIZATION  
OF PROTONS

INSTITUUT-LORENTZ  
voor theoretische natuurkunde  
Nieuwsteeg 16-Leiden-Nederland

T.J.B. SWANENBURG



30 JAN. 1968

A STUDY OF  
THE DYNAMIC POLARIZATION  
OF PROTONS

INSTITUUT-LORENTZ  
voor theoretische natuurkunde  
Nieuwsteeg 18-Leiden-Nederland

PROEFSCHRIFT

TER VERKRIJGING VAN DE GRAAD VAN DOCTOR  
IN DE WISKUNDE EN NATUURWETENSCHAPPEN AAN  
DE RIJSUNIVERSITEIT TE LEIDEN, OP GEZAG VAN  
DE RECTOR MAGNIFICUS DR P. MUNTENDAM,  
HOOGLEERAAR IN DE FACULTEIT DER GENEES-  
KUNDE, TEN OVERSTAAN VAN EEN COMMISSIE UIT  
DE SENAAT TE VERDEDIGEN OP WOENSDAG  
18 OKTOBER 1967 TE 14 UUR

DOOR

TEUNIS JOHANNES BOUDEWIJN  
SWANENBURG

GEBOREN TE GOUDA IN 1938

*kast dissertaties*

DRUKKERIJ J. H. PASMANS - 'S-GRAVENHAGE

A STUDY OF  
THE DYNAMIC POLARIZATION  
OF PROTONS

PROMOTOR: PROF. DR N. J. POULIS



Dit werk vormt een onderdeel van het onderzoekprogramma van de Stichting voor Fundamenteel Onderzoek der Materie en is mogelijk gemaakt door financiële steun van de Nederlandse Organisatie voor Zuiver Wetenschappelijk Onderzoek.

## STELLINGEN

### I

De bewering van Borghini, dat de lekfactor  $f$  bij dynamische kernpolarisatie-experimenten in magnetisch verdunde kristallen kleiner is dan één, is onjuist.

Borghini, M., C.R. Acad. Sci., **262**, 337 (1966).

### II

De magnetisatiemetingen van Anderson en Giauque aan  $\text{CuSO}_4 \cdot 5\text{H}_2\text{O}$  geven geen nieuwe informatie omtrent het gedrag van de twee niet-equivalente Cu-ionen in de eenheidscel van dit kristal.

Anderson, R.J. en Giauque, W.F., Journ. Chem. Phys., **46**, 2413 (1967).

### III

De beïnvloeding van de spin-roosterrelaxatietijd van Nd-ionen in  $\text{La}_2\text{Mg}_3(\text{NO}_3)_{12} \cdot 24\text{H}_2\text{O}$  door het toevoegen van kleine hoeveelheden Pr aan deze kristallen verdient nader onderzoek, omdat een resonant cross-relaxatieproces onmogelijk is.

Dit proefschrift, hoofdstuk VI.  
Bloembergen, N., Shapiro, S., Pershan, P.S. en Artman, J.O., Phys. Rev. **114**, 445 (1959).

### IV

Het gebrek aan onderricht in de mogelijkheden van de digitale elektronische rekenmachine werkt remmend op de ontwikkeling van wetenschap, techniek en automatisering van bestuurlijke informatie-verzorging.

### V

Gelet op de technische mogelijkheden van dit ogenblik verdient het aanbeveling het onderzoek naar het ontstaan van kosmische  $\gamma$  straling te richten op een nauwkeurige bepaling van de spectrale verdeling van deze straling.

### VI

Voor een juiste interpretatie van kernspin-roosterrelaxatietijden in verdunde paramagnetische zouten is het noodzakelijk de  $b/C$ -waarde van het electronspinsysteem te kennen.

Dit proefschrift, hoofdstuk III.

## VII

De conclusie van Konowalow en Carra, dat de door hen gebruikte Morse-potentiaal bij de beschrijving van ketenmoleculen beter voldoet dan de 12-6 Lennard-Jones-potentiaal, is triviaal.

Konowalow, D.D. en Carra, S., *Nuovo Cimento*, **44**, 133 (1966).

## VIII

Om na te gaan of bij de spin-roosterrelaxatie van kernspins in verdunde paramagnetische kristallen bij lage temperatuur twee tijdconstanten optreden, verdient het aanbeveling dit relaxatieproces met behulp van de spin-echo methode te bestuderen.

## IX

Op grond van theoretische overwegingen is het niet te verwonderen dat geen schending van ladingsconjugatie-symmetrie gevonden wordt bij electron-positron annihilatie.

Mills, A.P. en Berko, S., *Phys. Rev. Letters*, **18**, 420 (1967).

## X

De experimenten van Teichler-Zaller en Hoch geven minder informatie over de kwantitatieve bijdrage van de cyclische fosforylering tot het fotosyntheseprocess dan de auteurs suggereren.

Teichler-Zaller, D. en Hoch, G., *Arch. Biochem. Biophys.*, **120**, 227 (1967).

## XI

Het bepalen van kernspin-roosterrelaxatietijden in  $\text{CuSO}_4 \cdot 5\text{H}_2\text{O}$  is van groot belang voor het verkrijgen van informatie over de fluctuatiefrequentie van de magnetische momenten van de Cu-ionen in dit kristal.

## XII

Om het veelal overbodige en soms onjuiste commentaar van sportverslaggevers bij een via de televisie uitgezonden voetbalwedstrijd te vermijden, verdient het aanbeveling deze verslaggevers te verplichten de door henzelf verzorgde uitzending op een later tijdstip nogmaals bij te wonen.

## Contents

INTRODUCTION AND SURVEY	7
CHAPTER I. THEORETICAL DESCRIPTION OF DYNAMIC NUCLEAR POLARIZATION	9
I-1. Description of nuclear dynamic polarization based on the rate equations	10
I-2. Description of saturation in solids in a rotating frame of reference	25
I-3. Dynamic polarization in the rotating frame	33
I-4. Improvement of the theory of dynamic polarization in the rotating frame	46
CHAPTER II. EXPERIMENTAL ARRANGEMENT AND PROCEDURE	49
II-1. Electron resonance equipment	49
II-2. Nuclear resonance equipment	53
II-3. Crystals	55
CHAPTER III. SPIN - LATTICE RELAXATION	58
III-1. Theory of proton spin-lattice relaxation in dilute paramagnetic crystals	58
III-2. Spin-lattice relaxation of the paramagnetic ions	64
III-3. Results on proton spin-lattice relaxation times	68
CHAPTER IV. DYNAMIC POLARIZATION OF PROTONS IN $(La, Nd)_2Mg_3(NO_3)_{12} \cdot 24H_2O$	77
IV-1. Experimental results	77
IV-2. Discussion of the experimental results	87
IV-3. Concluding remarks	92
CHAPTER V. DYNAMIC POLARIZATION OF PROTONS IN $(La, Ce)_2Mg_3(NO_3)_{12} \cdot 24H_2O$	94
V-1. Experimental results	95
V-2. Discussion of the experimental results	102
V-3. Concluding remarks	106

CHAPTER VI. THE INFLUENCE OF PARAMAGNETIC IMPURITIES OF THE DYNAMIC POLARIZATION OF PROTONS	108
VI-1. Experimental results	110
VI-2. Discussion of the experimental results	120
VI-3. Concluding remarks	130
SAMENVATTING	132

## Introduction and survey

The work described in this thesis is concerned with the dynamic polarization of protons in dilute paramagnetic crystals in the temperature region between 1 °K and 4 °K. This study was undertaken in order to investigate the polarization process under different, well-defined experimental conditions, and to obtain information about the coupling of the protons with the electron spins in the sample. Furthermore, the collective behaviour of spin systems under the influence of strong radiofrequency fields is investigated.

The possibility of increasing the magnetization of protons to a value which is close to the magnetization of the paramagnetic ions in the sample is of great interest for elementary particle physics. The polarized protons are used as scattering centres for incident particles, so that the spin-dependent part of the scattering cross-section can be determined.

In chapter I two different theoretical descriptions of the polarization process are given; the first one is based on the calculation of the populations of the Zeeman levels of the individual spins, the second theory gives the behaviour of the temperatures of the spin systems as a whole in a rotating frame of reference.

The experimental arrangement and the procedure followed in the measurements are discussed in chapter II. In view of the importance of the spin-lattice relaxation times of the spins that participate in the polarization process, in chapter III a theory is presented which describes the nuclear spin-lattice interaction in terms of the spin-spin and the spin-lattice relaxation times of the paramagnetic ions. The observed values of the proton spin-lattice relaxation times in the crystals in which the polarization was studied are explained on the basis of this theory.

All polarization experiments were performed in single crystals of  $\text{La}_2\text{Mg}_3(\text{NO}_3)_{12}\cdot 24\text{H}_2\text{O}$  (LaMN), to which a certain amount of paramagnetic rare earth ions was added. These crystals with Nd ions as polarizing spins represent the most simple system for studying the polarization process: only one paramagnetic spin species is present, the spin-lattice interaction of which is well understood. The experimental results obtained in these crystals are given in chapter IV.

Chapter V deals with the results obtained in LaMN crystals containing Ce ions. For an adequate description of the proton polarization the phonon bottleneck in the Ce spin-lattice relaxation has to be taken into account.

The influence of paramagnetic impurities different from the polarizing spins was studied in single crystals of LaMN with 2.0% Nd and various amounts of Ce or Pr. The experimental results are discussed in chapter VI.

## Chapter I

THEORETICAL DESCRIPTION OF NUCLEAR  
DYNAMIC POLARIZATION*Introduction*

In 1953 Overhauser suggested that it should be possible to enhance the magnetization of nuclei by saturating the resonance of the conduction electrons in metals<sup>1)</sup>. This enhancement is due to the hyperfine coupling between the nuclei and the electrons; nuclear transitions are then induced when the electrons are flipped by an rf field.

This idea has been extended to many other systems containing two different spin species, such as paramagnetic ions in hyperfine interaction with their own nuclei<sup>2)</sup>, paramagnetic ions in liquids, interacting with the nuclei of the solvent<sup>3)</sup>. However, the only substances in which considerable nuclear magnetizations have been obtained so far are dilute paramagnetic crystals where the protons of the water of hydration have a weak dipolar coupling with the paramagnetic ions<sup>4)</sup>. The dynamic polarization in these crystals will be considered in this thesis.

The electron-nuclear double resonance experiments are performed by placing the sample in a microwave cavity operated at a frequency  $\nu \approx 10^{10}$  Hz, in a static magnetic field  $H_0$ . If the frequency of the microwave field is equal to  $\nu = \nu_e \pm \nu_n$ , where  $\nu_e$  and  $\nu_n$  are the Larmor frequencies of the electron and the nuclear spins respectively, "forbidden" transitions are induced which simultaneously flip an electron spin  $S$  and a nuclear spin  $I$ . When the microwave irradiation is strong enough to saturate the forbidden transition, the nuclear polarization will be enhanced by a factor of the order of  $10^2$  in favorable cases. Simultaneous observation of the nuclear resonance absorption is used as a measure of this nuclear polarization.

In part I-1 this method of nuclear dynamic polarization will be described on the basis of the rate equations for the Zeeman levels of the individual spins<sup>5)</sup>. From the rate equations for the populations of these levels the nuclear magnetization can be calculated. Although this approach gives in a simple way a qualitative explanation of the principal features of dynamic polarization experiments, it is known that saturation of spin transitions in solids cannot be described adequately by these rate equations. Therefore in parts I-2 and I-3 a more correct approach will be presented.

## I-1. Description of nuclear dynamic polarization based on the rate equations

### I-1.1. The rate equations

A dilute paramagnetic crystal containing  $n_e$  paramagnetic ions with  $S = \frac{1}{2}$  and  $I = 0$ , and  $n_n$  nuclear spins with  $I = \frac{1}{2}$  belonging to atoms different from the paramagnetic ions, is placed in a constant, homogeneous magnetic field  $H_0$  in the  $z$  direction. The angular frequencies of the two spin species are given by  $\omega_e = \gamma_e H_0$  and  $\omega_n = \gamma_n H_0$ . The Hamiltonian for the spin systems is

$$H = \pi\omega_e \sum_{j=1}^{n_e} S_z^j + \pi\omega_n \sum_{i=1}^{n_n} I_z^i + H_{SS} + H_{SI} + H_{II} \quad (I.1)$$

The first two terms are the electron and nuclear Zeeman Hamiltonians, the other terms represent the spin-spin interactions. If the external field  $H_0$  is so strong that the spin-spin interactions are much smaller than the Zeeman terms, the eigenvalues of the Hamiltonian(I.1) are defined to a good approximation by the quantum numbers  $S_z$  and  $I_z$ . The energy level diagram of a "typical pair" consisting of one spin  $S$  and one spin  $I$  is shown in fig.I.1. The sample can be considered as a large number of such pairs; the terms  $H_{SS}$ ,  $H_{SI}$  and  $H_{II}$  are then responsible for the broadening of these energy levels. Moreover the interaction  $H_{SI}$  contains operator products of the form  $I_{\pm} S_z$  which allow for transitions of the type  $(I_z, S_z) \rightarrow (I_z \pm 1, S_z \pm 1)$  and  $(I_z, S_z) \rightarrow (I_z \pm 1, S_z \mp 1)$ . These transitions represent the simultaneous flipping of a spin  $S$  and a spin  $I$ , which leads to a change in the distribution of the nuclear spins over the energy levels, resulting in a nuclear polarization.

In fig.I.1. all possible transitions between the four energy levels are indicated. Their influence will first be discussed rather generally, and then the rate equations will be presented. The transitions should be divided into two groups: those that are brought about by the crystal lattice (the relaxation transitions), and those induced by the microwave field.

The first group of transitions is responsible for the establishment of an equilibrium distribution over the energy levels. It is assumed that the crystal lattice vibrations (phonons) provide a thermal reservoir at a temperature  $T_L$ . Interactions between these phonons and the electron spins  $S$  induce transitions of the type  $(S_z = \pm \frac{1}{2}) \rightarrow (S_z = \mp \frac{1}{2})$  at a rate  $w \text{ sec}^{-1}$ . Because the lattice is assumed to be in internal

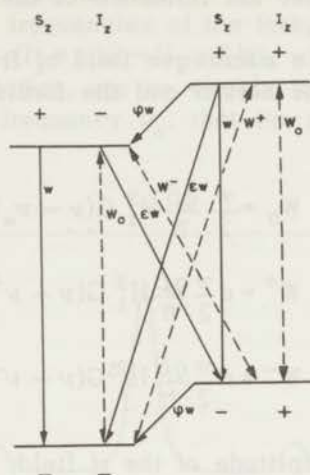


Fig. 1.1. Energy level diagram of a "typical pair" consisting of one spin  $S$  and one spin  $I$ . The levels are characterized by the quantum numbers  $S_z$  and  $I_z$ . The magnitudes of the different transitions are given in the text.

thermal equilibrium, the effect of this spin-lattice coupling is that the distribution of the spins  $S$  over the two possible orientations  $S_z = \pm \frac{1}{2}$  will be given by a Boltzmann factor

$$\frac{n_e^+}{n_e^-} = \exp\left(-\frac{\hbar\omega_e}{kT_L}\right) \quad (I.2)$$

where  $n_e^+$  and  $n_e^-$  are the numbers of the electron spins for which  $S_z = +\frac{1}{2}$  or  $S_z = -\frac{1}{2}$  respectively.

The terms  $I_{\mp} S_z$  of the dipole interaction  $H_{SI}$  induce relaxation transitions for the nuclei accompanied by an electron transition. The rate of this process is given by  $\epsilon w \text{ sec}^{-1}$ , where  $\epsilon$  is equal to

$$\epsilon = \frac{g}{4} \cos^2 \theta \sin^2 \theta \left(\frac{g\beta}{H_0 r^3}\right)^2 \quad (I.3)$$

where  $g\beta$  is the magnetic moment of the spin  $S$ ,  $r$  the distance between  $S$  and  $I$ , and  $\theta$  the angle between  $\vec{r}$  and  $\vec{H}_0$ <sup>6)</sup>. All other mechanisms that may cause a nuclear relaxation transition without interference of the spins  $S$  are combined in a term  $\phi w \text{ sec}^{-1}$ . The equilibrium distri-

butions obtained under the influence of these relaxation transitions are shown in fig. I.2a.

Application of a microwave field of frequency  $\nu$ , perpendicular to  $H_0$  will induce the normal and the forbidden transitions with the average rates

$$W_0 = \frac{\pi}{2} \frac{g\beta}{\hbar} H_1^2 G(\nu - \nu_0) \quad (I.4)$$

$$W^+ = \epsilon \frac{\pi}{2} \frac{g\beta}{\hbar} H_1^2 G(\nu - \nu^+) \quad (I.5)$$

$$W^- = \epsilon \frac{\pi}{2} \frac{g\beta}{\hbar} H_1^2 G(\nu - \nu^-) \quad (I.6)$$

where  $2H_1$  is the amplitude of the rf field, and  $G$  is the normalized paramagnetic resonance lineshape:

$$\int_0^{\infty} G(\nu) d\nu = 1.$$

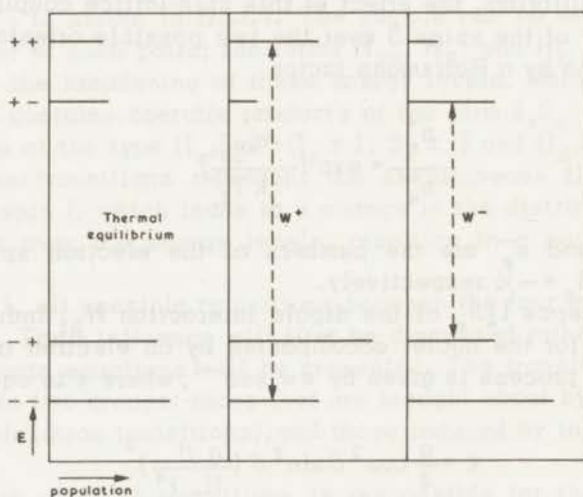


Fig. I.2. Relative populations of the energy levels of fig. I.1.  
 a. in thermal equilibrium.  
 b. saturation of the  $W^+$  transition.  
 c. saturation of the  $W^-$  transition.

The lineshapes of the three transitions are assumed to be the same, and  $\nu^\pm = \nu_e \pm \nu_n$  are the frequencies of the forbidden transitions. The pure nuclear transitions ( $I_z = \pm 1/2 \rightarrow I_z = \mp 1/2$ ), which are used to monitor the dynamic polarization, are so weakly induced by a second rf field at the resonance frequency  $\nu_n$ , that the polarization is not disturbed by this rf field.

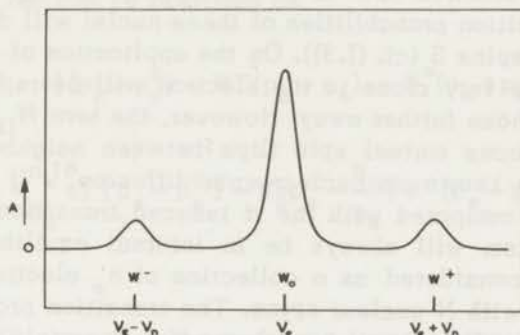


Fig. I.3. Idealized paramagnetic resonance spectrum of a system of electron spins which are in weak dipolar coupling with nuclear spins.

The microwave resonance absorption will show a central line at a frequency  $\nu_e$  and two satellites at  $\nu^+$  and  $\nu^-$ . The intensity of these forbidden lines is smaller than that of the main line by the factor  $\epsilon$  of (I.3). The spectrum is shown in fig. I.3. If the sample is strongly irradiated at a frequency  $\nu^+$ , the populations of the levels  $I_z = -1/2, S_z = -1/2$  and  $I_z = +1/2, S_z = +1/2$  become equal. The nuclear relaxation rate  $(\varphi + \epsilon)w$  should then be small compared with the induced transition rate  $W^+$ . If simultaneously the electron relaxation is fast enough to maintain the equilibrium Boltzmann distribution of the spins  $S$ , the nuclear polarization, defined as  $p_n = (n_n^+ - n_n^-)/(n_n^+ + n_n^-)$ , is found to be equal to

$$p_n \approx + \frac{\hbar \omega_e}{2 k T_L} \quad (\text{I.7})$$

which is  $\omega_e/\omega_n$  times larger than the thermal equilibrium value

$$p_n^0 \approx - \frac{\hbar \omega_n}{2 k T_L}$$

The populations of the energy levels are shown in fig.I.2b. Irradiation of the other forbidden transition  $W^-$  yields a nuclear enhancement equal to that of (I.7), but reversed in sign (fig.I.2c).

Until now a large number of typical pairs, each one consisting of one spin S and one spin I has been considered. However in most dilute paramagnetic crystals the number of protons  $n_n$  will exceed the number of electron spins  $n_e$ . To take this into account it will be assumed that one electron spin is in interaction with  $n_n/n_e = N$  nuclear spins. The transition probabilities of these nuclei will depend on their distance to the spins S (cf. (I.3)). On the application of an rf field the nuclei which are very close to the electron will be rapidly polarized compared with those further away. However, the term  $H_{II}$  in the Hamiltonian (I.1) induces mutual spin flips between neighbouring nuclei. This process is known as nuclear spin diffusion<sup>6</sup>). If this diffusion process is fast compared with the rf induced transition rate, the nuclear spin system will always be in internal equilibrium, and the sample can be considered as a collection of  $n_e$  electron spins, each one interacting with  $N$  nuclear spins. The transition probabilities  $\epsilon w$ ,  $\varphi w$  etc. defined before for each nuclear spin separately should now be considered as average values.

The rate equations for the populations of the nuclear Zeeman levels under the simultaneous action of the rf transition rates and the thermal relaxation rates can be written as

$$\begin{aligned}
 -\frac{dn_n^-}{dt} = \frac{dn_n^+}{dt} = & n_n^- \varphi w \left(1 - \frac{\beta_L \omega_n}{2}\right) - n_n^+ \varphi w \left(1 + \frac{\beta_L \omega_n}{2}\right) + \\
 & + n_n^- \frac{n_e^-}{n_e} \left[ W^- + \epsilon w \left(1 - \frac{\beta_L \omega_e}{2} - \frac{\beta_L \omega_n}{2}\right) \right] + \\
 & + n_n^- \frac{n_e^+}{n_e} \left[ W^+ + \epsilon w \left(1 + \frac{\beta_L \omega_e}{2} - \frac{\beta_L \omega_n}{2}\right) \right] + \\
 & - n_n^+ \frac{n_e^-}{n_e} \left[ W^+ + \epsilon w \left(1 - \frac{\beta_L \omega_e}{2} + \frac{\beta_L \omega_n}{2}\right) \right] + \\
 & - n_n^+ \frac{n_e^+}{n_e} \left[ W^- + \epsilon w \left(1 + \frac{\beta_L \omega_e}{2} + \frac{\beta_L \omega_n}{2}\right) \right] \quad (I.8)
 \end{aligned}$$

where  $\beta_L = \hbar/kT_L$ . The relaxation probabilities  $\varphi w$  and  $\epsilon w$  are weighted

by the appropriate Boltzmann factors. The factors  $n_e^\pm/n_e$  represent the probability that an electron spin in one of the  $S_z = \pm 1/2$  levels is in interaction with a nuclear spin. An equation very similar to (I.8) is valid for the electron populations.

By making use of the nuclear polarization  $p_n$  defined before, and the electron polarization  $p_e = (n_e^+ - n_e^-)/(n_e^+ + n_e^-)$  and their respective equilibrium values  $p_n^0 = -\beta_L \omega_n/2$  and  $p_e^0 = -\beta_L \omega_e/2$ , (I.8) and its equivalent for  $dn_e^\pm/dt$  can be rewritten as

$$\frac{dp_n}{dt} = -2w[\varphi + \epsilon](p_n - p_n^0) - W^-(p_n - p_e) - W^+(p_n + p_e) \quad (\text{I.9})$$

$$\frac{dp_e}{dt} = -2w\left[1 + \frac{n_n}{n_e}\epsilon\right](p_e - p_e^0) - W_0 p_e - \frac{n_n}{n_e}[W^-(p_e - p_n) + W^+(p_e + p_n)] \quad (\text{I.10})$$

(I.9) and (I.10) show that the response times of the two spin systems in the absence of microwave fields ( $W_0 = W^+ = W^- = 0$ ) are equal to

$$T_{1n} = [2w(\varphi + \epsilon)]^{-1} \quad (\text{I.11})$$

$$T_{1e} = [2w(1 + \frac{n_n}{n_e}\epsilon)]^{-1} \quad (\text{I.12})$$

where  $T_{1n}$  and  $T_{1e}$  are the nuclear and electron spin-lattice relaxation times. If  $W^+$  or  $W^- \neq 0$ , (I.9) and (I.10) are coupled, and  $p_e$  and  $p_n$  each display two characteristic times  $\tau_1$  and  $\tau_3$ .

The steady state values of  $p_e$  and  $p_n$ , following from (I.9) and (I.10) are given by

$$p_n = \frac{-\beta_L \omega_e (W^- - W^+) T_{1n}}{2[1 + W_0 T_{1e} + (W^- + W^+) f T_{1n}] [1 + (W^- + W^+) T_{1n}] - (W^- - W^+)^2 f T_{1n}^2} \quad (\text{I.13})$$

$$p_e = \frac{-\beta_L \omega_e [1 + (W^- + W^+) T_{1n}]}{2[1 + W_0 T_{1e} + (W^- + W^+) f T_{1n}] [1 + (W^- + W^+) T_{1n}] - (W^- - W^+)^2 f T_{1n}^2} \quad (\text{I.14})$$

where  $f = n_n/n_e$ ,  $T_{1e}/T_{1n} = N \cdot T_{1e}/T_{1n}$ . (I.13) and (I.14) show that the denominator increases as the square of the rf power at very high power levels, so that both the nuclear and the electron polarizations vanish. This is illustrated in fig. I.4 for a case where the paramagnetic resonance linewidth  $2\omega_L$  is equal to the separation of the forbidden transitions  $2\omega_n$ .

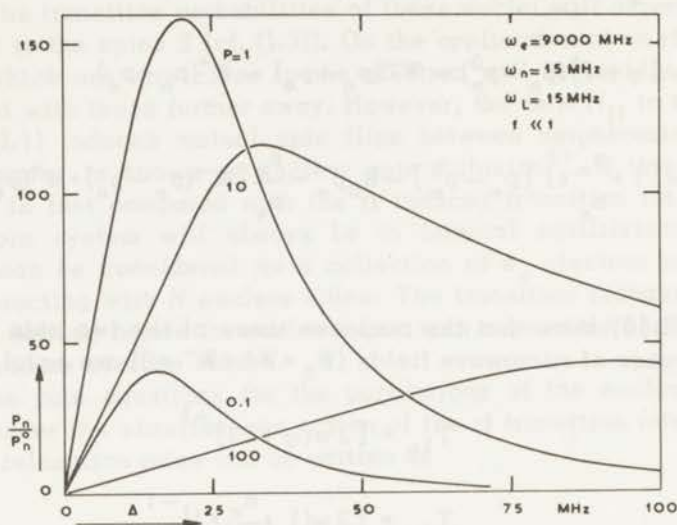


Fig. I.4. Proton polarization factor as a function of the irradiation frequency  $\Delta = \omega_e - \omega$  for several values of the micro-wave power in the cavity, calculated from (I.13).

## I-1.2. Special solutions

In this section several special cases will be discussed in which the general solutions (I.13) and (I.14) take a simpler form so that their meaning is understood more easily.

### a. Spectrum resolved

If the paramagnetic resonance spectrum has the form as illustrated in fig. I.3, so that the normal and forbidden transitions are separated, irradiation of one of the transitions will leave the others unaffected. On the application of a microwave field with frequency  $\nu^-$

only the  $W^-$  transition is induced, and from (I.13) and (I.14) the polarizations are found to be

$$p_n = \frac{-\beta_L \omega_e}{2} \frac{W^- T_{1n}}{1 + W^- T_{1n}(1+f)} \quad (\text{I.15})$$

$$p_e = \frac{-\beta_L \omega_e}{2} \frac{1 + W^- T_{1n}}{1 + W^- T_{1n}(1+f)} \quad (\text{I.16})$$

In the limit of very high microwave power, so that  $W^- T_{1n} \gg 1$ , the maximum obtainable nuclear polarization becomes

$$p_n^{\text{max}} = p_e = \frac{-\beta_L \omega_e}{2} \frac{1}{1+f} \quad (\text{I.17})$$

This value of  $p_n$  should be compared with that from (I.7). The nuclear enhancement is seen to be reduced by a factor  $1/(1+f)$ . The meaning of the "leakage factor"  $f$  can be understood from the following: each electron spin has to polarize  $N$  nuclear spins, which stay polarized during a time of the order of  $T_{1n}$ . After flipping one spin  $I$  it takes about  $T_{1e}$  seconds before the electron spin is available for flipping the next spin  $I$ . So for obtaining the full polarizing effect it is essential that  $T_{1n} \gg NT_{1e}$ , or  $f \ll 1$ . From (I.11) and (I.12) follows that  $f \approx N(\epsilon + \varphi)$ .

The time-dependent solutions of (I.9) and (I.10) can also be calculated. As stated before, the equations are coupled if  $W^- \neq 0$  or  $W^+ \neq 0$ . The time constants displayed by  $p_e$  and  $p_n$ ,  $\tau_1$  and  $\tau_3$  are given by

$$\tau_1 = T_{1e} \frac{1}{(1 + W^- T_{1n})} \quad (\text{I.18})$$

$$\tau_3 = T_{1n} \left[ 1 - \frac{W^- T_{1n}}{1 + W^- T_{1n}(1+f)} \right] \quad (\text{I.19})$$

If  $p_n = p_n^0 \approx 0$  and  $p_e = p_e^0$  and  $W^-$  (or  $W^+$ ) is switched on at  $t = 0$ , then

$$p_n(t) \approx p_n(\infty) \left[ 1 - \exp\left(-\frac{t}{\tau_3}\right) \right] \quad (\text{I.20})$$

which shows that  $\tau_3$  can be considered as the nuclear polarization time. The dependence of  $p_n$  of (I.15) and  $\tau_3$  on microwave power is shown in fig. I.5 for several values of the factor  $f$ .

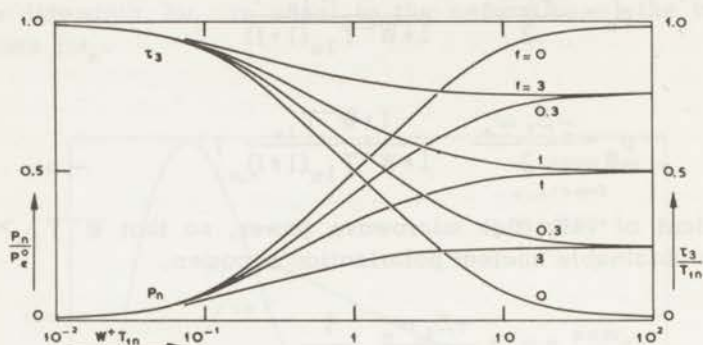


Fig. I.5. Proton polarization factor and polarization time as a function of the microwave power in the cavity for several values of  $f$ , calculated from (I.15) and (I.19) for a resolved spectrum.

The situation discussed in this section where the forbidden transitions were completely resolved, can only be realized in external magnetic fields larger than  $10^4$  Oe. The width of the electron resonance line is at least of the order of magnitude of the nuclear resonance frequency in lower fields, so that  $W^+$ ,  $W^-$  and  $W_0$  overlap each other. In the treatment of this case a distinction has to be made between homogeneously and inhomogeneously broadened electron resonance lines.

b. Spectrum not resolved; homogeneously broadened electron resonance line

If the broadening is homogeneous, that is if the paramagnetic resonance linewidth is due to the dipolar interaction  $H_{SS}$ , all electron spins will participate in each of the three transitions  $W_0$ ,  $W^-$  and  $W^+$ . The nuclear polarization is then given by the general solution (I.13)

$$p_n = \frac{-\beta_L \omega_e (W^- - W^+) T_{1n}}{2 [1 + W_0 T_{1e} + (W^- + W^+) f T_{1n}] [1 + (W^- + W^+) T_{1n}] - (W^- - W^+)^2 f T_{1n}^2} \quad (\text{I.21})$$

which was illustrated in fig. I.4.

The characteristic times  $\tau_1$  and  $\tau_3$  of the spin systems under the influence of relaxation and rf induced transitions cannot be calculated so easily as in the case of section a. Because the nuclear polarization time  $\tau_3$  contains the same information on the polarization process as the polarization  $p_n$  itself, (I.9) and (I.10) have been solved numerically for several practical cases. Fig. I.6 shows  $\tau_3$  as a function of microwave power for four values of the irradiation frequency  $\Delta = \omega_e - \omega$ , calculated for a sample where the electron resonance line had a half width of 20 MHz. The lineshape was assumed to be Lorentzian, which is in good agreement with the experimentally observed shape. For all values of  $\Delta$  the response time  $\tau_3$  tends to zero for high power levels, independent of the value of  $f$ , which was 2.4 in this special case. These calculations should be compared with (I.19), which was derived for the case that the spectrum was resolved;  $\tau_3$  then goes to zero only if  $f=0$ . Results very similar to those of fig.I.6 have been obtained for other crystals where the transitions  $W_0$ ,  $W^+$  and  $W^-$  overlapped each other.

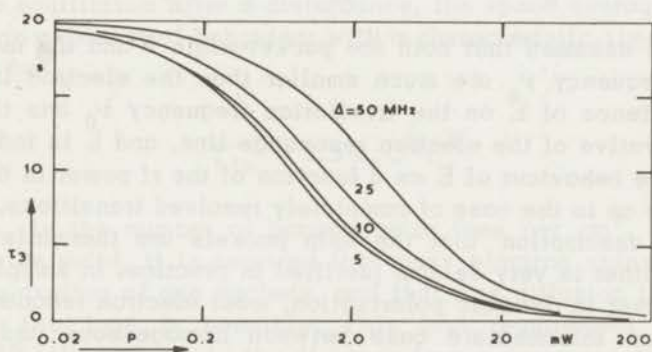


Fig. I.6. Proton polarization as a function of the microwave power in the cavity for several values of the irradiation frequency  $\Delta$ , calculated from (I.9) and (I.10).

c. Spectrum not resolved; inhomogeneously broadened electron resonance line

In many substances, especially in those where the electron spins are very dilute, the term  $H_{SS}$  in the Hamiltonian is very small. The width of the electron line is not primarily due to electron spin-spin interactions in that case, but to lattice imperfections or to inter-

actions with neighbouring nuclei. Electron spins which have the same surroundings will have equal Larmor frequencies, and will show a narrow resonance line, because of the smallness of  $H_{SS}$ . The observed lineshape  $G(\nu)$  is then the envelope of a large number of these narrow "spin packets", which are assumed to be thermally isolated from each other.

If such a substance is irradiated with an rf field of frequency  $\nu_0$ , a fraction  $\delta G(\nu_0)$  of the electron spins will be saturated, where  $\delta$  is the width of such a spin packet. But the packets for which  $\nu_0$  is equal to  $\nu^+$  or  $\nu^-$  will have their  $W^+$  or  $W^-$  transitions saturated. The remaining spins do not participate in the polarization process. The nuclear enhancements due to these packets,  $p_n^+$  and  $p_n^-$ , are given by  $p_n^0$  of (I.15), multiplied by the fraction of the electron spins that contribute to the polarization; the net enhancement factor is equal to the sum of these two contributions

$$E = \frac{p_n^+ + p_n^-}{p_n^0} = - \frac{2\delta\nu_0 W^+ T_{1n}}{1 + W^+ T_{1n} (1+f)} \left( \frac{dG}{d\nu} \right)_{\nu_0} \quad (\text{I.22})$$

It has been assumed that both the packet-width  $\delta$  and the nuclear resonance frequency  $\nu_n$  are much smaller than the electron linewidth. The dependence of  $E$  on the irradiation frequency  $\nu_0$  has the shape of the derivative of the electron resonance line, and  $E$  is independent of  $\gamma_n$ <sup>7)</sup>. The behaviour of  $E$  as a function of the rf power in the cavity is the same as in the case of completely resolved transitions.

The assumption that the spin packets are thermally isolated from each other is very seldom justified in practice. In samples which are of interest in dynamic polarization, most electron resonance lines represent an intermediate case between homogeneous and inhomogeneous broadening.

### I-1.3. The influence of nuclear spin diffusion on the polarization process

In the discussion of part I-1.1 it was assumed that nuclear spin diffusion was fast compared with the rate at which forbidden transitions are induced. The nuclear spin system is then always in internal equilibrium. However, if the electron spins are very dilute, the polarization has to be transported over a large distance from the nuclei which are close to the paramagnetic ion. Although the probability for a mutual spin flip between neighbouring nuclei is very high ( $\sim 10^5$  sec<sup>-1</sup> for protons), the time necessary for the transportation of polar-

ization over  $100 \text{ \AA}$  is still of the order of seconds. When the polarization time of the nuclei close to the ion is of the same order, the nuclear spin system will not be in internal equilibrium.

The probabilities for the forbidden transitions  $W^+$  and  $W^-$  depend in the same way on the distance  $r$  between the nucleus and the paramagnetic ion as the relaxation probability  $\epsilon w$ . So diffusion effects in dynamic polarization can be treated analogous to nuclear relaxation. The equation describing the evolution of  $p_n$  in the presence of spin diffusion is given by

$$\frac{dp_n}{dt} = -C \sum_k |\vec{r} - \vec{r}_k|^{-6} (p_n - p_n^0) + D \nabla^2 p_n \quad (\text{I.23})$$

where  $C = 3(g\beta)^2/10H_0^2 T_{1e}$ ;  $\vec{r}$  and  $\vec{r}_k$  are the positions of a nuclear spin and the  $k$ -th electron spin;  $D = aW^2$  is the diffusion constant,  $a$  the lattice constant and  $W$  the probability for a mutual nuclear spin flip between nearest neighbours<sup>6)</sup>. The polarization is treated here as a continuous space variable. If the nuclear spin system is allowed to return to equilibrium after a disturbance, the space average of  $p_n$  will display an exponential behaviour with a characteristic time  $T_{1n}$ , which is given by

$$T_{1n}^{-1} = 8.5 n_0 C^{1/2} D^{3/4} \quad (\text{I.24})$$

where  $n_0$  is the number of paramagnetic ions per  $\text{cm}^3$ . In order for (I.24) to be valid, it is required that many electron spins participate in the relaxation of one nucleus, and that free diffusion in the region between two ions is possible. This last requirement means that  $b = (C/D)^{1/4} \ll R$ , where  $b$  is the distance from a paramagnetic ion where the local field due to this ion is equal to the field from the surrounding nuclei, and  $R$  the distance between the paramagnetic ions<sup>8)</sup>.

In the presence of a microwave field inducing the transitions  $W_0$ ,  $W^+$  and  $W^-$ , the equation for  $p_n$  will be given by (I.9) to which a term describing the spin diffusion has to be added. Moreover, account has to be taken of the fact that the transition probabilities for a certain nuclear spin depend on  $|\vec{r} - \vec{r}_k|$

$$\begin{aligned} \frac{dp_n}{dt} = & -C \sum_k |\vec{r} - \vec{r}_k|^{-6} (p_n - p_n^0) - 2w\varphi(p_n - p_n^0) + \\ & -\Gamma^- \sum_k |\vec{r} - \vec{r}_k|^{-6} (p_n - p_e^0) + \Gamma^+ \sum_k |\vec{r} - \vec{r}_k|^{-6} (p_n + p_e^0) \end{aligned} \quad (\text{I.25})$$

where  $\Gamma^\pm = \frac{1}{2}\gamma H_1^2 T_{1e} G(\nu - \nu^\pm) C$ . It has been assumed that  $f \ll 1$ , so that the thermal equilibrium value  $p_e^0$  of the electron polarization can be used in (I.25). With the same validity conditions as for (I.24), where  $b$  is now equal to

$$b = [(C + \Gamma^- + \Gamma^+)/D]^{1/4}$$

the steady state value of the space average polarization  $\bar{p}_n$  is given by

$$\bar{p}_n = p_e^0 \frac{\Gamma^- - \Gamma^+}{C + \Gamma^- + \Gamma^+} \frac{1}{1 + \varphi w \tau_3'} \quad (\text{I.26})$$

where

$$(\tau_3')^{-1} = 8.5 n_0 (C + \Gamma^- + \Gamma^+)^{1/4} D^{3/4} \quad (\text{I.27})$$

If the microwave power is switched on at  $t=0$ ,  $\bar{p}_n$  shows an exponential behaviour with a polarization time  $\tau_3$  given by

$$(\tau_3)^{-1} = 8.5 n_0 (C + \Gamma^- + \Gamma^+)^{1/4} D^{3/4} + 2\varphi w \quad (\text{I.28})$$

If the spectrum is resolved and one of the forbidden transitions, e.g.  $\Gamma^-$  is excited, we can take  $\Gamma^- = \frac{1}{2} S_0 C$ , where  $S_0 = (\gamma H_1)^2 T_{1e} T_{2e}$ . Substitution of  $\Gamma^-$  and  $\tau_3'$  into (I.26) yields

$$\bar{p}_n = p_e^0 \left( \frac{S_0}{2 + S_0} \right) \frac{8.5 n_0 C^{1/4} D^{3/4} (1 + \frac{1}{2} S_0)^{1/4}}{2\varphi w + 8.5 n_0 C^{1/4} D^{3/4} (1 + \frac{1}{2} S_0)^{1/4}} \quad (\text{I.29})$$

Eq.(I.29) shows that in the limit of very high rf power ( $S_0 \rightarrow \infty$ ) the nuclear polarization is equal to that given by (I.15) which was deduced without referring to spin diffusion. If extraneous nuclear relaxation can be neglected ( $\varphi = 0$ ), the dependence on microwave power in (I.29) is also the same as in (I.15). But if  $\varphi w$  is comparable to  $8.5 n_0 C^{1/4} D^{3/4}$  the dependence of  $\bar{p}_n$  on  $S_0$  becomes weaker. This is illustrated in fig.I.7 for several values of  $\varphi w$ .

The polarization time  $\tau_3$  of (I.28) shows a dependence on microwave power which is also much weaker than that given by (I.19) (fig.I.7). The fact that  $\tau_3$  tends to zero for high rf fields even if the spectrum is resolved, is a result of the assumption that  $f \ll 1$ . If  $f$  cannot be

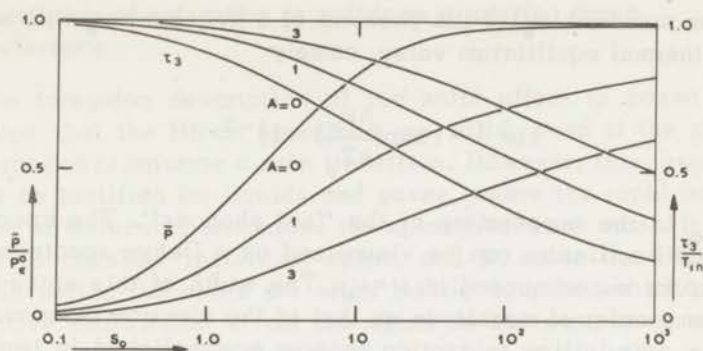


Fig. 1.7. Proton polarization factor and polarization time as a function of the microwave power in the cavity in the presence of nuclear spin diffusion, calculated from (I.29) and (I.28).

$$A = 2\phi w / 8.5n_0 C^{1/4} D^{3/4} \quad f \ll 1$$

neglected,  $\tau_3$  will be different from zero if the forbidden lines are well resolved; however for overlapping transitions  $\tau_3$  tends to zero in the limit of strong rf fields.

#### I-1.4. The influence of a phonon bottleneck on the polarization process

As discussed in part I-1.1, the interaction between the phonons of the lattice and the electron spin system is responsible for the spin-lattice relaxation time  $T_{1e}$ . It was assumed that these phonons were in equilibrium at a temperature  $T_L$ , which is equal to the temperature of the surrounding helium bath. The average energy of the lattice oscillators is  $\bar{E} = (\frac{1}{2} + k)h\nu$ , where  $k$  is the average phonon excitation number, which takes the value at thermal equilibrium

$$k(\nu) = \left[ \exp\left(\frac{h\nu}{kT_L}\right) - 1 \right]^{-1} \quad (\text{I.30})$$

If the electron spin-lattice relaxation is determined by a direct process, which is usually the case at temperatures of about 1°K, a relaxation transition creates a phonon of energy  $h\nu_e$ . If the rate at which these transitions take place is higher than the rate at which these phonons distribute their energy over the entire phonon spectrum, the

excitation number  $k(\nu_e)$  of the phonons of a frequency  $\nu_e$  will be higher than its thermal equilibrium value, namely

$$k(\nu_e) = \left[ \exp\left(\frac{h\nu_e}{kT_p}\right) - 1 \right]^{-1} \quad (\text{I.31})$$

where  $T_p$  is the temperature of the "hot phonons". The spectrum of the lattice oscillators can be visualized as a Debye spectrum with a narrow spike superimposed at  $\nu = \nu_e$ . The width of this spike will be of the same order of magnitude as that of the electron resonance line.

The spin-lattice relaxation is now accomplished in two steps: the spins at a temperature  $T_S$  relax to phonons at a temperature  $T_p$ , and these hot phonons return to their equilibrium temperature  $T_L$  at a rate  $1/\tau_{ph}$ . To take this phonon bottleneck into account in the calculations of the nuclear polarization, it is necessary to introduce an extra equation to the rate equations (I.9) and (I.10), which describes the evolution of the hot phonon temperature  $T_p$ . It can be shown that under stationary conditions  $T_p$  is given by

$$\frac{T_p}{T_L} = \frac{1 + \sigma}{1 + \sigma(p_e/p_e^0)} \quad (\text{I.32})$$

where  $\sigma$  is the so-called bottleneck factor defined as the (energy exchange rate between spins and phonons)/(energy exchange rate between phonons and bath).  $\sigma$  is proportional to the electron spin concentration and inversely proportional to the paramagnetic resonance linewidth.

The dependence of the nuclear polarization on the rf power and on the irradiation frequency is now extremely complicated. In the relatively simple case of a resolved spectrum,  $p_n$  can be found from a biquadratic equation<sup>10</sup>). However, it is evident that a phonon bottleneck will always reduce the polarization factor in the limit of strong saturation of the forbidden transition. The electron polarization is smaller when a phonon bottleneck is present, and (I.17) shows that  $p_n$  can never become larger than  $p_e$ .

## I-2. Description of saturation in solids in a rotating frame of reference

The foregoing description of the solid effect is based on the assumption that the Bloch equations are valid, even if the rf fields are so strong as to saturate a spin transition. However, this assumption can only be justified for liquids and gases, where the rapid motion of the atoms or molecules uncouples the spins from each other. It is then possible to consider individual spins, and to solve the Bloch equations. In solids the spins are often tightly coupled, which requires a collective description of all the spins in the sample as a single system with many degrees of freedom.

Although an attempt to describe the behaviour of a spin system in a solid still in terms of the Bloch equations is reasonably successful as to the imaginary part  $\chi''$  of the rf susceptibility<sup>11)</sup>, there is a glaring discrepancy between theory and experiment in the behaviour of the real part  $\chi'$  when the spin system is strongly saturated. This failure of the Bloch equations to predict the evolution of a nuclear spin system in solids under the influence of strong rf fields was demonstrated by Redfield<sup>12)</sup>. He indicated the correct approach to the problem for the case that the spin system is strongly saturated. Provotorov solved the more general problem of arbitrary saturation parameters<sup>13)</sup>.

Since dynamic polarization is obtained by strong saturation of spin transitions in solids, as outlined in I-1, Solomon suggested to extend Redfield's theory to this problem<sup>14)</sup>. As an introduction to this approach of dynamic polarization in I-2.1 a review of Redfield's theory will be given, and in I-2.2 the extension by Provotorov is discussed. Section I-2.3 deals with the idea of the mixing of spin temperatures. These conceptions will be applied to the problem of dynamic polarization in I-3<sup>15)</sup>.

### I-2.1. Very strong saturation

A sample containing  $n_e$  identical spins  $S$  is submitted to a constant, homogeneous magnetic field  $H_0$  in the  $z$  direction, and an rf field  $H_1$  along the  $x$  axis with amplitude  $H_1$ , and frequency  $\omega$ . The Larmor frequency of the spins  $S$  in the field  $H_0$  is  $\omega_e = -\gamma_e H_0$ ; and the total Hamiltonian of the system is

$$\begin{aligned} H &= \omega_e \pi \sum_j S_z^j + 2\omega_1 \pi \sum_j S_x^j \cos \omega t + H_{SS} \\ &= \pi \omega_e S_z + 2\omega_1 \pi S_x \cos \omega t + H_{SS} \end{aligned} \quad (I.33)$$

where  $\omega_1 = -\gamma_e H_1$  and  $H_{SS}$  represents the spin-spin interaction. We want to calculate the steady state value of the magnetization of the sample in the presence of the rf field  $\vec{H}_1$  and the spin-lattice interaction, characterized by the relaxation time  $T_{1e}$ . It is assumed that the spin-spin interactions are sufficiently strong to maintain a uniform temperature within the spin system, which may be different from the lattice temperature  $T_L$ , and that the effect of  $T_{1e}$  is to change this temperature slowly until equilibrium is reached.

The Hamiltonian (I.33) is explicitly time-dependent and cannot be used in this form for a thermodynamical description of the system. However, if a transformation to a frame of reference rotating at a frequency  $\omega$  is performed by means of the unitary operator  $U = \exp(-i\omega S_z t)$ , the Hamiltonian becomes

$$H' = \pi(\omega_e - \omega)S_z + \pi\omega_1 S_x + H'_{SS} \quad (\text{I.34})$$

The Zeeman part of  $H'$  is now independent of time. On the other hand,  $H'_{SS} = U^{-1}H_{SS}U$  will now contain the time explicitly. If the dc field  $H_0$  is assumed to be much larger than the local field due to the spin-spin interactions, the time-dependent terms in  $H'_{SS}$  can be neglected and only the terms commuting with  $U$  have to be taken into account.

In the rotating frame of reference we have a constant effective field  $\vec{H}'_e$  with

$$\gamma_S H'_e = [(\omega_e - \omega)^2 + \omega_1^2]^{1/2} \quad (\text{I.35})$$

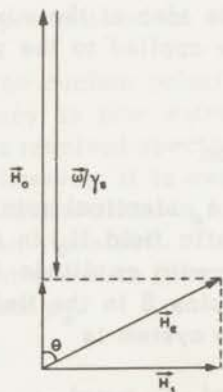


Fig. I.8. The external magnetic field  $\vec{H}_0$ , the rf field  $\vec{H}_1$  and the effective field  $\vec{H}'_e$  in a frame rotating with a frequency  $\omega$ .

making an angle  $\theta$  with  $\vec{H}_0$ , where  $\theta$  (fig. I.8) is given by

$$\tan \theta = \frac{\omega_1}{\omega_e - \omega} \quad (\text{I.36})$$

The original assumption of Redfield is that the statistical behaviour of the spin system in this rotating frame can be described by means of a spin temperature  $T_S$ . That is, the density matrix  $\rho'$  in that frame has the form

$$\rho' = \frac{\exp(-\frac{H'}{kT_S})}{\text{Trace} \exp(-\frac{H'}{kT_S})} \quad (\text{I.37})$$

which reduces for sufficiently high temperatures to

$$\rho' \approx 1 - \frac{H'}{kT_S} = 1 - \alpha H' = 1 - \alpha Z' - \alpha H'_{SS} \quad (\text{I.38})$$

where  $\alpha = 1/kT_S$ . The expectation value of the Hamiltonian (I.34),  $\langle H' \rangle = \text{Trace}(\rho' H')$  is then given by

$$\langle H' \rangle = \langle Z' \rangle + \langle H'_{SS} \rangle \approx \alpha \hbar [(\omega_e - \omega)^2 + \omega_1^2 + \omega_L^2] \quad (\text{I.39})$$

where  $\omega_L^2 = \text{Trace}(H'_{SS})^2 / \text{Trace}(S_z)^2$ . The local field  $H_L = \omega_L / \gamma_e$  is related to the second moment of the unsaturated resonance line by  $H_L^2 = \frac{1}{3} \Delta H^2$ .

It can be shown that the spin-lattice relaxation rate of  $\langle H'_{SS} \rangle$  is twice as fast as that of  $\langle Z' \rangle$  if there is no correlation between the relaxation of two neighbouring spins. The variations of  $\langle Z' \rangle$  and  $\langle H'_{SS} \rangle$  due to the coupling with the lattice are then given by

$$\frac{\partial}{\partial t} \langle Z' \rangle = -\frac{1}{T_{1e}} [\langle Z' \rangle - \langle Z' \rangle_0] = -\frac{1}{T_{1e}} [\langle Z' \rangle - \frac{\omega_e - \omega}{\omega_e} Z_0] \quad (\text{I.40})$$

$$\frac{\partial}{\partial t} \langle H'_{SS} \rangle = -\frac{2}{T_{1e}} \langle H'_{SS} \rangle \quad (\text{I.41})$$

where  $Z_0 = \hbar \beta_L \omega_e^2$  is the thermal equilibrium value of the Zeeman

energy in the laboratory frame, and  $\beta_L = 1/kT_L$  the inverse lattice temperature. Under stationary conditions the expectation value of the total Hamiltonian  $\langle H' \rangle$  is constant, so from (I.40) and (I.41) follows for the inverse spin temperature  $\alpha$

$$\alpha = \frac{(\omega_e - \omega)\omega_e}{(\omega_e - \omega)^2 + \omega_1^2 + 2\omega_L^2} \beta_L \quad (\text{I.42})$$

or

$$\frac{T_L}{T_S} = \frac{H_0 H_e \cos \theta}{H_e^2 + 2H_L^2} \quad (\text{I.43})$$

where  $\theta$  is the same as in fig. I.8. The magnetic moment  $\vec{M}$  of the spin system in the rotating frame is aligned along the effective field  $\vec{H}_e$ . It is related to its thermal equilibrium value in the laboratory frame  $M_0$  by

$$M = M_0 \frac{H_e}{H_0} \cdot \frac{T_L}{T_S} = M_0 \frac{H_e^2 \cos \theta}{H_e^2 + 2H_L^2} \quad (\text{I.44})$$

From (I.42) it can be concluded that for exact resonance ( $\Delta = \omega_e - \omega = 0$ )

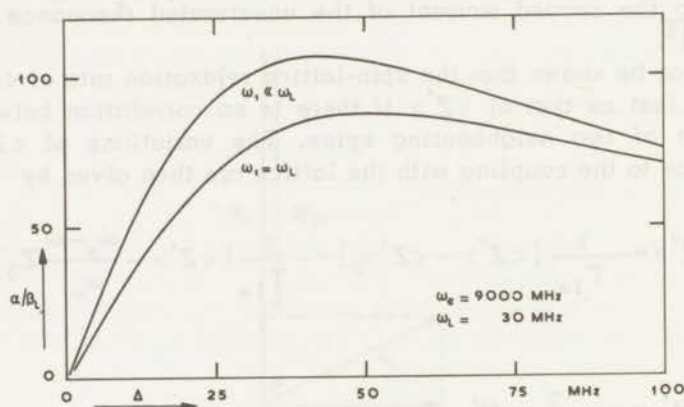


Fig. I.9. Inverse temperature of the spin system as a function of the irradiation frequency  $\Delta$  for two values of the rf field strength, calculated from (I.42).

the inverse spin temperature  $\alpha=0$ . For  $\Delta = \pm(\omega_1^2 + 2\omega_L^2)^{1/2}$  the value of  $\alpha$  obtains a maximum, respectively a minimum equal to

$$\frac{\alpha}{\beta_L} = \pm \frac{\omega_e}{2(\omega_1^2 + 2\omega_L^2)^{1/2}} \quad (I.45)$$

The dependence of  $\alpha/\beta_L$  as a function of  $\Delta$  is plotted in fig.I.9 for  $\omega_1 \ll \omega_L$  and for  $\omega_1 = \omega_L$ . From now on we will assume that  $\omega_1 \ll \omega_L$ . This condition is fulfilled in most paramagnetic saturation experiments.

### I-2.2. Arbitrary value of the saturation parameter

In the foregoing section it was stated that the influence of the spin-lattice relaxation was so small that one unique spin temperature could be defined for the Hamiltonian (I.34), in spite of the fact that the relaxation rates of the Zeeman- and the spin-spin part of the Hamiltonian are different. It is evident that this assumption can only be true if the rf induced transition rate is much larger than the spin-lattice relaxation rate.

Provotorov has shown that in the intermediate case of weak saturation in solids where  $T_2 \ll T_1$ , a temperature has to be assigned to the Zeeman term as well as to the spin-spin term of the Hamiltonian. In general these temperatures will be different, but in the limit of very strong saturation they become equal (Redfield). In this theory of Provotorov the density matrix in the rotating frame is thus of the form

$$\rho' = \frac{\exp(-aZ' - \gamma H'_{SS})}{\text{Trace} \exp(-aZ' - \gamma H'_{SS})} \approx 1 - aZ' - \gamma H'_{SS} \quad (I.46)$$

where  $Z'$  and  $H'_{SS}$  are the same as in I-2.1, and  $\alpha = 1/kT_S$  and  $\gamma = 1/kT_{SS}$  are their inverse temperatures. The expectation value of the Hamiltonian  $\langle H' \rangle$  is given by

$$\langle H' \rangle = \langle Z' \rangle + \langle H'_{SS} \rangle = \alpha(\Delta^2 + \omega_1^2) + \gamma\omega_L^2 \approx \alpha\Delta^2 + \gamma\omega_L^2 \quad (I.47)$$

Provotorov has shown from first principles that the time variations of  $\langle Z' \rangle$  and  $\langle H'_{SS} \rangle$  due to the rf field are given by

$$\frac{\partial}{\partial t} \langle Z' \rangle = -W_0(\Delta) \left[ \langle Z' \rangle - \frac{\Delta^2}{\omega_L^2} \langle H'_{SS} \rangle \right] \quad (I.48)$$

$$\frac{\partial}{\partial t} \langle H'_{SS} \rangle = -\frac{\Delta^2}{\omega_L^2} W_0(\Delta) \left[ \langle H'_{SS} \rangle - \frac{\omega_L^2}{\Delta^2} \langle Z' \rangle \right] \quad (I.49)$$

$W_0(\Delta)$  is the rf induced transition probability per unit time, proportional to  $H_1^2$ .  $W_0$  is identical with the induced transition probability used in the rate equations of I-1. By substitution of  $\langle Z' \rangle$  and  $\langle H'_{SS} \rangle$ , (I.48) and (I.49) can be rewritten as

$$\frac{\partial}{\partial t} \alpha = -W_0(\Delta)(\alpha - \gamma) \quad (I.50)$$

$$\frac{\partial}{\partial t} \gamma = -\frac{\Delta^2}{\omega_L^2} W_0(\Delta)(\gamma - \alpha) \quad (I.51)$$

Eq.(I.50) shows that the rf field tries to equalize the temperatures of  $Z'$  and  $H'_{SS}$ . (I.51) can be deduced from (I.50) when the conservation of the total spin energy given by (I.47) is taken into account. For exact resonance ( $\Delta = 0$ ) the spin-spin interaction temperature does not change under the influence of the rf field. If on the other hand  $\Delta \neq 0$ , a photon of the rf field has not the right energy necessary for an average spin flip. The difference,  $\hbar(\omega_e - \omega)$  has to be given off or taken up by the spin-spin energy.

The variations of  $\langle Z' \rangle$  and  $\langle H'_{SS} \rangle$  due to the spin-lattice coupling are the same as in the preceding section, so the total derivatives of  $\alpha$  and  $\gamma$  are given by

$$\frac{d}{dt} \alpha = -W_0(\Delta)(\alpha - \gamma) - \frac{1}{T_{1e}} \left( \alpha - \frac{\omega_e}{\Delta} \beta_L \right) \quad (I.52)$$

$$\frac{d}{dt} \gamma = -\frac{\Delta^2}{\omega_L^2} W_0(\Delta)(\gamma - \alpha) - \frac{2}{T_{1e}} (\gamma - \beta_L) \quad (I.53)$$

Under steady state conditions the left hand side of these equations is zero, and the solutions for  $\alpha$  and  $\gamma$  are found to be

$$\frac{\alpha}{\beta_L} = \frac{\omega_e}{\Delta} \frac{2\omega_L^2 + W_0 T_{1e} \Delta^2}{2\omega_L^2 + W_0 T_{1e} (\Delta^2 + 2\omega_L^2)} \quad (\text{I.54})$$

$$\frac{\gamma}{\beta_L} = \frac{\omega_e}{\Delta} \frac{W_0 T_{1e} \Delta^2}{2\omega_L^2 + W_0 T_{1e} (\Delta^2 + 2\omega_L^2)} \quad (\text{I.55})$$

The behaviour of  $\alpha$  and  $\gamma$  as a function of  $\Delta$  is shown in fig. I.10 for several values of the saturation parameter  $W_0 T_{1e}$ . For the shape function included in  $W_0$  a Lorentzian lineshape has been assumed with a half width  $H_{1/2} = \omega_L / \gamma$ . For high power levels both  $\alpha$  and  $\gamma$  tend to become equal to the solution for  $\alpha$  given in (I.42) and plotted in fig. I.9.

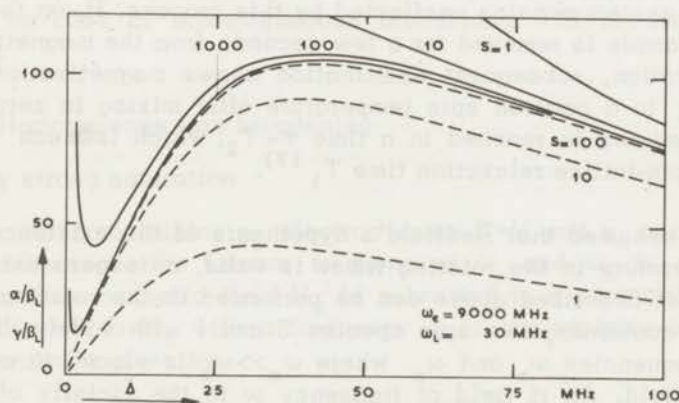


Fig. I.10. Inverse temperatures of the Zeeman and of the spin-spin part of the Hamiltonian (I.34) as a function of the irradiation frequency  $\Delta$  for several values of the saturation parameter  $S = W_0 T_{1e}$ , calculated from (I.54) and (I.55).

### I-2.3. Thermal mixing of spin temperatures

In solids containing two different spin species  $S$  and  $I$  experiments can be performed in which mixing of the temperatures of the the two spin systems occurs. If the two systems are prepared so as to have different spin temperatures before mixing, they will have a common temperature after mixing, which is determined by the initial

temperatures and the heat capacities of the two systems. This thermal mixing occurs only when mutual flip processes, induced by spin-spin interactions between these systems, can take place without change of the total energy<sup>16)</sup>. This requirement is fulfilled when the two spins have the same or nearly the same Larmor frequencies. The mixing time  $\tau$  will be of the order of the spin-spin relaxation time, multiplied by a factor giving the overlap of the two resonance lines.

Two examples of experiments of this type will be given, one on mixing described in the laboratory frame, and one in the rotating frame.

a. When a crystal of lithium fluoride is placed in a strong magnetic field, the Larmor frequencies of the  $\text{Li}^7$  and  $\text{F}^{19}$  nuclei are different. The system can be described by assigning to each of the spin systems a temperature of its own. If by means of a strong rf field one spin species is saturated, it will take a time of the order of  $T_1$ , i.e. several minutes, before equilibrium with the lattice is restored. The other spin system remains unaffected by this process. If, on the other hand the sample is removed for a few seconds from the magnetic field after saturation, subsequent examination shows magnetizations corresponding to a common spin temperature after mixing in zero field. Complete mixing is reached in a time  $\tau \approx T_2$ , which is much shorter than the spin-lattice relaxation time  $T_1$ <sup>17)</sup>.

b. If it is assumed that Redfield's hypothesis of the existence of a spin temperature in the rotating frame is valid, an experiment analogous to that described above can be performed in the rotating frame. A sample containing two spin species S and I with widely different Larmor frequencies  $\omega_e$  and  $\omega_n$  where  $\omega_e \gg \omega_n$  is placed in a strong magnetic field. An rf field of frequency  $\omega$  in the vicinity of  $\omega_e$  is applied. The Larmor frequency of the spins S in a frame rotating with an angular frequency  $\omega$  is  $\omega_e - \omega = \Delta$ . Because  $\omega_e \gg \omega_n$ , this rf field will not affect the spins I, and their Larmor frequency is still given by  $\omega_n$ . If  $\Delta \approx \omega_n$ , the two spin systems are in good heat contact with each other and will obtain equal temperatures in the rotating frame<sup>14)</sup>. The temperature of the spins S is given by (I.42) in the case of strong saturation.

Because of the mixing the temperature of the spins I has the same value in the rotating frame; however, this temperature is the same in both frames of reference, so (I.42) gives directly the cooling factor of the spins I in the laboratory frame. If the spins S are identified with electron spins, and the spins I with nuclei, this experiment gives the enhancement of the nuclear polarization if the sample is

strongly irradiated at a frequency  $\omega = \omega_e - \omega_n$ . So the description above is a new approach to the experiment discussed in I-1 in terms of Zeeman levels and rate equations. As can already be seen from (I.42) the results for the nuclear polarization factor are different from those deduced in I-1. In the next part of this chapter a more detailed discussion of this approach will be given.

### I-3. Dynamic polarization in the rotating frame

As discussed in the preceding section, an adequate description of dynamic polarization of nuclei in solids requires an approach similar to that given by Redfield and Provotorov for one spin species. Recently Borghini has worked out this polarization theory, described in principle in the last section of I-2.3, in detail<sup>15)</sup>. As in Redfield's theory it is assumed that the line broadening is homogeneous, in order to make it possible to assign one unique spin temperature to the system. The case of inhomogeneous broadening will be discussed in I-3.2.c.

#### I-3.1. Homogeneous line broadening

##### a. Very strong saturation

A solid containing  $n_e$  electron spins  $S = \frac{1}{2}$  and  $n_n$  nuclear spins  $I = \frac{1}{2}$  with respective Larmor frequencies  $\omega_e$  and  $\omega_n$  in a constant homogeneous magnetic field  $H_0$  is submitted to a strong rf field  $H_1$ , perpendicular to  $H_0$  with a frequency  $\omega$  in the vicinity of  $\omega_e$ . The Hamiltonian is given by

$$H = \hbar\omega_e S_z + 2\hbar\omega_1 S_x \cos \omega t + \hbar\omega_n I_z + H_{SS} + H_{SI} + H_{II} \quad (I.56)$$

where  $S_z = \sum_j S_z^j$ ,  $S_x = \sum_j S_x^j$ ,  $I_z = \sum_i I_z^i$  and  $\omega = \gamma_e H_1$ . The last three terms represent the spin-spin interactions. The canonical transformation  $U = \exp(-i\omega S_z t)$  leads again to a time-independent Hamiltonian in the rotating frame

$$H' = \hbar\Delta S_z + \hbar\omega_1 S_x + \hbar\omega_n I_z + H'_{SS} + H'_{SI} + H_{II} \quad (I.57)$$

where  $H'_{SI}$  is the secular part of the S-I interaction, and  $\Delta = \omega - \omega_e$ . Since the effective Larmor frequencies in the rotating frame,  $\Delta$  and  $\omega_n$ ,

are of the same order of magnitude in dynamic polarization experiments, we can assume that the thermal mixing is complete so that it is allowed to assign a single spin temperature  $T_S$  to the whole Hamiltonian  $H'$ . The density matrix in the rotating frame is then

$$\rho' \approx 1 - \alpha Z'_S - \alpha H'_{SS} - \alpha Z'_I - \alpha H'_{SI} - \alpha H_{II} \quad (I.58)$$

where  $\alpha = 1/kT_S$ . From (I.57) and (I.58) the expectation value of  $H'$  can be calculated

$$\begin{aligned} \langle H' \rangle &= \langle Z'_S \rangle + \langle Z'_I \rangle + \langle H'_{SS} \rangle + \langle H'_{SI} \rangle + \langle H_{II} \rangle = \\ &= \alpha \left[ \Delta^2 + \frac{\text{Trace}(I_z)^2}{\text{Trace}(S_z)^2} \omega_n^2 + \frac{\text{Trace}(H'_{SS})^2 + \text{Trace}(H'_{SI})^2 + \text{Trace}(H_{II})^2}{\text{Trace}(S_z)^2} \right] \end{aligned} \quad (I.59)$$

The variations of the different terms in (I.59) due to the coupling with the lattice can be written in the same way as (I.40) and (I.41). The argument that  $\langle H' \rangle$  is constant under steady state conditions yields for the common inverse spin temperature

$$\frac{\alpha}{\beta_L} = \frac{\omega_e \Delta}{\Delta^2 + 2\omega_L'^2 + N(T_{1e}/T_{1n})\omega_n^2} \quad (I.60)$$

where  $N = n_n/n_e$  and  $T_{1e}$  and  $T_{1n}$  are the electron and nuclear spin-lattice relaxation times;  $\omega_L'^2$  is now defined by

$$2\omega_L'^2 = \frac{2 \text{Trace}(H'_{SS})^2 + \text{Trace}(H'_{SI})^2}{\text{Trace}(S_z)^2} \quad (I.61)$$

In the derivation of (I.60) it has been assumed that  $\omega_1 \ll \omega_L'$ , and terms of the order of  $T_{1e} \text{Trace}(H_{II})^2 / T_{1n} \text{Trace}(H'_{SS})^2$  have been omitted.

Since the temperature of the nuclear spins is the same in both frames of reference, (I.60) directly gives the enhancement of the nuclear polarization in the laboratory frame. The behaviour of  $\alpha/\beta_L$  as a function of  $\Delta$  is plotted in fig. I.11 for several values of  $f = NT_{1e}/T_{1n}$ . The maximum and minimum values of  $\alpha/\beta_L$  are obtained for

$$\Delta = \pm (2\omega_L'^2 + f\omega_n^2)^{1/2} \quad (\text{I.62})$$

and they are equal to

$$\left(\frac{\alpha}{\beta_L}\right)_{\max, \min} = \pm \frac{\omega_e}{2(2\omega_L'^2 + f\omega_n^2)^{1/2}} \quad (\text{I.63})$$

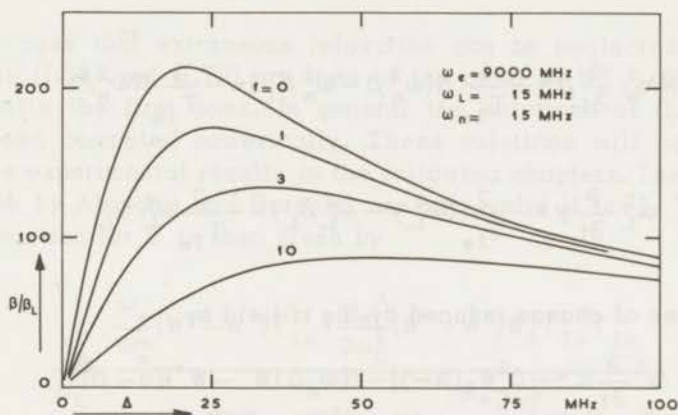


Fig. I.11. Inverse temperature of the spin system as a function of the irradiation frequency  $\Delta$  for several values of  $f$ , calculated from (I.60).

#### b. Arbitrary value of the saturation parameter

Consider again a sample containing spins S and spins I, represented by the Hamiltonian (I.57) in the rotating frame. If the spin-lattice relaxation rates are not slow compared with the rf induced transition probability, different temperatures have to be assigned to the various parts of the Hamiltonian, just as in the case of one spin species. The density matrix will then be of the form

$$\rho' \approx 1 - \hbar\alpha\Delta S_z - \hbar\beta\omega_n I_z - \gamma H'_{SS} \quad (\text{I.64})$$

where contributions from  $H'_{SI}$  and  $H_{II}$  are left out. The omission of  $H_{II}$  with respect to  $H'_{SS}$  is certainly justified because the concentration of the paramagnetic ions is always of the order of 1% in polar-

ization experiments. The omission of  $H'_{SI}$  simplifies the calculations while the results are not affected seriously.

The expectation values of  $\langle Z'_S \rangle$ ,  $\langle Z'_n \rangle$  and  $\langle H'_{SS} \rangle$  can be calculated in the same way as before. The variations of these expectation values due to interaction with the lattice are given by

$$\Delta^2 \frac{\partial}{\partial t} \alpha = -\frac{1}{T_{1e}} \Delta^2 \left( \alpha - \frac{\omega_e}{\Delta} \beta_L \right) \quad (I.65)$$

$$N\omega_n^2 \frac{\partial}{\partial t} \beta = -\frac{1}{T_{1n}} N(\omega_n^2 \beta - \omega_n^2 \beta_L) \approx -\frac{1}{T_{1n}} N\omega_n^2 \beta \quad (I.66)$$

$$\omega_L^2 \frac{\partial}{\partial t} \gamma = -\frac{2}{T_{1e}} (\omega_L^2 \gamma - \omega_L^2 \beta_L) \approx -\frac{2}{T_{1e}} \omega_L^2 \gamma_L \quad (I.67)$$

and the rates of change induced by the rf field by

$$\Delta^2 \frac{\partial}{\partial t} \alpha = -\Delta^2 W_0 (\alpha - \gamma) - N\omega_n \Delta (W^- - W^+) (\alpha - \beta) \quad (I.68)$$

$$N\omega_n^2 \frac{\partial}{\partial t} \beta = -N\omega_n^2 W^- \left[ (\beta - \alpha) + \left(1 - \frac{\Delta}{\omega_n}\right) (\alpha - \gamma) \right] + \\ -N\omega_n^2 W^+ \left[ (\beta - \alpha) + \left(1 + \frac{\Delta}{\omega_n}\right) (\alpha - \gamma) \right] \quad (I.69)$$

$$\omega_L^2 \frac{\partial}{\partial t} \gamma = -\Delta^2 W_0 (\gamma - \alpha) - N\omega_n^2 \left[ W^- \left(1 - \frac{\Delta}{\omega_n}\right) + W^+ \left(1 + \frac{\Delta}{\omega_n}\right) \right] (\gamma - \beta) \quad (I.70)$$

where  $W^-$  and  $W^+$  are the probabilities for the forbidden transitions, defined by (I.5) and (I.6). The first terms in  $\partial\alpha/\partial t$  and  $\partial\gamma/\partial t$  of (I.68) and (I.70) are the same as those in (I.50) and (I.51). We introduced a second term in  $\partial\alpha/\partial t$  which represents the influence of the nuclear polarization on the electron spin system<sup>18</sup>. In many of our experiments this term is necessary to describe the polarization process completely. Conservation of spin energy is accounted for by means of the second term in  $\partial\gamma/\partial t$ . Eq. (I.69) describes the tendency of  $\beta$  to become equal to  $\alpha$  under the influence of  $W^\pm$ . When an rf quantum with energy  $\hbar\omega$  is absorbed or emitted, causing a change of  $\hbar(\omega_e \pm \omega_n)$

in the Zeeman energy, the difference  $\hbar(\omega_e - \omega \pm \omega_n) = \hbar(\Delta \pm \omega_n)$  has to be supplied or taken up by the spin-spin energy.

As before, the forbidden transition probabilities have a maximum at  $\Delta = \pm \omega_n$  and a width of the order of  $\omega_L$ . Their relative magnitude is given by

$$W^+(\Delta = \omega_n) = W^-(\Delta = -\omega_n) = W_0(\Delta = 0) \cdot \frac{T_{1e}}{T_{1n}} \quad (\text{I.71})$$

for the case that extraneous relaxation can be neglected. The last terms in (I.68) and (I.70) are then of the order of  $NT_{1e}/T_{1n} = f$  compared with the first ones. In general the solutions of (I.65)-(I.70) have been computed numerically. These solutions will be compared with the experimental results in the following chapters. The equations as given by Abragam and Borghini are only valid if  $f \ll 1$ . The steady state solution for  $\beta$  is then given by

$$\frac{\beta}{\beta_L} = \frac{\frac{\omega_e}{\omega_n} (W^- - W^+) T_{1n} + \frac{\omega_e \Delta}{2\omega_L^2} (W^- + W^+) W_0 T_{1e} T_{1n}}{(1 + W^- T_{1n} + W^+ T_{1n}) (1 + \frac{\Delta^2 + 2\omega_L^2}{2\omega_L^2} W_0 T_{1e})} \quad (\text{I.72})$$

To demonstrate the difference between this spin temperature theory and that based on the rate equations, (I.72) should be compared with (I.21) which is the general result from Jeffries' theory. There are two important phenomena for which the predictions from (I.72) deviate strongly from those of (I.21):

1. According to (I.72)  $\beta/\beta_L$  tends to a constant value in the limit of high rf power, while (I.21) predicts that the polarization factor goes to zero in this case.
2. The maximum obtainable enhancement calculated from (I.21) is  $\omega_e/\omega_n$ , whereas (I.72) predicts  $\omega_e/(2\omega_L\sqrt{2})$  in the limit of high rf power. Thus if  $\omega_n > 2\omega_L\sqrt{2}$ , the polarization factor following from the spin temperature theory is higher than that predicted from the rate equations.

Also the time-dependent solutions of (I.65)-(I.70) can be computed. Since the equations are coupled, every spin temperature will exhibit three time constants, with different coefficients. The solutions for  $\alpha$  and  $\gamma$  are mainly determined by two characteristic times  $\tau_1$  and  $\tau_2$  which are of the order of  $T_{1e}$ . The nuclear polarization is described

by the third one,  $\tau_3$ . This polarization time is, analogous to the relaxation time  $T_{1n}$ , the response time of the average value of the nuclear polarization when the microwave power is turned on. These time-dependent solutions have been computed numerically on the TR-4 computer of the Technische Hogeschool in Delft, for the crystals used in the polarization experiments. The equations were solved by hand, and then the coefficients were evaluated by the computer. The usual approximation methods for the solution of first order differential equations are of little value here, because at high power level  $\tau_1$  and  $\tau_2$  are of the order of  $10^{-5}$  seconds, which implies a step length of  $10^{-6}$  seconds, while the time necessary for the establishment of equilibrium  $\tau_3$  is of the order of  $10^2$  seconds.

The result of such a calculation of  $\tau_3$  in a crystal of  $\text{La}_2\text{Mg}_3(\text{NO}_3)_{12} \cdot 24\text{H}_2\text{O}$  containing 1.0% Ce is shown in fig. I.12. For small values of  $\Delta$   $\tau_3$  becomes constant at relatively low rf power, because for small  $\Delta$  the electron resonance line is strongly saturated. In that case the ratio of polarizing and relaxing transitions is no longer proportional

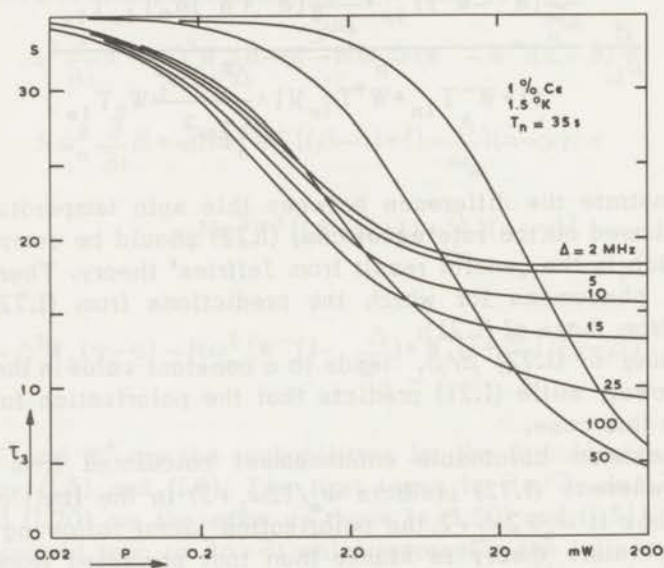


Fig. I.12. Proton polarization time as a function of the microwave power in the cavity for several values of the irradiation frequency  $\Delta$ . The curves have been calculated numerically from (I.65) - (I.70) for a single crystal of LaMN containing 1.0% Ce.

to  $W_0$ . On the other hand, far in the wings of the line a much larger  $H_1^2$  is necessary to obtain saturation. Since here the ratio  $W^\pm/W_0$  is larger, very short polarization times are found at high microwave power.  $\tau_3$  is always different from zero, although the transitions are not resolved. This result differs appreciably from that following from Jeffries' theory, given in fig. I.6.

### I-3.2. Special solutions

#### a. Spectrum resolved

If  $\omega_L \ll \omega_n$ , so that the transitions are well resolved, saturation of one of the forbidden transitions, say  $W^-$  does not affect  $W^+$  or  $W_0$ . (I.72) then reduces to

$$\frac{\beta}{\beta_L} = \frac{\omega_e}{\omega_n} \frac{W^- T_{1n}}{1 + W^- T_{1n}} \quad (\text{I.73})$$

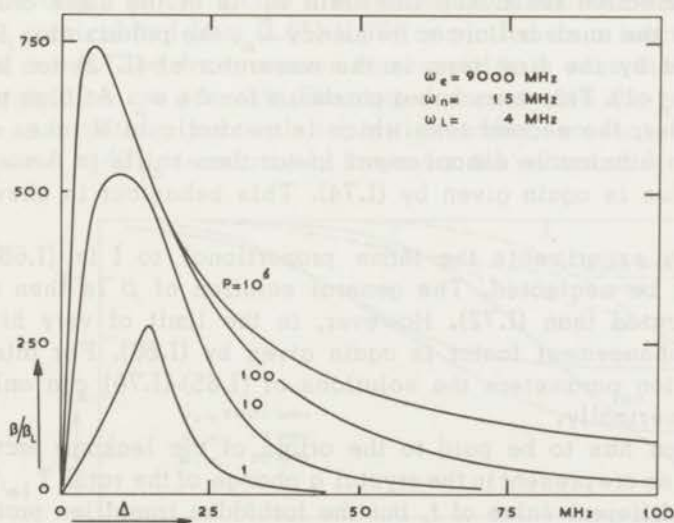


Fig. I.13. Proton polarization factor as a function of the irradiation frequency  $\Delta$  for several values of the microwave power in the cavity;  $\omega_n > 2\omega_L\sqrt{2}$  so the maximum polarization is larger than  $\omega_e/\omega_n = 600$ .

which is exactly the same expression as that found from the rate equations if  $f$  is neglected (cf. (I.15)). This is not surprising, because the spin-spin interaction does not take part in the polarization process.

If the spectrum is not completely resolved, while at the same time  $\omega_n > 2\omega_L\sqrt{2}$ , the nuclear polarization shows the behaviour illustrated in fig.I.13. Irradiation with a frequency  $\Delta \approx \omega_n$  yields an enhancement which is given approximately by (I.73). However, for values of  $\Delta$  in the vicinity of  $\omega_L\sqrt{2}$  a larger polarization factor is found for high rf power. In the limit of very strong saturation the inverse nuclear spin temperature is then equal to

$$\frac{\beta}{\beta_L} = \frac{\omega_e \Delta}{\Delta^2 + 2\omega_L^2} \quad (\text{I.74})$$

which is the same value as that found from Redfield's theory (I.42).

#### b. Homogeneous line broadening; $\omega_L \gtrsim \omega_n$

If the electron resonance linewidth  $\omega_L$  is of the same order of magnitude as the nuclear Larmor frequency  $\omega_n$ , the polarization factor is determined by the first term in the numerator of (I.72) for low rf power ( $W^\pm T_{1n} < 1$ ). This term has a maximum for  $\Delta \approx \omega_n$ . At high power levels however, the second term which is quadratic in  $W$  takes over. The maximum obtainable enhancement factor then shifts to  $\Delta = \omega_L\sqrt{2}$ , while its value is again given by (I.74). This behaviour is shown in fig.I.14.

In many experiments the terms proportional to  $f$  in (I.68) and (I.70) cannot be neglected. The general solution of  $\beta$  is then much more complicated than (I.72). However, in the limit of very high rf power the enhancement factor is again given by (I.60). For intermediate saturation parameters the solutions of (I.65)-(I.70) can only be computed numerically.

Attention has to be paid to the origin of the leakage factor  $f$ . If no impurities are present in the crystal a change of the ratio  $T_{1e}/T_{1n}$  results in a different value of  $f$ , but the forbidden transition probabilities  $W^\pm$  will also change (cf. (I.71)). On the other hand if  $T_{1n}$  is shortened by the addition of impurities, then  $W^+$  and  $W^-$  are not influenced, because they are only due to the coupling of the nuclei with the polarizing spins. The microwave power necessary to obtain the maximum polarization will then be larger, since the condition  $W^\pm T_{1n} \gg 1$

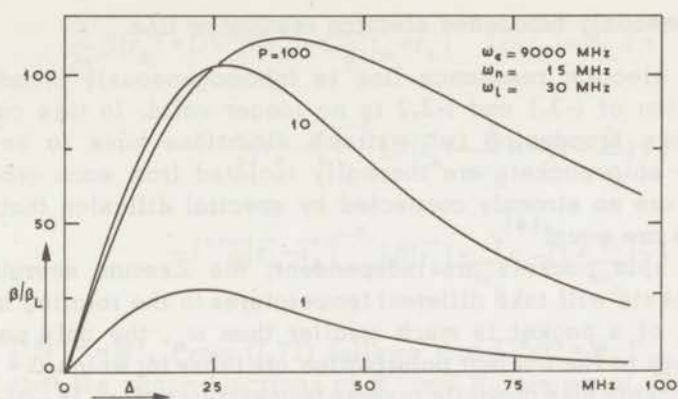


Fig. I.14. Proton polarization factor as a function of the irradiation frequency  $\Delta$  for several values of the microwave power in the cavity; for high power levels the maximum polarization shifts to  $\Delta = \omega_L \sqrt{2}$ .

is more difficult to satisfy as  $T_{1n}$  is shorter. Examples of this behaviour will be shown in chapter VI.

The behaviour of the nuclear polarization time  $\tau_3$  depends also on the origin of the factor  $f$ . An example is shown in fig. I.15, where  $\tau_3/T_{1n}$  calculated from (I.65)-(I.70) is plotted as a function of microwave power. The drawn curves correspond to a case that  $f=2.4$  while no impurities are present. The dotted curves give the results for the same parameters, but with impurities added, so that  $f=12$ . In this last case  $\tau_3/T_{1n}$  is relatively larger for all values of  $\Delta$ .

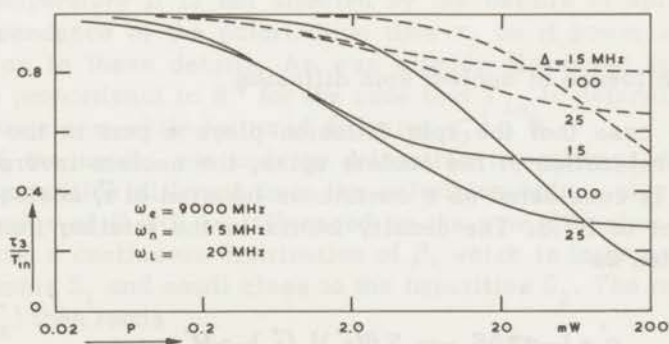


Fig. I.15. Proton polarization times as a function of the microwave power in the cavity, for several values of the irradiation frequency  $\Delta$ . The drawn curves were calculated for a crystal for which  $f=2.4$ , while no impurities are present. The dotted lines refer to the same crystal, but with impurities added so that  $f=12.0$ .

### c. Inhomogeneously broadened electron resonance line

If the electron resonance line is inhomogeneously broadened, the description of I-3.1 and I-3.2 is no longer valid. In this case of inhomogeneous broadening two extreme situations have to be considered: the spin packets are thermally isolated from each other, or the packets are so strongly connected by spectral diffusion that their temperatures are equal<sup>19)</sup>.

If the spin packets are independent, the Zeeman energies of different packets will take different temperatures in the rotating frame. If the width of a packet is much smaller than  $\omega_n$ , the only packets that contribute to the nuclear polarization are those for which  $\Delta = \pm\omega_n$ . These two packets take opposite inverse temperatures  $\alpha(+\omega_n) = -\alpha(-\omega_n)$ . Just as in I-1.3 the dependence of the nuclear enhancement on the irradiation frequency will then be proportional to the derivative of the electron resonance lineshape.

If, on the contrary, spectral diffusion is sufficiently strong to equalize the temperatures of the narrow spin packets, the inverse temperature in the rotating frame can be shown to be

$$\frac{\alpha}{\beta_L} = \frac{\omega_e \Delta}{\Delta^2 + \omega^2}$$

where  $\omega_e$  is the mean frequency of the distribution and  $\overline{\omega^2}$  its second moment. So in this case the dependence of the nuclear polarization on  $\Delta$  is the same as in the case of a homogeneously broadened line.

### I-3.3. The influence of nuclear spin diffusion

In the case that the spin diffusion plays a part in the polarization and relaxation of the nuclear spins, the nuclear inverse spin temperature is considered as a continuous function of  $\vec{r}$ , analogous to the treatment in I-1.3. The density matrix in the rotating frame can then be written as

$$\rho' = 1 - \alpha \hbar \Delta S_z - \omega_n \sum_k \beta(\vec{r}_k) I_z(\vec{r}_k) - \gamma H'_{SS} \quad (\text{I.75})$$

and the equation for  $\beta(\vec{r}_k)$  can be deduced from (I.66) and (I.69), combined with the diffusion equation (I.23)

$$\begin{aligned}
\frac{\partial}{\partial t} \beta(\vec{r}_k) = & D \nabla^2 \beta(\vec{r}_k) - C \sum_{\vec{e}} |\vec{r}_e - \vec{r}_k|^{-6} [\beta(\vec{r}_k) - \beta_L] + \\
& - \Gamma^- \sum_{\vec{e}} |\vec{r}_e - \vec{r}_k|^{-6} [\beta(\vec{r}_k) - \frac{\Delta}{\omega_n} \alpha - (1 - \frac{\Delta}{\omega_n}) \gamma] + \\
& - \Gamma^+ \sum_{\vec{e}} |\vec{r}_e - \vec{r}_k|^{-6} [\beta(\vec{r}_k) + \frac{\Delta}{\omega_n} \alpha - (1 + \frac{\Delta}{\omega_n}) \gamma] \quad (I.76)
\end{aligned}$$

where  $\Gamma^{\pm} r^{-6} = W^{\pm}$ . From (I.71) follows that  $\Gamma^{\pm}/C = W_0 T_{1e}$  when assumed that the shape functions of  $W^{\pm}$  and  $W_0$  are equal. The diffusion equation can be rewritten as

$$\frac{d\beta}{dt} = D \nabla^2 \beta - \Gamma \sum_{\vec{e}} |\vec{r}_e - \vec{r}_k|^{-6} (\beta - \beta_{st}) \quad (I.77)$$

where  $\Gamma = \Gamma^- + \Gamma^+ + C$  and  $\beta_{st}$  is given by

$$\beta_{st} = \frac{\Delta}{\omega_n} \frac{\Gamma^- - \Gamma^+}{\Gamma} \alpha - \frac{(\frac{\Delta}{\omega_n} - 1) \Gamma^- - (\frac{\Delta}{\omega_n} + 1) \Gamma^+}{\Gamma} \gamma + \frac{C}{\Gamma} \beta_L \quad (I.78)$$

which is of course identical to the earlier expression (I.72), since in the stationary state spin diffusion has no influence on the nuclear polarization. Although the stationary value of the nuclear inverse spin temperature  $\beta$  is not affected by the details of spin diffusion, the dependence of the polarization time  $\tau_3$  on rf power is very sensitive as to these details. As was already discussed in I-1.3,  $\tau_3^{-1}$  will be proportional to  $W^{1/4}$  for the case that  $T_{1n}$  is determined by spin diffusion alone, while for rapid diffusion  $\tau_3^{-1} \propto W$ .

If the nuclei can undergo relaxation transitions with paramagnetic impurities different from the polarizing spins, also the steady state value of  $\beta$  will be influenced by the spin diffusion. Then there will exist a continuous distribution of  $\beta$ , which is large near the polarizing spins  $S_1$  and small close to the impurities  $S_2$ . The rate equation for  $\beta(\vec{r}_k)$  then reads

$$\frac{\partial}{\partial t} \beta(\vec{r}_k) = D \nabla^2 \beta(\vec{r}_k) - \Gamma_1 \sum_{\vec{r}_1} |\vec{r}_1 - \vec{r}_k|^{-6} (\beta - \beta_1) - \Gamma_2 \sum_{\vec{r}_2} |\vec{r}_2 - \vec{r}_k|^{-6} (\beta - \beta_2) \quad (I.79)$$

where  $\vec{r}_1$  and  $\vec{r}_2$  are the positions of the spins  $S_1$  and  $S_2$ . Eq.(I.79) shows that  $S_1$  and  $S_2$  tend to polarize or relax the nuclear spin system to different inverse temperatures  $\beta_1$  and  $\beta_2$ . The space average value of  $\beta$  in the stationary state, following from (I.79) is given by

$$\frac{\beta}{\beta_L} = \frac{\beta_0}{\beta_L} \frac{N_1 b_1}{N_2 b_2 + N_1 b_1} \quad (\text{I.80})$$

where  $\beta_0$  denotes the inverse temperature that would be given to the nuclei if only the spins  $S_1$  were present;  $b_1$  and  $b_2$  are equal to  $(\Gamma_1/D)^{1/4}$  and  $(\Gamma_2/D)^{1/4}$  respectively, while  $N_1$  and  $N_2$  represent the numbers of the spins  $S_1$  and  $S_2$ . In (I.80)  $b_2$  will depend on the rf power since the spins  $S_1$  are the polarizing spins, while  $b_2$  is constant. If the available power is sufficient to make  $N_1 b_1 \gg N_2 b_2$ , the influence of the impurities  $S_2$  is negligible and the nuclear enhancement will be the same as if only the spins  $S_1$  were present. Obviously this argument only holds, just as in I-1.3, as long as the factor  $f$  is neglected. If this factor is taken into account, it turns out that the high transition probability necessary to surpass the impurity influence results in a higher electron spin temperature, which causes a smaller nuclear polarization. In the experiments that will be described in chapter VI this influence of nuclear spin diffusion will be of importance.

#### I-3.4. Influence of a phonon bottleneck

In (I.40) and (I.41), describing the coupling of the electron spins with the crystal lattice,  $\beta_L$  was assumed to represent the inverse lattice temperature. In crystals where a phonon bottleneck is present, this assumption is no longer true, and  $\beta_L$  will be the inverse temperature of the phonons on speaking terms, as discussed in I-1.4. Just as before it is then necessary<sup>20)</sup> to introduce an equation describing the evolution of this phonon temperature  $1/\beta_L$

$$\frac{d}{dt} \left( \frac{1}{\beta_L} \right) = - \frac{A}{T_{1e}^*} \omega_e \Delta \left( \alpha - \frac{\omega_e}{\Delta} \beta_L \right) - \frac{1}{\tau_{ph}} \left( \frac{1}{\beta_L} - \frac{1}{\beta_L^0} \right) \quad (\text{I.81})$$

where  $A$  is the relative number of spins and phonons on speaking terms, and  $T_{1e}^*$  spin-phonon relaxation time. The second term on the right hand side describes the relaxation of the hot phonons to their

equilibrium value given by the bath temperature  $1/\beta_L^0$ . The rate of this process is given by  $1/\tau_{ph}$ .

With the assumption that  $f \ll 1$ , the stationary values for  $\beta$  and  $\beta_L$  are found to be

$$\frac{\beta}{\beta_L^0} = \frac{\frac{\omega_e}{\omega_n} (W^- - W^+) T_{1n} + \frac{\omega_e \Delta}{2\omega_L^2} (W^- + W^+) W_0 T_{1e} T_{1n}}{(1 + W^+ T_{1n} + W^- T_{1n}) [1 + W_0 T_{1e} \frac{\Delta^2 + 2(1+\sigma)\omega_L^2}{2\omega_L^2}]} \quad (I.82)$$

$$\frac{\beta_L}{\beta_L^0} = \frac{2\omega_L^2 + W_0 T_{1e} (\Delta^2 + 2\omega_L^2)}{2\omega_L^2 + W_0 T_{1e} [\Delta^2 + 2(1+\sigma)\omega_L^2]} \quad (I.83)$$

where  $\sigma$  is the bottleneck coefficient. The only difference in this solution for  $\beta$  with the earlier expression (I.72) is that the factor 2 multiplying  $\omega_L^2$  is replaced by  $2(1+\sigma)$ . This is a consequence of the fact that the Zeeman relaxation of the electrons is slowed down by a factor  $(1+\sigma)$ , while the relaxation of  $\langle H'_{SS} \rangle$  is not affected by the phonon bottleneck because of the much smaller heat capacity of the spin-spin interactions.

Fig.I.16 shows the nuclear enhancement factor for the same parameters as in fig.I.14, but now including a bottleneck factor  $\sigma=5$ . At the highest power levels the maximum enhancement is now obtained for  $\Delta = \omega_L \sqrt{(1+\sigma)2}$ , instead of  $\omega_L \sqrt{2}$  in the case where no bottleneck exists. The value of this maximum is reduced by a factor  $\sqrt{\sigma+1}$ . In chapter V several experiments are described where the influence of a phonon bottleneck is clearly demonstrated.

There is no doubt that the collective description of the spin systems that participate in the polarization process is more rigorous from a theoretical viewpoint than that based on the rate equations. In fact the experiments that will be discussed in the following chapters indicate that a quantitative agreement between theory and experiment is obtained in many practical cases.

In the equations (I.65)-(I.70) describing the electron and the nuclear polarization the influence of  $H'_{SI}$  was neglected with respect to  $H'_{SS}$  (cf.(I.64)). So it may be expected that in crystals with a large concentration of paramagnetic ions the experimental results will be in better agreement with these theoretical predictions than in crystals

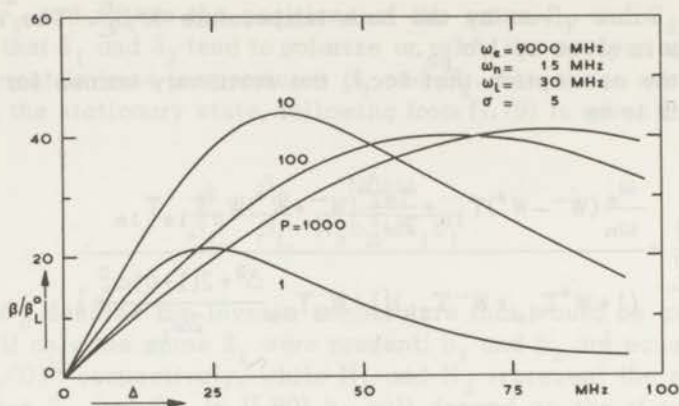


Fig. I.16. Proton polarization factor as a function of the irradiation frequency  $\Delta$  for several values of the micro-wave power in the cavity in the presence of a phonon bottleneck; for high power levels the maximum polarization shifts to  $\Delta = \omega_L \sqrt{2(1+\sigma)}$ .

containing only a small amount of these ions. However, the opposite is true: serious discrepancies between theory and experiment occur in crystals with the largest concentration of paramagnetic ions. In the following we will indicate how (I.65)-(I.70) should be changed to account for these observed discrepancies.

#### I-4. Improvement of the theory of dynamic polarization in the rotating frame

As will be shown in chapter III the nuclear spin-lattice relaxation is in general not only determined by the electron spin-lattice relaxation, but also by the electron spin-spin interactions. Especially in those crystals where the electron spin concentration is large these spin-spin interactions may determine the nuclear relaxation time completely.

##### I-4.1. The relaxation equation for the nuclear spins

If the spin-spin interactions of the electrons contribute considerably to the nuclear relaxation rate, there are two relaxation processes in parallel, so that (I.66) can be written formally as

$$\frac{\partial}{\partial t} \beta = -\frac{1}{T_{1n}} (\beta - \beta_L) - \frac{1}{T'_{1n}} (\beta - \beta_L) \quad (\text{I.84})$$

where  $(T'_{1n})^{-1}$  is the rate at which the nuclear spin system comes into equilibrium with the lattice by the interaction with the electron Zeeman system. The second term describes the return to thermal equilibrium via the electron spin-spin interactions. It has been shown both theoretically and experimentally that  $T'_{1n}$  is inversely proportional to the number of paramagnetic ions  $n_e^{10}$ . In chapter III we will show that in many practical cases  $T''_{1n}$  is given by

$$T''_{1n} = \frac{N\omega_n^2}{2\omega_L^2} T_{1e} \quad (I.85)$$

which means that the nuclear relaxation time is equal to the spin-lattice relaxation time of the electron spin-spin system  $T_{1e}/2$  multiplied by the ratio of the heat capacities of the nuclear Zeeman system and of the electron spin-spin system. This ratio is approximately proportional to  $n_e^{-3}$ . Thus for large concentrations of paramagnetic ions the second term in (I.84) will determine the nuclear relaxation rate.

#### I-4.2. Consequencies for the nuclear polarization

In I.3 the forbidden transition probability was calculated from (I.71), where the measured value of the nuclear spin-lattice relaxation time was used. However, it will be clear from the foregoing that this value is no longer a measure for the magnitude of  $W^\pm$  if electron spin-spin interactions contribute to  $T_{1n}$ . Then  $T'_{1n}$  of (I.84) should be used to calculate  $W^\pm/W_0$ . The second term of (I.84) can then be considered as a term describing the extraneous relaxation of the nuclei via the electron spin-spin system. The relative importance of this extraneous relaxation will increase strongly with increasing paramagnetic ion concentration. Thus for higher concentration the microwave power which is necessary to obtain the maximum polarization will increase, because the condition  $W^\pm T_{1n} \gg 1$  is then more difficult to satisfy. An example of this behaviour, which is analogous to that observed when paramagnetic impurities are present in the crystal, will be given in chapter IV.

## References

1. Overhauser, A.W., Phys.Rev. **92**, 411 (1953).
2. Jeffries, C.D., Phys.Rev. **106**, 164 (1957).
3. Allais, E., C.R.Acad.Sci. **246**, 2123 (1958).
4. Abragam, A. and Proctor, W.G., C.R.Acad.Sci. **246**, 2253 (1958).
5. Leifson, O.S. and Jeffries, C.D., Phys.Rev. **122**, 1781 (1961).
6. Bloembergen, N., Commun. Kamerlingh Onnes Lab., Leiden No. 277b; Physica **15**, 386 (1949).
7. Abragam, A., Principles of Nuclear Magnetism (Oxford University Press, 1961), Chapter IX.
8. De Gennes, P.G., J.Phys.Chem.Solids, **3**, 345 (1958).
9. Faughan, B.W. and Strandberg, M.W.P., J.Phys.Chem.Solids **19**, 155 (1961).
10. Jeffries, C.D., Technical Report UCB-34P20-T-1 (1966), University of California (unpublished).
11. Bloembergen, N., Purcell, E.M. and Pound, R.V., Phys.Rev. **73**, 619 (1948).
12. Redfield, A.G., Phys.Rev. **98**, 1787 (1955).
13. Provotorov, B.N., J.Exptl.Theoret. Phys. **41**, 1582 (1961).
14. Solomon, I., Proc. of the Int. Conf. on Magn. and Elec. Res. and Relax., Eindhoven, 1962 (North Holland Publ. Co., A'dam).
15. Abragam, A. and Borghini, M., Progr. in Low Temp. Phys. Vol.IV. Ed. C.J. Gorter (North Holland Publ. Co., A'dam 1964).
16. Abragam, A., Principles of Nuclear Magnetism, Chapter V.
17. Abragam, A. and Proctor, W.G., Phys.Rev. **109**, 1441 (1958).
18. Swanenburg, T.J.B., van den Heuvel, G.M. and Poulis, N.J., Commun. Leiden No. 354a, Physica **33**, 707 (1967).
19. Bloembergen, N., Shapiro, S., Pershan, P.L. and Artman, J.O., Phys.Rev. **114**, 445 (1959).
20. Borghini, M., Phys. Letters **20**, 228 (1966).
21. Schmutge, J.T. and Jeffries, C.D., Phys.Rev. **A 138**, 1785 (1965).

## Chapter II

## EXPERIMENTAL ARRANGEMENT AND PROCEDURE

*Introduction*

Electron-nuclear double resonance experiments are performed in general in an apparatus which enables the simultaneous observation of the electron paramagnetic resonance and the nuclear resonance. In dynamic polarization the electron Larmor frequency is generally of the order of 10 to 100 GHz, so that the proton resonance frequency is in the rf region from 10 to 100 MHz.

The sample in which the dynamic polarization is to be studied is placed in a microwave cavity. The external magnetic field  $H_0$  is then adjusted at one of the forbidden transitions, and the intensity of the proton resonance signal is used as a measure of the increase of the proton polarization. In most experimental set ups the coil for the observation of the nuclear resonance is mounted inside the cavity<sup>1)</sup>. In our arrangement however it is wound around the cavity, and slits in the sidewalls permit the penetration of the rf field into the cavity.

The cavity is placed in a liquid helium cryostat between the poles of a Bruker Physik BE-20 C8 electromagnet. The power supply of this magnet has a long term current stability of 5 parts in  $10^6$ . Small field modulation coils are mounted between the pole caps. The coils are fed with a 50 Hz current when the resonance signals are displayed on the screen of an oscilloscope, or with a small current of a variable frequency between 30 and 1000 Hz when phase sensitive detection is used.

The construction of the cavity together with the microwave spectrometer will be discussed in II-1. In II-2 a description will be given of the nuclear resonance apparatus. The preparation of the single crystals of  $\text{La}_2\text{Mg}_3(\text{NO}_3)_{12}\cdot 24\text{H}_2\text{O}$  (LaMN) with different amounts of Nd, Ce or Pr ions at the La sites will be described in II-3.

*II-1. Electron resonance equipment**II-1.1. Double resonance cavity*

The microwave cavity is a rectangular X-band cavity operating in the  $\text{TE}_{102}$  mode. The internal dimensions are 44 x 22 x 6 mm. The construction is shown in fig. II.1. The LaMN crystal, which has a volume of about  $8 \times 5 \times 2 \text{ mm}^3$ , is inserted in a piece of styrofoam

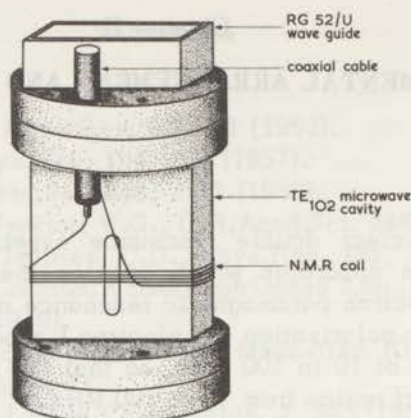


Fig. II.1. The microwave cavity. The n.m.r. coil is wound around the cavity.

that fits close in the cavity. The lower part of the cavity can be removed to give access to the interior. In the middle of the sidewalls narrow slits are made that permit the penetration of the rf field of the n.m.r. coil. The Q-factor of the cavity is about 3000 at helium temperatures<sup>2,3</sup>.

The advantages of this cavity construction are that new crystals can easily be inserted without changing the n.m.r. coil and that the Q-factor of the coil is so small due to losses in the copper walls of the cavity, that there is only a very weak rf field at the site of the crystal. If the nuclear relaxation time  $T_{1n}$  is shorter than 500 seconds the resonance signal can be continuously monitored with an rf voltage of 15 mV across the coil without causing more than 5% saturation. A normal coil with comparable dimensions would already cause appreciable saturation if  $T_{1n}$  was of the order of 50 seconds at the same rf voltage. Furthermore, the homogeneity of the microwave field over the crystal has been measured to be within 5%. Such uniformity seems to be very difficult to obtain when the coil is mounted inside the cavity. The field pattern is then always distorted by the presence of the copper wires of the coil.

One of the major disadvantages of the geometry of the cavity is of course that, due to the low Q-factor of the coil, the signal-to-noise ratio of the n.m.r. signal is low. This difficulty is, however, only important in measuring the thermal equilibrium proton signal. The polarized signals are large enough to be recorded easily.

## II-1.2. Microwave apparatus for dynamic polarization experiments

The block diagram of the microwave set up used in the dynamic polarization experiments is shown in fig.II.2. A Varian V-58 klystron, delivering a power of about 300 mW at 9000 MHz is connected to the cavity, which is placed in a liquid helium cryostat. A thinwalled stainless steel waveguide is used to reduce the heat input. The power level in the cavity can be regulated by means of a 60 db calibrated attenuator. A 26 db crossguide coupler to which a bolometer mount is connected enables a continuous monitoring of the klystron power. The power reflected from the cavity is measured via a 10 db directional coupler with a second bolometer mount. The microwave power in the cavity can then easily be calculated from the incident and the reflected power.

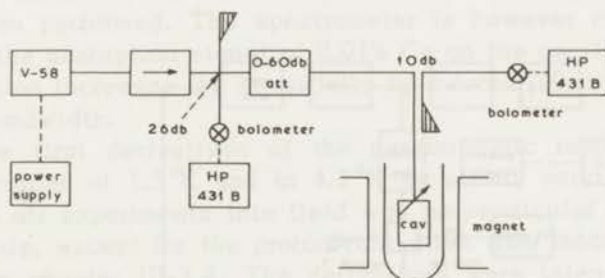


Fig. II.2. Block diagram of the microwave apparatus used in the dynamic polarization experiments.

In principle this arrangement can also be used for the observation of the paramagnetic resonance signals. However, for low concentrations of the paramagnetic ions in the crystal the change of the reflection coefficient of the cavity when the field  $H_0$  is adjusted at resonance is too small to be detected directly by the bolometer bridge. Furthermore, the Nd resonance signal can be observed at low temperatures with a microwave power of only  $10^{-6}$  W because of the relatively long spin-lattice relaxation time. This makes bolometer or video detection impossible. Therefore the microwave apparatus was extended to a more sensitive set up, which easily enables the observation of 0.01% Ce or Nd in the crystals.



frequency of the cavity. If there is a difference in frequency, a 10 kHz component will be present at the receiver output, which is fed into a 10 kHz lock-in amplifier. The resultant dc voltage is added to the reflector voltage from the power supply, so that the klystron frequency is corrected automatically<sup>4</sup>).

About  $10^{-3}$  W of the microwave signal of the V-58 klystron is fed via the E-arm of a hybrid T to the 1N23B diode, and mixed with the signal from the local oscillator. The 30 MHz component of the resultant voltage is amplified, and connected to a 30 MHz discriminator circuit. The dc correction voltage produced by this AFC unit is added in the right phase to the reflector voltage from the local oscillator power supply. The frequency difference is thus maintained at 30 MHz. The power delivered by the V-58 klystron is continuously monitored on a bolometer bridge.

No measurements of the sensitivity of this microwave system have been performed. The spectrometer is however capable of displaying the absorption signal of 0.01% Ce on the oscilloscope. Lock-in detection increases the sensitivity by a factor 10 to 100 depending on the bandwidth.

The first derivatives of the paramagnetic resonance signals were recorded at 1.5°K and at 4.2°K by slowly varying the external field. In all experiments this field was perpendicular to the crystal-line z axis, except for the proton relaxation time measurements described in chapter III-3.4. The derivatives were integrated by hand, and the linewidths were determined from these integrated signals.

## II-2. Nuclear resonance equipment

### II-2.1. Measurement of the polarization factor

The nuclear resonance spectrometer consists of a modified Pound-Watkins oscillator, which operates in the frequency range from 9 MHz to 15 MHz. Polarization measurements on LaMN,Nd were carried out at a frequency of about 9.5 MHz, and those on LaMN,Ce at  $\nu \approx 14$  MHz. Under normal operating conditions the rf voltage across the coil is 10 to 100 mV, depending on the dc feedback voltage. As mentioned before, an oscillating amplitude of 15 mV permits a continuous observation of proton signals without saturation if the relaxation time is shorter than 500 seconds.

The linear response of the oscillator has been checked for several operating points by comparing the measured proton enhancement factor E with that measured with a twin-T bridge. The two

observed values of  $E$  were always equal within the accuracy of the measurements, which is about 5%. A second check of the linearity is provided by the observation of the decay of an enhanced proton signal after switching off the microwave power. Always a purely exponential decay was observed, which would not have been the case if the oscillator had a nonlinear response.

After one stage of rf amplification the proton signal is rectified and fed into the PAR HR-8 lock-in amplifier. The block diagram is shown in fig.II.4.

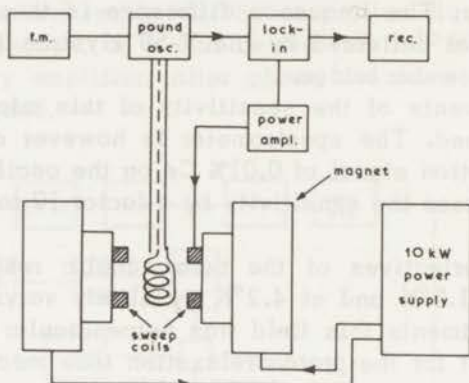


Fig. II.4. Block diagram of the n.m.r. apparatus used in the dynamic polarization experiments.

The course of the measurement of the polarization factor is as follows: the V-58 klystron is tuned at the resonance frequency of the cavity. The magnetic field  $H_0$  is then adjusted in the vicinity of the paramagnetic resonance value. At a certain microwave power level in the cavity the proton resonance signal is then recorded by motor-tuning the oscillator through the proton resonance frequency.

The magnetic field is then increased by one or two oersted and the proton signal is again recorded. If the magnetic field is shifted so far from resonance that the polarization factor has become very small, the klystron is switched off and the thermal equilibrium proton resonance signal is measured several times. Because of the unfavorable signal-to-noise ratio a long time constant is used in this case. After every change of the field  $H_0$  or of the microwave power, sufficient time was allowed for the polarization to reach a steady state.

## II-2.2. Measurement of the polarization and relaxation times

As mentioned before, the proton spin-lattice relaxation times were determined from the decay of a polarized signal after suddenly switching off the microwave power. The exponential signal thus obtained is replotted on a semilog graph, and the time constant can easily be calculated. In this manner relaxation times down to a few seconds can be measured. This limit is determined by the response time of the apparatus, which is about 0.3 seconds.

The polarization times were measured by recording the build-up of the polarization after switching on the klystron. This was repeated several times for the same power level. Then another cavity power was chosen, and again the build-up time was determined. The exponential curves were always replotted for the calculation of the polarization time  $\tau_3$ .

The accuracy of the measurements of E and  $\tau_3$  depends mainly on the polarization factor and frequency stability of the klystron. It is, however, always better than 10%. For all measurements of the polarization factor and of the polarization time the rf voltage across the coil was taken so low, that saturation of the proton resonance signal could be neglected with respect to the other inaccuracies of the measurements, which are of the order of a few percent.

## II-3. Crystals

### II-3.1. Preparation

The single crystals of  $\text{La}_2\text{Mg}_3(\text{NO}_3)_{12} \cdot 24\text{H}_2\text{O}$  in which a small amount of the La ions is replaced by one or two other rare earth ions, were grown from a saturated aqueous solution. A vessel with the solution containing a mixture of LaMN and CeMN or NdMN is placed in a desiccator which is kept at a temperature of  $0^\circ$  to  $5^\circ\text{C}$ . At higher temperatures the evaporation of water is so fast that the crystals begin to grow at the surface. Under the conditions mentioned clear crystals of 300-500 mg were prepared in a few days. The flat hexagonal plates were cut down to the dimensions necessary for the experiment ( $8 \times 5 \times 2$  mm).

Because a small amount of paramagnetic ions in the crystal, different from those added on purpose, has a great influence on the nuclear relaxation time and on the enhancement factor, the origin and the purity of the chemicals used is given below:

$\text{La}(\text{NO}_3)_3 \cdot 6\text{H}_2\text{O}$	Lindsay Chem.Co, Code 549; La 99.997%; Pr 0.001%; Fe 0.0001%.
$\text{Mg}(\text{NO}_3)_2 \cdot 6\text{H}_2\text{O}$	Mallinckrodt Anal.Reagent. Fe 0.0005%.
$\text{Nd}(\text{NO}_3)_3 \cdot 6\text{H}_2\text{O}$	Hopkin and Williams, Code 5990; Fe 0.001%; Pr 0.005%.
$\text{Ce}(\text{NO}_3)_3 \cdot 6\text{H}_2\text{O}$	Merck A.G. Fe 0.005%; Pr 0.005%.
$\text{Pr}(\text{NO}_3)_3 \cdot 6\text{H}_2\text{O}$	Hopkin and Williams, Code 7190.

The Nd salts contained the normal isotopic composition (~80% even isotopes; 12%  $^{143}\text{Nd}$ ; 8%  $^{145}\text{Nd}$ ).

In some of the crystals part of the measurements were repeated several times, sometimes with intervals of a few months. Always the same relaxation times and the same polarization factors were observed.

### II-3.2. Concentration of the paramagnetic rare earth ions in the crystals

In order to be able to make a quantitative comparison between the observed polarization factors and the theoretical predictions, the concentration of the polarizing spins in the crystals should be known. In general this concentration will not be the same as that in the solution.

Arc spectrography has shown that in a small crystal grown from a solution of LaMN containing 1.0% Nd, only 0.2% Nd is present<sup>5,6</sup>. If the crystal is allowed to grow on, the Nd concentration increases. Because our crystals were always prepared from a relatively large amount of solution, we have assumed in all our calculations that the Nd concentration in the crystals is only 20% of that of the solution.

The percentage of Ce in the crystals is presumably close to that of the solution. Susceptibility measurements on a LaMN,Ce crystal grown from a solution containing 10% Ce indicate that the Ce concentration in the crystal is about 9%<sup>7</sup>.

For the Pr ion no precise data are available. The intensity of the paramagnetic resonance line does not give any information, because the g-values are  $g_{//} = 1.55$  and  $g_{\perp} = 0$ . Crystal field distortions make the observation of paramagnetic resonance possible. The con-

centration however is not important, because the Pr ion was never used as polarizing spin.

Although in the following chapters results are given for one crystal for each concentration, many more measurements have been carried out. The data show that crystals grown from solutions containing the same amount of paramagnetic rare earth ions give the same results as to the proton spin-lattice relaxation times and the polarization factors.

### References

1. Abragam, A. and Borghini, M., Progr. in Low Temp. Phys. Vol. IV. Ed. C.J. Gorter (North Holland Publ. Co., A'dam 1964).
2. Hardeman, G.E.G., Philips Res. Repts. **15**, 587 (1960).
3. Tchao, Y-H., Thesis, Paris (1961).
4. We are very much indebted to Drs. E. Lijphart for the design of this 10 kHz frequency stabilizing unit.
5. Dost, H., private communication mentioned in Schultz, C., Thesis, Berkeley (1964).
6. Raynaud, H. and Cittanova, A., private communication mentioned in Borghini, M., C.R. Acad. Sci. **262**, 337 (1966).
7. Lubbers, J., private communication.

## Chapter III

## SPIN-LATTICE RELAXATION

*Introduction*

The spin-lattice relaxation times of the paramagnetic ions as well as those of the protons in the crystal play a dominant part in the dynamic polarization process. One of the requirements for obtaining the maximum polarization factor

$$E = \frac{\beta}{\beta_L} = \frac{\omega_e \Delta}{\Delta^2 + 2\omega_L^2}$$

is, that the factor  $f = NT_{1e}/T_{1n} \ll 1$ , as discussed in chapter I. This means that for a fixed paramagnetic ion concentration  $T_{1n}/T_{1e} \gg N$ . Furthermore, the maximum obtainable polarization is also strongly influenced by the occurrence of a phonon bottleneck in the electron spin-lattice relaxation.

In view of the importance of the relaxation times the measurements of  $T_{1e}$  and  $T_{1n}$  that have been carried out in the crystals in which the dynamic polarization process was studied, will be given in this chapter. In III-1 a theoretical description of the nuclear spin-lattice relaxation mechanism is presented, which takes the influence of the electron dipole-dipole interaction into account. The dependence of  $T_{1n}$  on the concentration of the paramagnetic ions is different from the one predicted by earlier theories<sup>1,2,3</sup>). In III-3 the values of  $T_{1e}$  are summarized; in III-3 the measurements of  $T_{1n}$  in single crystals of LaMN containing different amounts of one or the two paramagnetic rare earth ions are discussed.

### III-1. Theory of proton spin-lattice relaxation in dilute paramagnetic crystals

#### III-1.1. Relaxation equations

The interaction of a nuclear spin with the surrounding crystal lattice is calculated in general by evaluating the spectral intensity  $J(\omega)$  of the fluctuating field at the position of the nucleus<sup>4</sup>). In dilute paramagnetic crystals where only a dipolar coupling between the nuclei and the paramagnetic ions is present,  $J(\omega)$  is known to be deter-

mined only by the fluctuations of the  $z$  component of the spin  $S$  of the paramagnetic ions<sup>1)</sup>.

There are two mechanisms that may induce a change of the orientation of the spins  $S$ : their interaction with the lattice and their interaction with each other. The spectral density due to the first process will have a Debye distribution with a correlation time  $\tau_c$  equal to the spin-lattice relaxation time  $T_{1e}$

$$J_1(\omega) = \frac{1}{3} g^2 \beta^2 S(S+1) \frac{T_{1e}}{1 + \omega^2 T_{1e}^2} \quad (\text{III.1})$$

The spectral distribution due to the spin-spin interaction  $J_2(\omega)$  will not have a Debye shape because of the correlation between two neighbouring spins. However, apart from a factor of order unity the magnitude of  $J_2(\omega)$  will still be given by (III.1) where  $T_{1e}$  is replaced by  $T_{2e}$ .

The intensities  $J_1(\omega)$  and  $J_2(\omega)$  determine the rate at which the nuclear spin system comes into equilibrium with the electron Zeeman system denoted by  $Z_e$ , and with the electron spin-spin system  $H_{SS}$  respectively. The transition probabilities of the nuclear spins are given by

$$W_1 = \frac{9}{4} \gamma_n^2 r_{IS}^{-6} \sin^2 \theta \cos^2 \theta J_1(\omega_n) \quad (\text{III.2})$$

$$W_2 = \frac{9}{4} \gamma_n^2 r_{IS}^{-6} \sin^2 \theta \cos^2 \theta J_2(\omega_n) \quad (\text{III.3})$$

where  $r_{IS}$  is the distance between the nuclear spin and the paramagnetic ion, and  $\theta$  the angle between  $\vec{r}_{IS}$  and  $\vec{H}_0$ <sup>1)</sup>. The nuclear Larmor frequency in the field  $H_0$  is given by  $\omega_n$ . According to Provotorov's theory (cf. (I-2.2))  $Z_e$  and  $H_{SS}$  may have different temperatures if  $T_{2e} \ll T_{1e}$ <sup>5)</sup>. In the absence of a microwave field which tries to equalize their temperatures, there is no contact between  $Z_e$  and  $H_{SS}$  if the electron resonance linewidth  $\omega_L$  is much smaller than the Larmor frequency  $\omega_e$ . A relaxation process of the Kronig-Bouwkamp type is then impossible<sup>6)</sup>.

The electron Zeeman system is coupled with the lattice with a spin-lattice relaxation time  $T_{1e}$ . The rate at which the spin-spin system comes into equilibrium with the lattice is given by  $2/T_{1e}$  (cf. (I-2.1)).

The problem to be solved is to calculate the rate at which the

nuclear Zeeman system  $Z_n$  returns to equilibrium after a disturbance. The thermal block diagram illustrating the model that is used for the description of the relaxation process is shown in fig. III.1.

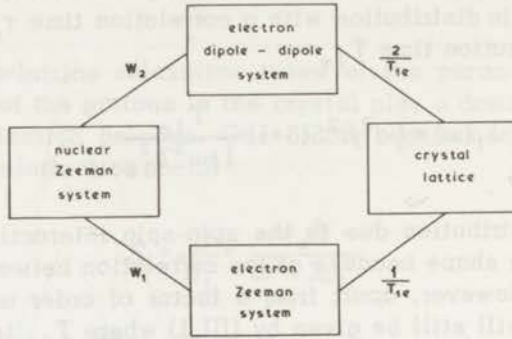


Fig. III.1. Thermal block diagram for the description of the nuclear spin-lattice relaxation process.

The equations describing the rates of change of the expectation values of  $Z_n$ ,  $Z_e$  and  $H_{SS}$  are given by

$$\frac{d}{dt} \langle Z_n \rangle_n = -W_2 \{ \langle Z_n \rangle_n - \langle Z_n \rangle_{SS} \} - W_1 \{ \langle Z_n \rangle_n - \langle Z_n \rangle_e \} \quad (\text{III.4})$$

$$\frac{d}{dt} \langle H_{SS} \rangle_{SS} = W_2 \{ \langle Z_n \rangle_n - \langle Z_n \rangle_{SS} \} - \frac{2}{T_{1e}} \{ \langle H_{SS} \rangle_{SS} - \langle H_{SS} \rangle_L \} \quad (\text{III.5})$$

$$\frac{d}{dt} \langle Z_e \rangle_e = W_1 \{ \langle Z_n \rangle_n - \langle Z_n \rangle_e \} - \frac{1}{T_{1e}} \{ \langle Z_e \rangle_e - \langle Z_e \rangle_L \} \quad (\text{III.6})$$

where  $\langle Z_n \rangle_n = n_n \omega_n^2 / T_n = n_n \beta_n \omega_n^2$  is the expectation value of the nuclear Zeeman energy when the nuclear spin system is at a temperature  $T_n$ . Likewise  $\langle Z_n \rangle_{SS} = n_n \beta_{SS} \omega_n^2$ ,  $\langle Z_n \rangle_e = n_n \beta_e \omega_n^2$  and  $\langle Z_n \rangle_L = n_n \beta_L \omega_n^2$ . The corresponding electron spin-spin energies and the electron Zeeman energies are given by  $\langle H_{SS} \rangle_{SS} = n_e \beta_{SS} \omega_L^2$ ,  $\langle H_{SS} \rangle_L = n_e \beta_L \omega_L^2$ ,  $\langle Z_e \rangle_e = n_e \beta_e \omega_e^2$  and  $\langle Z_e \rangle_L = n_e \beta_L \omega_e^2$ . It is to be noted that  $\omega_L$  is the Larmor frequency of the electron spins in the field due to

neighbouring electron spins. The equations given above can be re-written as

$$\frac{d}{dt}\beta_n = -W_2(\beta_n - \beta_{SS}) - W_1(\beta_n - \beta_e) \quad (\text{III.7})$$

$$\frac{d}{dt}\beta_{SS} = -\frac{N\omega_n^2}{\omega_L^2} W_2(\beta_{SS} - \beta_n) - \frac{2}{T_{1e}}(\beta_{SS} - \beta_L) \quad (\text{III.8})$$

$$\frac{d}{dt}\beta_e = -\frac{N\omega_n^2}{\omega_e^2} W_1(\beta_e - \beta_n) - \frac{1}{T_{1e}}(\beta_e - \beta_L) \quad (\text{III.9})$$

where  $N = n_n/n_e$ . The time-dependent solutions of these equations can of course be calculated in general. However, in order to show the relative influence of the different transition probabilities we will consider several situations where the solutions take a simple form.

### III-1.2. Special solutions

a.  $n_e \omega_e^2 \gg n_n \omega_n^2$

If the electron spin concentration is larger than  $\sim 10^{-3}\%$ ,  $n_e \omega_e^2 \gg n_n \omega_n^2$  because in general  $\omega_e \approx 10^3 \omega_n$ . The temperature of the electron Zeeman system  $1/\beta_e$  will then remain equal to the lattice temperature  $1/\beta_L$  during the nuclear relaxation process. Eq. (III.9) is then no longer important, while (III.7) reduces to

$$\frac{d}{dt}\beta_n = -W_2(\beta_n - \beta_{SS}) - W_1(\beta_n - \beta_L) \quad (\text{III.10})$$

The two equations (III.8) and (III.10) describing the evolution of  $\beta_n$  will have a solution of the form

$$\beta_n = A e^{-\frac{t}{\tau_1}} + B e^{-\frac{t}{\tau_2}} + C \quad (\text{III.11})$$

and thus the decay of  $\beta_n$  will show in general two time constants  $\tau_1$  and  $\tau_2$ .

In the crystals which are used in the dynamic polarization ex-

periments described in the following chapters the electron spin-lattice relaxation time  $T_{1e}$  is known to vary between  $10^{-4}$  and 1 sec, while the spin-spin relaxation time  $T_{2e}$  is in the range from  $10^{-9}$  to  $10^{-6}$  sec, depending on the paramagnetic ion concentration; the nuclear Larmor frequency  $\omega_n \approx 10^8$ . Substitution of these values in (III.1) shows that  $J_1(\omega_n) \ll J_2(\omega_n)$  so that

$$W_2 \gg W_1 \quad (\text{III.12})$$

Furthermore, measurements of the electron resonance linewidth  $\omega_L$  show that for concentrations up to about 20% the following condition is valid

$$\frac{N\omega_n^2}{\omega_L^2} \gg 1 \quad (\text{III.13})$$

The general time-dependent solution of  $\beta_n$  can be simplified by making use of these inequalities (III.12) and (III.13). The two time constants  $\tau_1$  and  $\tau_2$  are then given by

$$\tau_1^{-1} = \frac{\omega_L^2}{N\omega_n^2} \cdot \frac{2}{T_{1e}} + W_1 \quad (\text{III.14})$$

$$\tau_2^{-1} = \frac{N\omega_n^2}{\omega_L^2} W_2 \quad (\text{III.15})$$

In the concentration range up to 20% the coefficient A in (III.11) is very large compared with B, so that the principal change in  $\beta_n$  occurs with the time constant  $\tau_1$ , which can be identified with the observed relaxation time. This time behaviour of  $\beta_n$  is illustrated schematically in fig.III.2, curve 1;  $\beta_n - \beta_L$  first drops by a small amount with the short time constant  $\tau_2$ , and then goes slowly to equilibrium with a characteristic time  $\tau_1$ . If the paramagnetic ion concentration  $c$  increases,  $\omega_L^2/N$  increases as  $c^3$ , while  $W_1$  is proportional to  $c$ ;  $\tau_1$  decreases and  $\tau_2$  increases with increasing concentration. Also the coefficient B can be shown to increase (curve 2).

If the concentration becomes larger than  $\sim 20\%$ , (III.13) will no longer be valid. The time constants are then no longer given by (III.14) and (III.15). Calculation shows that  $\tau_1$  and  $\tau_2$  become comparable in magnitude, just as the coefficients A and B (curve 3). If the concen-

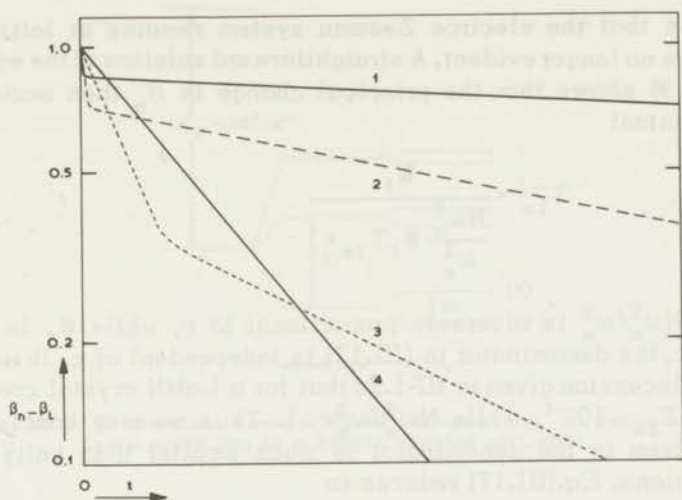


Fig. III.2. Behaviour of the nuclear inverse spin temperature as a function of time. The different curves are discussed in the text.

tration becomes so large that  $\omega_L^2 > N\omega_n^2$  the spin-spin system will remain at lattice temperature during the nuclear relaxation. The relaxation time is then given by

$$\tau_2^{-1} = W_2 + W_1 \approx W_2 \quad (\text{III.16})$$

This relaxation time is temperature-independent, because  $W_2$  is determined by  $T_{2e}$ , which is independent of temperature.

The solutions discussed above show that in the interval of paramagnetic ion concentrations between  $10^{-3}\%$  and 20% the main part of the decay of  $\beta_n$  is given by the time constant  $\tau_1$  from (III.14). As stated before, the first term in (III.14) is proportional to  $c^3$ , the second one proportional to  $c$ . Calculation shows, that the two terms are of comparable magnitude for  $c \approx 1\%$ , so that  $\tau_1 (\approx T_{1n})$  will vary as  $c^{-3}$  for  $1\% < c < 20\%$ , and proportional to  $c^{-1}$  for  $10^{-3}\% < c < 1\%$ . For higher concentrations the dependence of  $T_{1n}$  on  $c$  is determined by the concentration dependence of  $T_{2e}$ .

b.  $n_e \omega_e^2 < n_n \omega_n^2$

If the electron spin concentration is so low that  $\omega_e^2 < N\omega_n^2$ , the

assumption that the electron Zeeman system remains at lattice temperature, is no longer evident. A straightforward solution of the equations (III.7)-(III.9) shows that the principal change in  $\beta_n$  then occurs with a time constant

$$T_{1n}^{-1} = \frac{W_1}{\frac{N\omega_n^2}{\omega_e^2} W_1 T_{1e} + 1} \quad (\text{III.17})$$

Because  $N\omega_n^2/\omega_e^2$  is inversely proportional to  $c$ , while  $W_1$  is proportional to  $c$ , the denominator in (III.17) is independent of  $c$ . It is known from the discussion given in III-1.2a that for a LaMN crystal containing 1% Nd  $W_1 T_{1e} \approx 10^{-4}$ , while  $N\omega_n^2/\omega_e^2 \ll 1$ . Thus we may conclude that the first term in the denominator is much smaller than unity for all concentrations. Eq.(III.17) reduces to

$$T_{1n}^{-1} = W_1 \quad (\text{III.18})$$

which shows that  $T_{1n}^{-1}$  is proportional to the paramagnetic ion concentration  $c$  down to the lowest concentrations.

The measurement of  $T_{1n}$  for very small paramagnetic ion concentrations are difficult in practice because of the presence of unknown impurities in the crystals.

### III-2. Spin-lattice relaxation of the paramagnetic ions

The relevant part of the energy level diagram of the paramagnetic rare earth ions in LaMN is shown in fig.III.3. The spin-orbit splitting is usually of the order of  $10^3 \text{ cm}^{-1}$ , which is considerably larger than the crystal field splittings ( $\sim 10^2 \text{ cm}^{-1}$ ). For the ions which are of interest here the lowest state is a doublet, the degeneracy of which is removed by an external magnetic field  $H_0$ .

At liquid helium temperatures only this ground state will be occupied, and paramagnetic resonance is observed between the two levels  $|a\rangle$  and  $|b\rangle$  of this lowest state. The next higher states will in general not be populated at these low temperatures, but they may still be of great influence on the relaxation rate between the levels  $|a\rangle$  and  $|b\rangle$ <sup>7)</sup>.

It has been shown both theoretically and experimentally that the spin-lattice relaxation of the rare earth ions at low temperatures can occur through three different processes<sup>3)</sup>:

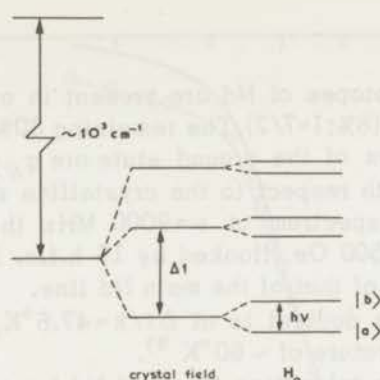


Fig. III.3. Schematic energy level diagram of a paramagnetic rare earth ion in a single crystal of LaMN.

- The direct process, where a spin flips from state  $|b\rangle$  to state  $|a\rangle$ , simultaneously with the creation of a phonon of energy  $\hbar\omega_e$ . The direct relaxation rate  $T_{1d}^{-1}$  is proportional to  $\coth(\hbar\omega_e/2kT)$ .
- The Raman process, which involves the simultaneous absorption of a phonon of energy  $\delta_1$  and the emission of another phonon of energy  $\delta_2 = \delta_1 + \hbar\omega_e$ , together with a spin flip from  $|b\rangle$  to  $|a\rangle$ . The Raman relaxation rate is proportional to  $T^7$  if the ground state is a non-Kramers doublet, or to  $T^9$  if it is a Kramers doublet.
- The Orbach process, which also implies a two phonon process: a phonon of energy  $\Delta 1$  is absorbed, with a simultaneous spin flip from  $|b\rangle$  to the next higher doublet at  $\Delta 1$ . Then a phonon of energy  $\Delta 1 + \hbar\omega_e$  is created, while the spin flips to  $|a\rangle$ . Clearly this process only works if there are phonons of energy  $\Delta 1$  present in the crystal, so  $\Delta 1$  should be smaller than  $k\theta$ , where  $\theta$  is the Debye temperature defined as  $k\theta = \hbar\Omega$  ( $\Omega$  is the cut-off frequency). The Orbach relaxation rate is proportional to  $\exp(-\Delta 1/kT)$ .

The direct process and the Orbach process are depending on a narrow phonon band, with a width of the order of the paramagnetic resonance linewidth. The relaxation rates due to these processes may be slowed down by a phonon bottleneck<sup>8)</sup>. In the Raman process however the spin energy is distributed over the whole phonon spectrum, so that a phonon bottleneck is very improbable.

For two of the ions that will be discussed (Ce and Pr) only the direct process shows a phonon bottleneck. The spin-bath relaxation rate  $T_{1b}^{-1}$  is then proportional to  $A [\coth(\hbar\omega_e/2kT)]^2$  where  $A$  depends on the concentration and the linewidth of the paramagnetic ions, and on the crystal size.

## III-2.1. Nd in LaMN

Two uneven isotopes of Nd are present in our crystals:  $^{143}\text{Nd}$  (12%;  $I=7/2$ ) and  $^{145}\text{Nd}$  (8%;  $I=7/2$ ). The remaining 80% are even isotopes with  $I=0$ . The  $g$ -values of the ground state are  $g_{\parallel}=0.362 \pm 0.01$  and  $g_{\pm}=2.702 \pm 0.006$  with respect to the crystalline  $z$  axis<sup>3)</sup>. The paramagnetic resonance spectrum at  $\nu=9000$  MHz thus consists of a central line at  $H_0 \approx 2500$  Oe, flanked by 16 h.f.s. lines each with an intensity of about 1% of that of the main Nd line.

The next higher doublet is at  $\Delta 1/k=47.6^\circ\text{K}$ , which is well below the Debye temperature of  $\sim 60^\circ\text{K}$ <sup>9)</sup>.

The spin-lattice relaxation times of Nd have been measured for  $z \perp H_0$  in an external field of 2.5 kOe in crystals containing 1% and 5% Nd. The data which do not depend on the Nd concentration, are very well fitted by the expression

$$T_{1e}^{-1} = 0.3 \coth\left(\frac{\hbar\omega_e}{2kT}\right) + 6.3 \times 10^9 \exp\left(-\frac{47.6}{T}\right) \quad (\text{III.19})$$

in the temperature region from  $0.3^\circ\text{K}$  to  $4.2^\circ\text{K}$ <sup>10)</sup>. At low temperatures the direct process prevails, while at high temperatures the Orbach process is most effective. The exponent of the Orbach term is in agreement with the energy of the excited level.

Measurements were also carried out in our laboratory by Dr Drewes and Drs Lijphart in one of our crystals. Their results are shown in fig.III.4, together with the relaxation times calculated from (III.19). The agreement is very good.

In III-3.4 experiments on the proton relaxation time  $T_{1n}$  as a function of the angle  $\theta$  between the crystalline  $z$  axis and the external field  $H_0$  are described. The electron spin-lattice relaxation time has been measured as a function of this angle<sup>11)</sup>. The results show that  $T_{1e}$  is independent of  $\theta$  in the region  $90^\circ > \theta > 50^\circ$ .

## III-2.2. Ce in LaMN

Only even isotopes are present in the crystals,  $^{140,142}\text{Ce}$  ( $I=0$ ). The  $g$ -values of the ground state are  $g_{\parallel}=1.83$  and  $g_{\pm}=0.024$ <sup>10,12)</sup>. The paramagnetic resonance spectrum at  $\nu=9000$  MHz consists of only one line in a field of about 3600 Oe.

The next higher doublet is found at  $\Delta 1/k=34.0^\circ\text{K}$ .

The relaxation rate shows, just as in the case of Nd, two processes in parallel. The Orbach process, which is predominant above

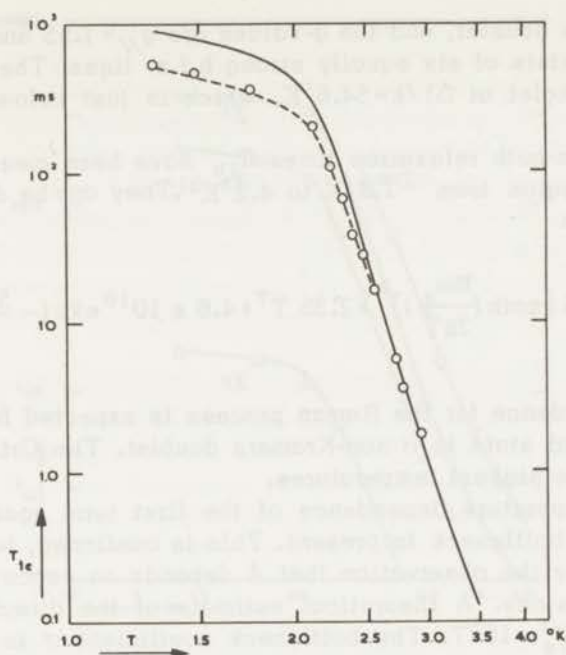


Fig. III.4. Nd spin-lattice relaxation time  $T_{1e}$  as a function of temperature. The circles represent the values measured at 9600 MHz, while the dotted curve gives the values of ref. 3. The solid line represents  $T_{1e}$  at 8600 MHz.

$T \approx 2.2^\circ\text{K}$ , is proportional to  $\exp(-34.0/T)$ , while now a phonon bottlenecked direct process is observed at the lowest temperatures. In crystals containing different amounts of Ce the spin-bath relaxation rate could be fitted by the expression

$$T_{1b}^{-1} = A \left[ \coth\left(\frac{\hbar\omega_e}{2kT}\right) \right]^2 + 2.7 \times 10^9 \exp\left(-\frac{34.0}{T}\right) \quad (\text{III.20})$$

in a field  $H_0 = 3600 \text{ Oe}^{10}$ . The coefficient  $A$  is inversely proportional to the Ce concentration and to the crystal size. For Ce concentrations of a few percent  $A$  is of order unity.

### III-2.3. Pr in LaMN

The only isotope present is  $^{141}\text{Pr}$  ( $I=5/2$ ). The ground state is

a non-Kramers doublet, and the  $g$ -values are  $g_{//} = 1.55$  and  $g_{\perp} = 0$ . The spectrum consists of six equally strong h.f.s. lines. The next higher level is a singlet at  $\Delta/k = 54.6^{\circ}\text{K}$ , which is just below the Debye temperature.

The spin-bath relaxation times  $T_{1b}$  have been measured in the temperature region from  $1.3^{\circ}\text{K}$  to  $4.2^{\circ}\text{K}$ <sup>3</sup>). They can be described by the expression

$$T_{1b}^{-1} = A \left[ \coth \left( \frac{\pi\omega_e}{2kT} \right) \right]^2 + 2.35 T^7 + 4.6 \times 10^{10} \exp \left( - \frac{54.6}{T} \right) \quad (\text{III.21})$$

The  $T^7$  dependence for the Raman process is expected from the fact that the ground state is a non-Kramers doublet. The Orbach term is dominant at the highest temperatures.

The temperature dependence of the first term again indicates that a phonon bottleneck is present. This is confirmed, just as in the case of Ce, by the observation that  $A$  depends on concentration and crystal dimensions. A theoretical estimate of the direct relaxation rate yields  $T_{1d}^{-1} \approx 10^5 T$ . The bottleneck coefficient  $\sigma$  is then of the order of  $10^3$ , so that the observed value of  $T_{1b}^{-1}$  at the lower temperatures is of the order of  $10^2 \text{ sec}^{-1}$ .

### III-3. Results on proton spin-lattice relaxation times

#### III-3.1. Proton spin-lattice relaxation in $(\text{La,Nd})\text{Mn}$

In single crystals of  $\text{LaMn}$  containing 0.5, 1.0, 2.0, 5.0 and 10% Nd the proton relaxation times have been measured in the temperature region from  $1.5^{\circ}\text{K}$  to  $4.0^{\circ}\text{K}$  in an external field  $H_0 \approx 2500 \text{ Oe}$ . The results are shown in fig. III.5 as a function of temperature for the various crystals. The behaviour of  $T_{1n}$  with temperature is roughly the same as that of the electron spin-lattice relaxation time  $T_{1e}$ , given in fig. III.4; a closer examination shows however, that for all crystals the temperature dependence of  $T_{1n}$  is slightly weaker than that of  $T_{1e}$ . This is probably due to the presence of unknown impurities in the crystal. This suggestion is confirmed by fig. III.6, where  $T_{1n}$  is plotted versus the Nd concentration  $c$ . This figure shows that for  $T = 1.5^{\circ}\text{K}$   $T_{1n}$  is independent of the Nd concentration if this concentration is less than  $\sim 1\%$ . At  $T = 2.5^{\circ}\text{K}$  the same behaviour is found for  $c < 0.5\%$ . At higher temperatures this effect is not observed, and then  $T_{1n}$  is approximately proportional to  $1/c$  for Nd concentrations below 2%.

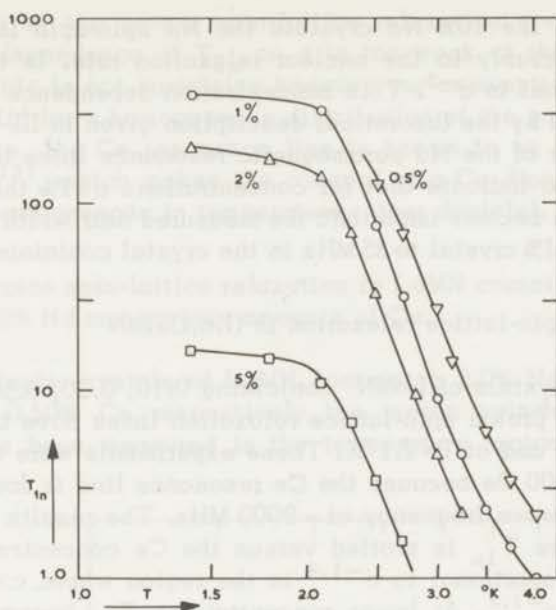


Fig. III.5. Proton spin-lattice relaxation time  $T_{1n}$  as a function of temperature for several Nd concentrations in the crystal.

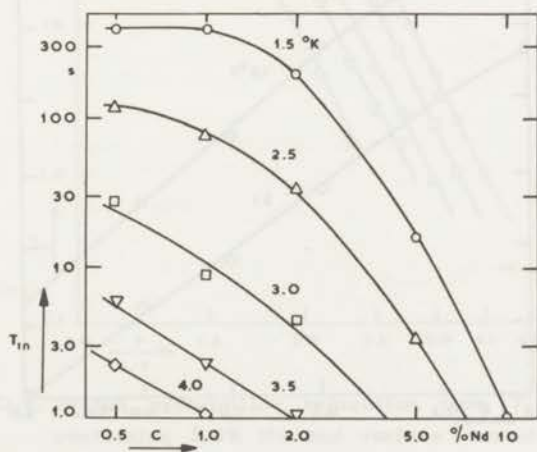


Fig. III.6. Proton spin-lattice relaxation time  $T_{1n}$  as a function of the Nd concentration in the crystal for several temperatures.

For the 5% and the 10% Nd crystals the Nd spin-spin interactions contribute appreciably to the nuclear relaxation rate. In this region  $T_{1n}$  is proportional to  $c^{-3}$ . This concentration dependence is exactly the one predicted by the theoretical description given in III-1.

The widths of the Nd paramagnetic resonance lines in the various crystals also indicate that for concentrations  $c > 1\%$  the Nd spin-spin interactions become important: the measured half width increases from 9 MHz in the 1% crystal to 35 MHz in the crystal containing 10% Nd.

### III-3.2. Proton spin-lattice relaxation in $(La,Ce)MN$

In single crystals of  $LaMN$  containing 0.10, 0.20, 0.50, 1.0, 2.0 and 5.0% Ce the proton spin-lattice relaxation times have been measured at  $T = 1.5^\circ K$  and at  $T = 2.1^\circ K$ . These experiments were carried out in a field  $H_0 \approx 3600$  Oe because the Ce resonance line is found at this field for a microwave frequency of  $\approx 9000$  MHz. The results are shown in fig. III.7, where  $T_{1n}$  is plotted versus the Ce concentration  $c$ . At  $2.1^\circ K$   $T_{1n}$  is proportional to  $c^{-1.4}$  in the region where  $c > 0.2\%$ , and at  $1.5^\circ K$   $T_{1n} \propto c^{-1.8}$ . At lower concentrations  $T_{1n}$  becomes proportional to  $1/c$ . This behaviour is in qualitative agreement with the

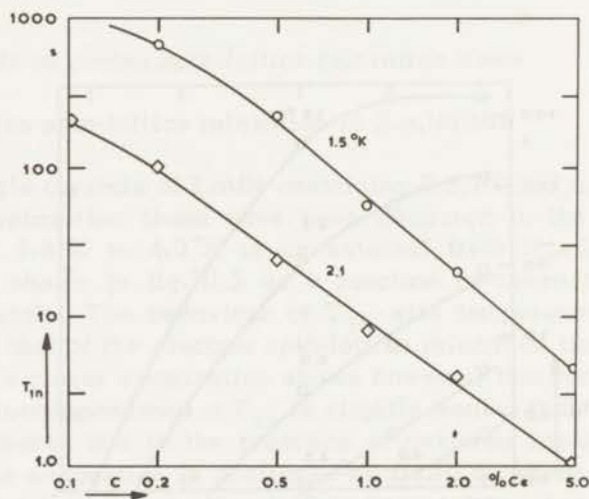


Fig. III.7. Proton spin-lattice relaxation time  $T_{1n}$  as a function of the Ce concentration in the crystal for two temperatures.

description of the proton spin-lattice relaxation given before. However, the dependence of  $T_{1n}$  on  $c$  is too weak at the higher concentrations. This is not surprising because our assumption that  $n_e \omega_L^2 \propto c^3$  is only valid for a homogeneous distribution of the paramagnetic ions. Furthermore, the Ce resonance line is known to be inhomogeneously broadened<sup>13)</sup>, which makes the concept of a Ce dipole-dipole system which is homogeneous in temperature rather doubtful.

### III-3.3. Proton spin-lattice relaxation in LaMN containing 2.0% Nd and various amounts of Ce

In single crystals of LaMN, containing 2.0% Nd and 0.02, 0.10, 0.20 and 0.50% Ce respectively, the proton spin-lattice relaxation times have been measured in the temperature region from 1.25°K to

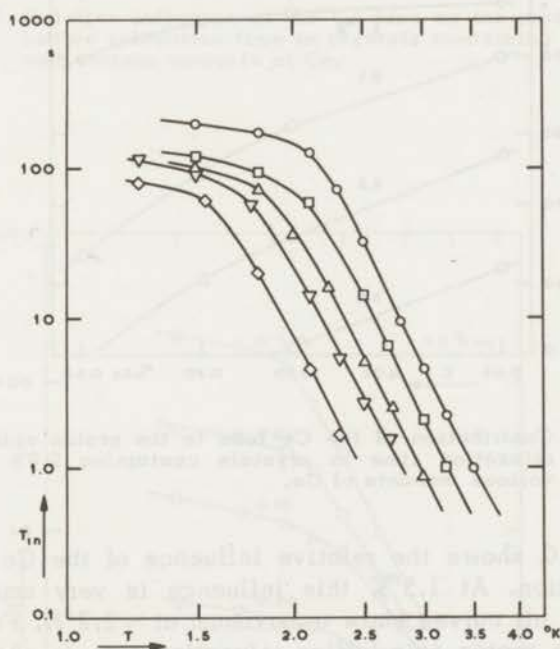


Fig. III.8. Proton spin-lattice relaxation time  $T_{1n}$  in crystals containing 2.0% Nd and various amounts of Ce as a function of temperature.

- |              |              |
|--------------|--------------|
| ○ — 0% Ce    | ▽ — 0.20% Ce |
| □ — 0.02% Ce | ◇ — 0.50% Ce |
| △ — 0.10% Ce |              |

3.5°K in an external field  $H_0 \approx 2500$  Oe. In fig.III.8  $T_{1n}$  is plotted versus  $T$  for the various crystals. The upper curve represents  $T_{1n}$  in a pure 2.0% Nd crystal. The results show that the proton relaxation times are shortened considerably by the addition of Ce, especially at temperatures above 2°K. The contribution of the Ce ions to the proton relaxation rate  $(T_{1n}'')^{-1}$  can be calculated by subtracting the contribution of the Nd spins  $(T_{1n}')^{-1}$  given by the upper curve, from the total observed relaxation rate. In fig.III.9  $T_{1n}''$  is shown as a function of the Ce concentration  $c$ . For the smallest concentrations  $T_{1n}''$  is proportional to  $c$ , except at 1.5°K where the influence of unknown impurities becomes apparent, just as in the case of Nd. The stronger dependence on  $c$  for higher concentrations mentioned already in the preceding section, is observed also in this case.

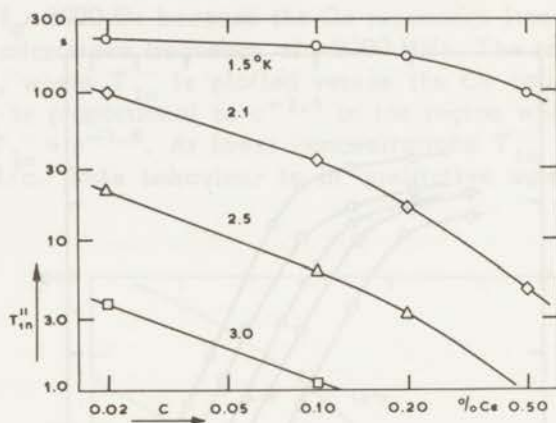


Fig. III.9. Contribution of the Ce ions to the proton spin-lattice relaxation time in crystals containing 2.0% Nd and various amounts of Ce.

Fig.III.10 shows the relative influence of the Ce ions on the proton relaxation. At 1.5°K this influence is very small even for 0.50% Ce, but all curves show a maximum at  $\sim 2.2^\circ\text{K}$ . For the 0.50% Ce crystal the proton spin-lattice relaxation time is shortened by a factor of about 30 in the temperature region from 2.0°K to 3.0°K.

#### III-3.4. Proton spin-lattice relaxation in LaMN containing 2.0% Nd and various amounts of Pr

In single crystals of LaMN containing 2.0% Nd and 0.02, 0.10

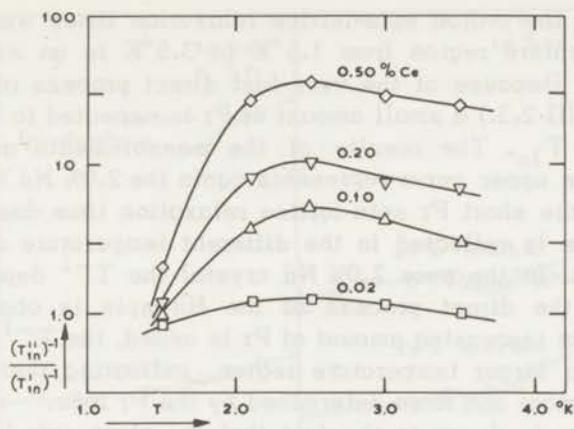


Fig. III.10. Relative influence of the Ce ions on the proton spin-lattice relaxation time in crystals containing 2.0% Nd and various amounts of Ce.

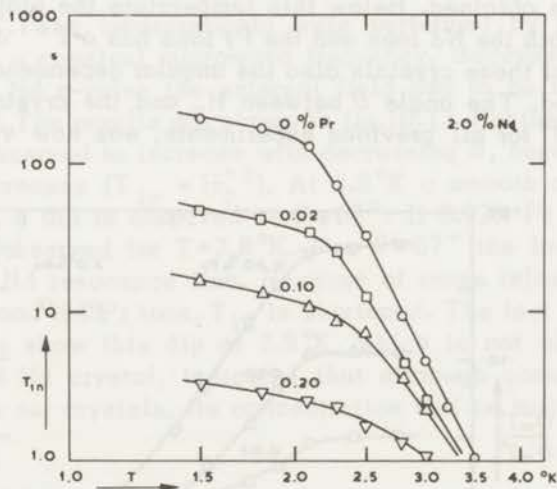


Fig. III.11. Proton spin-lattice relaxation time  $T_{ln}$  in crystals containing 2.0% Nd and various amounts of Pr as a function of temperature.

and 0.20% Pr the proton spin-lattice relaxation times were measured in the temperature region from 1.5°K to 3.5°K in an external field  $H_0 \approx 2500$  Oe. Because of the very fast direct process of the Pr ion in LaMN (cf. III-2.3.) a small amount of Pr is expected to have a large influence on  $T_{1n}$ . The results of the measurements are shown in fig. III.11. The upper curve represents again the 2.0% Nd crystal. The influence of the short Pr spin-lattice relaxation time due to the fast direct process is reflected in the different temperature dependences of the curves. In the pure 2.0% Nd crystal the  $T^{-1}$  dependence expected from the direct process of the Nd spin is observed below  $T=2.0$ °K. If an increasing amount of Pr is added, the  $T^{-1}$  dependence is found in a larger temperature region, indicating that the proton relaxation is more and more determined by the Pr ions.

Attention is drawn to the fact that the short spin-lattice relaxation time of the Pr ion is based on a theoretical estimate. A direct observation is impossible because of the occurrence of a phonon bottleneck as discussed in III-2.3. Our proton relaxation time measurements show unambiguously that a fast direct process is indeed present.

The relative influence of the Pr ions calculated in the way indicated before is shown in fig. III.12. The Pr influence increases rapidly with decreasing temperature, down to 2.1°K, where a constant value is obtained. Below this temperature the proton relaxation time due to both the Nd ions and the Pr ions has a  $T^{-1}$  dependence.

In two of these crystals also the angular dependence of  $T_{1n}$  has been measured. The angle  $\theta$  between  $H_0$  and the crystalline  $z$  axis, which was 90° for all previous experiments, was now varied between

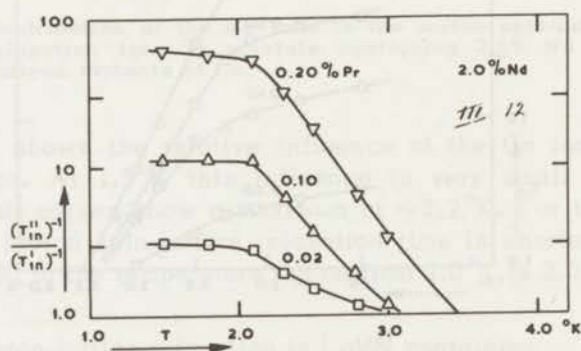


Fig. III.12. Relative influence of the Pr ions on the proton spin-lattice relaxation time in crystals containing 2.0% Nd and various amounts of Pr.

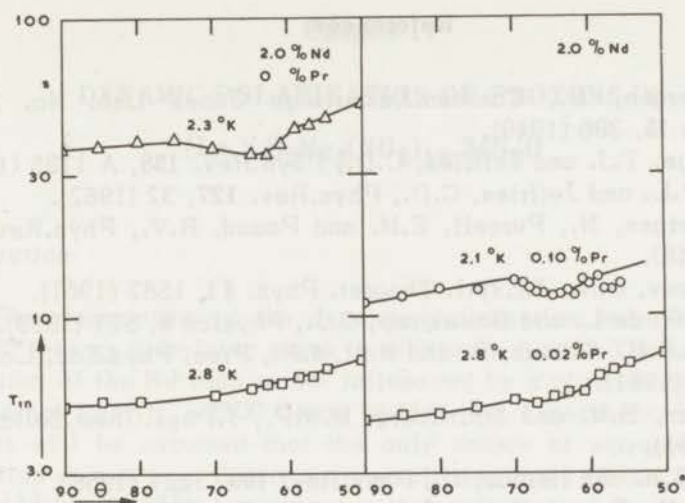


Fig. III.13. Proton spin-lattice relaxation time  $T_{1n}$  in crystals containing 2.0% Nd and various amounts of Pr as a function on the angle  $\theta$ . The figure on the left shows  $T_{1n}$  in a pure 2.0% Nd crystal; while the right hand side shows the influence of small amounts of Pr.

$90^\circ$  and  $50^\circ$ . The measurements were performed by polarizing the protons with a constant microwave frequency. Because of the anisotropy of the Nd g-value the external field had to be increased with decreasing  $\theta$ . The results are shown in fig.III.13. For the pure Nd crystal,  $T_{1n}$  is observed to increase with decreasing  $\theta$ , because the external field increases ( $T_{1n} \propto H_0^{+2}$ ). At  $2.8^\circ\text{K}$  a smooth curve is found, but at  $2.3^\circ\text{K}$  a dip is observed at  $\theta \approx 67^\circ$ . If 0.02% Pr is added, this dip is also observed for  $T=2.8^\circ\text{K}$ . For  $\theta=67^\circ$  the low field Pr line crosses the Nd resonance line. Because of cross relaxation between the Nd ions and the Pr ions,  $T_{1n}$  is shortened. The fact that 0.02% Pr is enough to show this dip at  $2.8^\circ\text{K}$ , which is not observed in the "pure" 2.0% Nd crystal, indicates that although some unwanted Pr is present in our crystals, its concentration will be much smaller than 0.02% Pr.

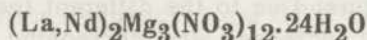
In this chapter only those data on  $T_{1n}$  are discussed which are necessary to make possible a quantitative comparison between the experimental results of the following chapters and the theoretical predictions. A more detailed analysis of the proton spin-lattice relaxation process in various crystals will be given in a forthcoming article.

## References

1. Bloembergen, N., Commun.Kamerlingh Onnes Lab. No. 277b, Physica **15**, 386 (1949).
2. Schmutge, T.J. and Jeffries, C.D., Phys.Rev. **138**, A 1785 (1965).
3. Scott, P.L. and Jeffries, C.D., Phys.Rev. **127**, 32 (1962).
4. Bloembergen, N., Purcell, E.M. and Pound, R.V., Phys.Rev. **73**, 679 (1948).
5. Provotorov, B.N., J.Exptl. Theoret. Phys. **41**, 1582 (1961).
6. Kronig, R. de L. and Bouwkamp, C.J., Physica **5**, 521 (1938).
7. Finn, C.P.B., Orbach, R. and Wolf, W.P., Proc. Phys.Soc.(London) **77**, 261 (1961).
8. Faughnan, B.W. and Strandberg, M.W.P., J.Phys.Chem.Solids **19**, 155 (1961).
9. Dieke, G.H. and Heroux, L., Phys.Rev. **103**, 1227 (1956).
10. Ruby, R.H., Benoit, H. and Jeffries, C.D., Phys.Rev. **127**, 51(1962).
11. Larson, G.H. and Jeffries, C.D., Phys.Rev. **141**, 461 (1966).
12. Lubbers, J., Thesis, Leiden (1967).
13. Abragam, A. and Borghini, M., Progr. in Low Temp. Phys. Vol.IV Ed.C.J. Gorter (North Holland Publ.Co, A'dam, 1964).

## Chapter IV

## DYNAMIC POLARIZATION OF PROTONS IN

*Introduction*

The description of the dynamic polarization process in LaMN with Nd ions as polarizing spins is relatively simple. The spin-lattice relaxation of the Nd ions is not influenced by a phonon bottleneck in an external field  $H_0 \approx 2500$  Oe as used in our experiments<sup>1)</sup>. Furthermore it will be assumed that the only source of extraneous proton relaxation comes from the hyperfine splitting lines of the uneven isotopes  $^{143}\text{Nd}$  and  $^{145}\text{Nd}$ , which give a contribution of about 20% to the nuclear relaxation rate. So the only quantities that are necessary to calculate the maximum obtainable polarization factor from the spin temperature theory given in I-3 are: the Nd resonance linewidth  $\omega_L$ , the irradiation frequency  $\Delta = \omega_e - \omega$  and the factor  $f = NT_{1e}/T_{1n}$ . The maximum obtainable polarization factor is then given by (I.63)

$$E = \frac{\beta}{\beta_L} = \frac{\omega_e \Delta}{\Delta^2 + 2\omega_L^2 + f\omega_n^2} \quad (\text{IV.1})$$

For intermediate power levels the polarization factor is found from the steady state solutions of (I.65)-(I.70). The time-dependent solutions of these equations can also be calculated to yield the response time of the proton spin system to a sudden increase of the microwave power, the polarization time  $\tau_3$ .

In IV-1 we will give the experimental results for the polarization factor  $E$  and for the polarization time  $\tau_3$  in single crystals of LaMN containing 0.5, 1.0, 2.0, 5.0 and 10% Nd<sup>2)</sup>. In IV-2 a comparison is made between these experimental data and the values of  $E$  and  $\tau_3$  calculated from (IV.1) and (I.65)-(I.70).

*IV-1. Experimental results**a. The leakage factor  $f$* 

The factor  $f = NT_{1e}/T_{1n}$  can be calculated from the Nd and the proton spin-lattice relaxation times given in chapter III, and from the

Nd concentration in the crystals, which is about 20% of that of the solution<sup>3)</sup>.

The values of  $f$  for the various crystals are shown in fig.IV.1 as a function of temperature. Due to the different temperature dependencies of  $T_{1e}$  and  $T_{1n}$   $f$  increases with decreasing temperature. Below 2.1°K, where both  $T_{1e}$  and  $T_{1n}$  obey approximately a  $T^{-1}$ -law,  $f$  tends to a constant value. From these data it can be expected on the basis of (IV.1) that the maximum obtainable enhancement factor in the liquid helium temperature range will be found at 4.2°K for all crystals, and that this enhancement will decrease with decreasing temperature<sup>4)</sup>.

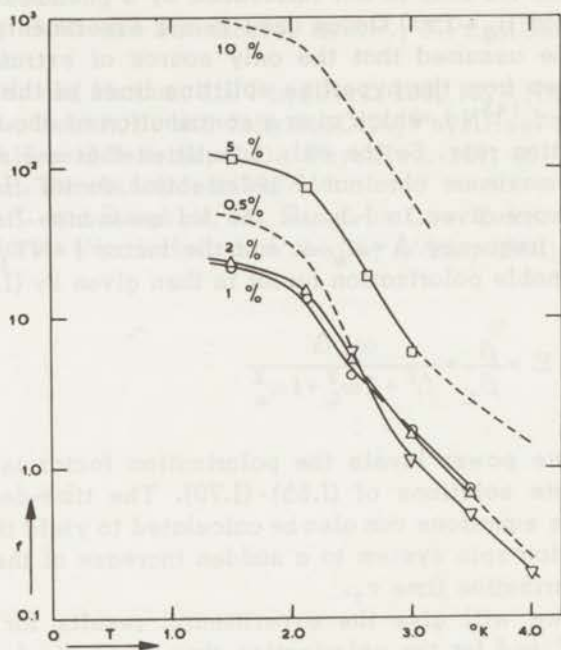


Fig. IV.1. Factor  $f = NT_{1e}/T_{1n}$  as a function of temperature for various Nd concentrations in the crystal.

In performing the experiments it turned out to be impossible to obtain the maximum enhancement factor at temperatures above  $T = 2.5$ °K. This is due to the fact that the maximum available microwave power in the cavity (200 mW) was not sufficient to saturate the forbidden transition completely. At 3.0°K and 3.5°K however the maximum obtainable enhancements could be extrapolated from the values found

at 0.2, 2.0, 20 and 200 mW cavity power. In the discussion the polarization factor  $E$  at a microwave power of 2.0 mW will be denoted by  $E_{2.0}$ , and the maximum of  $E_{2.0}$  as a function of  $\Delta$  by  $E_{2.0}^{max}$ , the extrapolated value defined above is denoted by  $E^{max}$ ; the corresponding values of the irradiation frequency  $\Delta$  are  $\Delta_{2.0}^{max}$  and  $\Delta^{max}$ .

b. 0.50% Nd

In the single crystal of LaMN with 0.50% Nd the polarization factor could only be measured in the temperature range from 2.5°K to 4.0°K because of the long proton relaxation times at lower temperatures. The behaviour of the enhancement factor at the maximum available power  $E_{200}$  is shown in fig.IV.2 as a function of  $\Delta$  for the temperatures 2.5, 3.0, 3.5 and 4.0°K. The curves for  $E_{200}$  at 4.0°K and 3.5°K are far from their maximum values; this is due to insufficient microwave power. The sharp drop in the enhancement factor  $E_{200}^{max}$  from 230 at 3.0°K to 80 at 2.5°K is expected from the increase of  $f$  (cf.fig. IV.1). Fig.IV.2 also shows that  $\Delta_{200}^{max}$  increases from 13 MHz at 4.0°K to 17 MHz at 2.5°K.

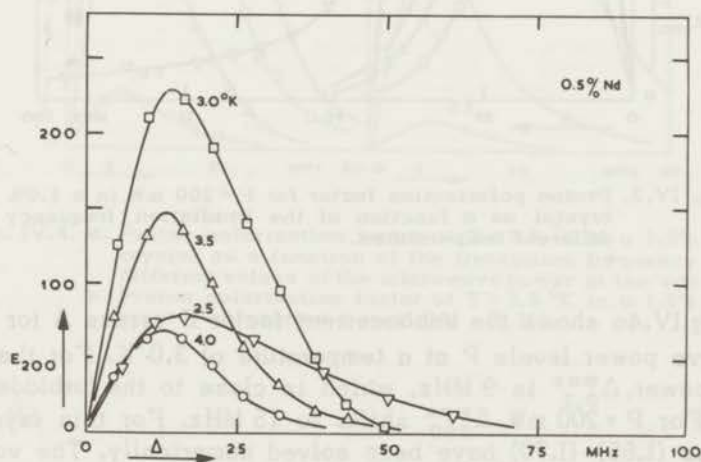


Fig. IV.2. Proton polarization factor for  $P = 200$  mW in a 0.5% Nd crystal as a function of the irradiation frequency for different temperatures.

c. 1.0% Nd

Measurements of the polarization factor were performed again

only between 2.5°K and 4.0°K. In this temperature region the values of  $f$  are slightly larger than in the 0.50% Nd crystal, and the corresponding values of  $E_{200}^{max}$  are indeed smaller than those observed in the preceding crystal.  $\Delta_{200}^{max}$  increases from 13 MHz at 4.0°K to 21 MHz at 2.5°K.

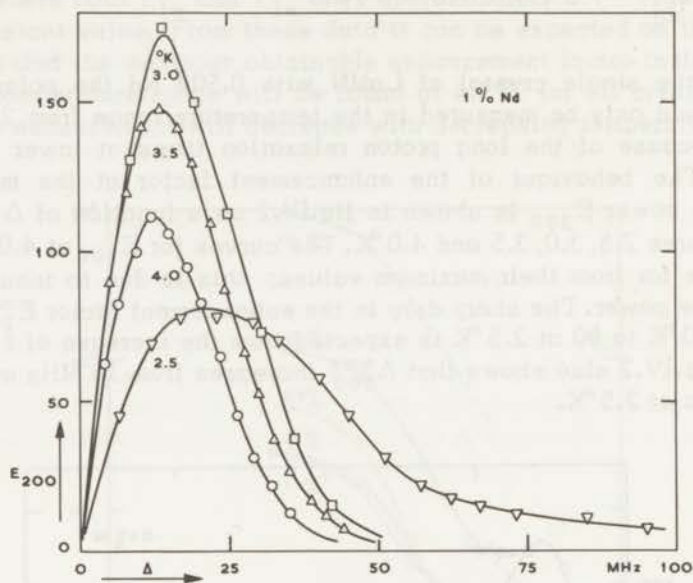


Fig. IV.3. Proton polarization factor for  $P = 200$  mW in a 1.0% Nd crystal as a function of the irradiation frequency for different temperatures.

Fig. IV.4a shows the enhancement factor  $E$  versus  $\Delta$  for various microwave power levels  $P$  at a temperature of 3.0°K. For the lowest cavity power,  $\Delta_{0.2}^{max}$  is 9 MHz, which is close to the forbidden transition. For  $P = 200$  mW,  $\Delta_{200}^{max}$  shifts to 15 MHz. For this crystal the equations (I.65)-(I.70) have been solved numerically. The values of the measured parameters used in these calculations are listed in table IV.I. It has been assumed that all three resonance lines  $G_0$ ,  $G^+$  and  $G^-$  have a Lorentzian shape with a half width equal to the measured value  $\omega_L = 9.0$  MHz. The results are shown in fig. IV.4b. A comparison with fig. IV.4a will be made in IV.2c.

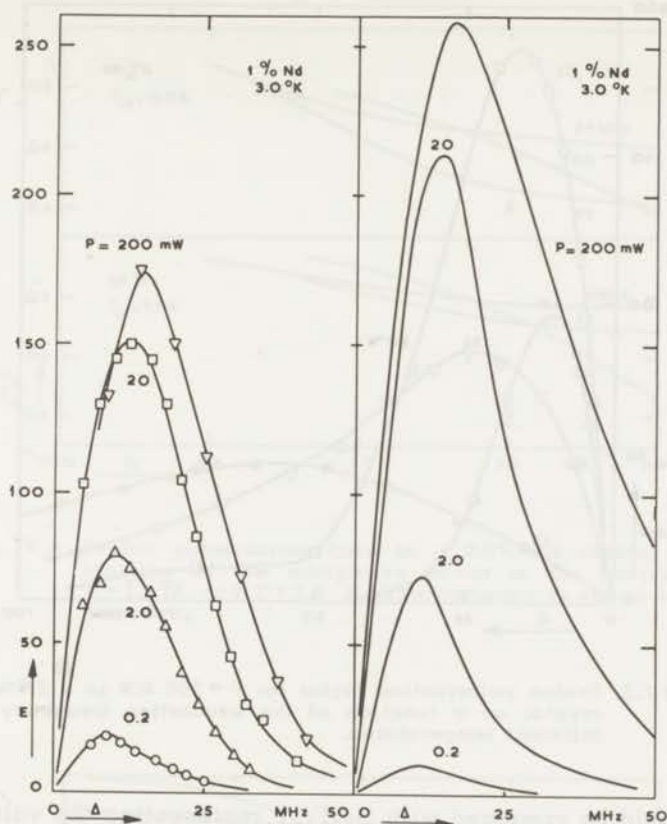


Fig. IV.4. a. Proton polarization factor at  $T = 3.0^{\circ}\text{K}$  in a 1.0% Nd crystal as a function of the irradiation frequency for different values of the microwave power in the cavity.  
 b. Proton polarization factor at  $T = 3.0^{\circ}\text{K}$  in a 1.0% Nd crystal calculated from (I.65) - (I.70).

#### d. 2.0% Nd

The linewidth  $\omega_L$  is equal to that in the 1.0% Nd crystal, and the factor  $f$  has also practically the same value at corresponding temperatures. The enhancement factors as shown in fig. IV.5 are in fact equal to those observed in the preceding crystal. At the lowest temperature  $E_{200}^{\max}$  is only 47, while at this temperature  $\Delta_{200}^{\max}$  has increased to 60 MHz.

Also the nuclear polarization times  $\tau_3$  have been determined in this crystal at  $T = 2.1^{\circ}\text{K}$  and at  $T = 2.8^{\circ}\text{K}$ . Fig. IV.6 shows the results,

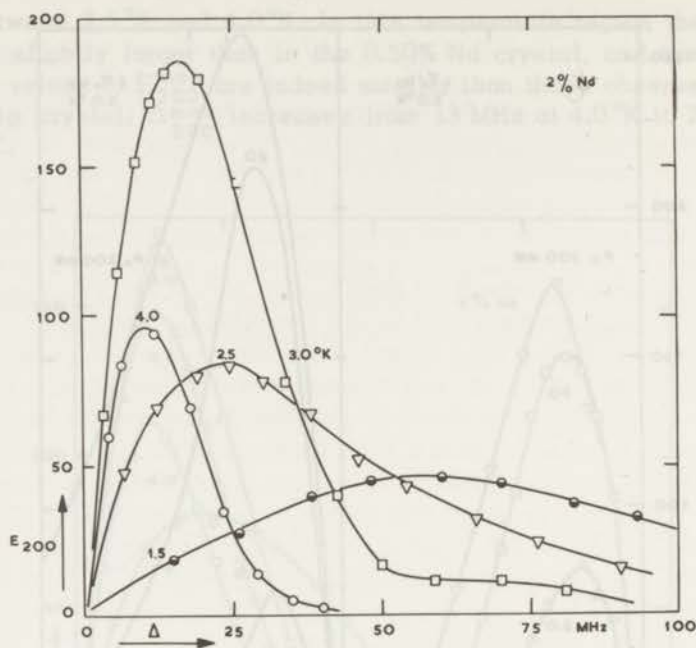


Fig. IV.5. Proton polarization factor for  $P = 200$  mW in a 2.0% Nd crystal as a function of the irradiation frequency for different temperatures.

which should be compared with fig. IV.7 representing the values of  $\tau_3$  calculated from (I.65) - (I.70). At 2.8 °K the agreement as to the dependence of  $\tau_3$  on  $\Delta$  is good, as can be seen from the behaviour of the curve for  $\Delta = 30$  MHz with respect to those for  $\Delta = 4$  MHz and  $\Delta = 15$  MHz. Also the dependence of  $\tau_3$  on microwave power is in agreement with the calculations, although all measured values of  $\tau_3$  are slightly too large. At  $T = 2.1$  °K the equations could only be solved for  $\Delta = 10$  MHz and  $\Delta = 100$  MHz. The calculated dependence of  $\tau_3$  on microwave power is clearly different from the observed behaviour at this temperature.

e. 5.0% Nd

The observed polarization factors in this crystal are considerably smaller than the corresponding values found in the crystals with a lower Nd concentration, as is to be expected from the increase of

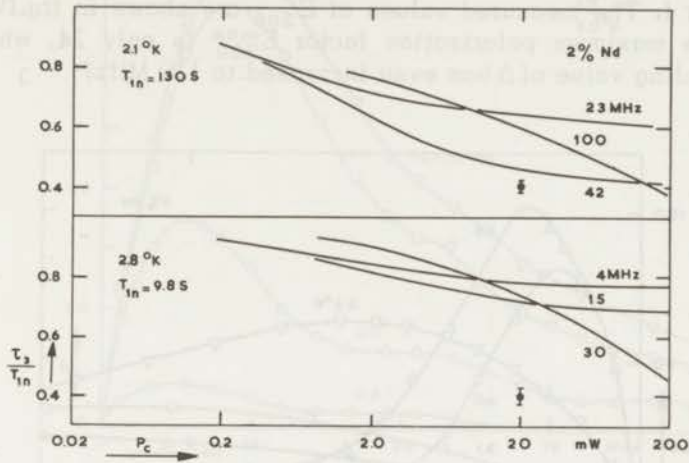


Fig. IV.6. Proton polarization time in a 2.0% Nd crystal as a function of the microwave power in the cavity, for  $T = 2.1^{\circ}\text{K}$  and  $T = 2.8^{\circ}\text{K}$ . The accuracy is shown by the error bar.

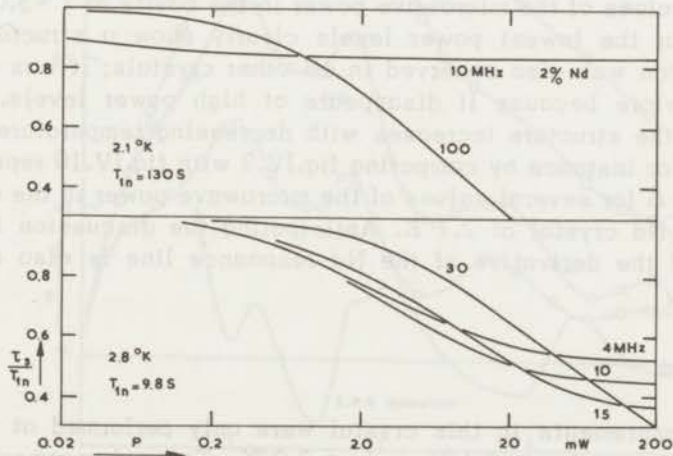


Fig. IV.7. Proton polarization time in a 2.0% Nd crystal as a function of the microwave power in the cavity for  $T = 2.1^{\circ}\text{K}$  and  $T = 2.8^{\circ}\text{K}$ , calculated from (I.65) - (I.70).

the factor  $f$ . The measured values of  $E_{200}$  are shown in fig.IV.8. At  $1.5^\circ\text{K}$  the maximum polarization factor  $E_{200}^{\text{max}}$  is only 24, while the corresponding value of  $\Delta$  has even increased to 110 MHz.

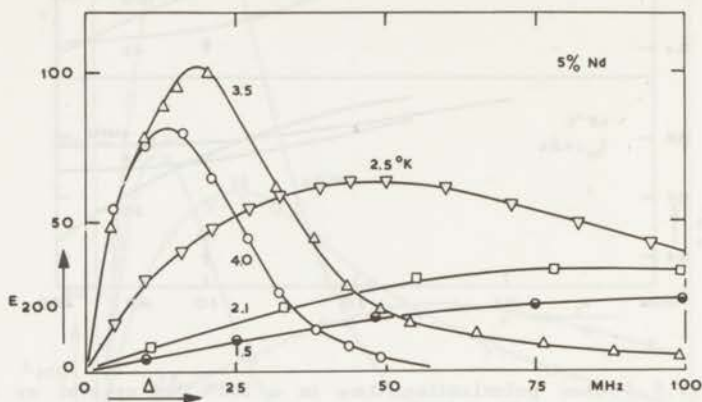


Fig. IV.8. Proton polarization factor for  $P = 200$  mW in a 5.0% Nd crystal as a function of the irradiation frequency for different temperatures.

In fig.IV.9 the enhancement factor  $E$  is plotted versus  $\Delta$  for several values of the microwave power in the cavity at  $T = 3.0^\circ\text{K}$ . The curves for the lowest power levels clearly show a structure. This phenomenon was also observed in all other crystals; it was not mentioned before because it disappears at high power levels. For all crystals the structure increases with decreasing temperature, as can be seen for instance by comparing fig.IV.9 with fig.IV.10 representing  $E$  versus  $\Delta$  for several values of the microwave power in the cavity in the 5.0% Nd crystal at  $2.1^\circ\text{K}$ . Anticipating the discussion in IV-2.e a part of the derivative of the Nd resonance line is also drawn in fig.IV.10.

#### f. 10% Nd

Measurements in this crystal were only performed at two temperatures, namely at  $2.1^\circ\text{K}$  and at  $3.0^\circ\text{K}$ . The enhancement factors were very small,  $E_{200}^{\text{max}} = 4$  and  $E_{200}^{\text{max}} = 8$  respectively, due to the short proton spin-lattice relaxation time;  $T_{1n}$  is of the order of one second at  $2.1^\circ\text{K}$ . The results on  $E_{200}$  as a function of  $\Delta$  are shown in fig.IV.11.

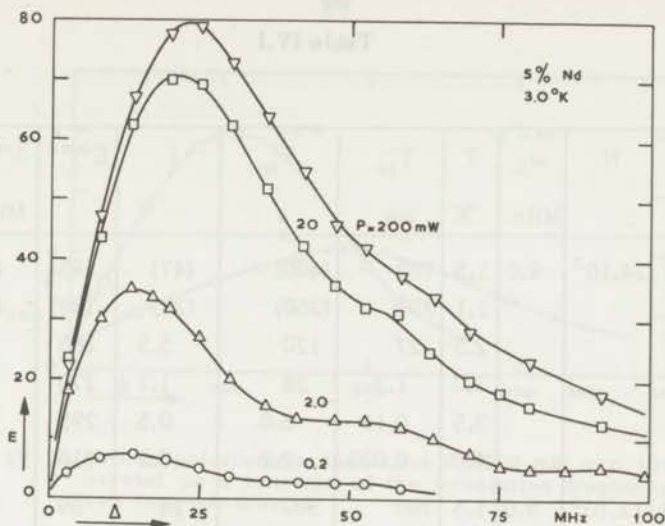


Fig. IV.9. Proton polarization factor at  $T = 3.0^\circ\text{K}$  in a 5.0% Nd crystal as a function of the irradiation frequency for different values of the microwave power in the cavity.

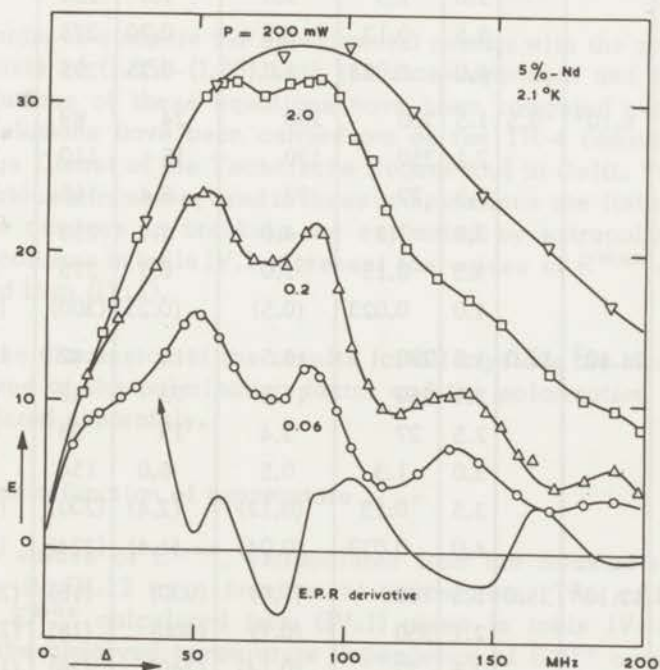


Fig. IV.10. Proton polarization factor at  $T = 2.1^\circ\text{K}$  in a 5.0% Nd crystal as a function of the irradiation frequency for different values of the microwave power in the cavity. Part of the derivative of the electron resonance line is also shown.

Table IV.I

%Nd	N	$\omega_L$	T	$T_{le}$	$T_{ln}$	f	$E^{max}$	$\Delta^{max}$
		MHz	°K	ms	s			MHz
0.5	$24.10^3$	9.0	1.5	780	(400)	(47)	(65)	(66)
			2.1	350	(350)	(24)	(89)	(48)
			2.5	27	120	5.5	165	26
			3.0	1.3	28	1.1	270	16
			3.5	0.13	6.0	0.5	295	14
			4.0	0.023	2.2	0.2	310	13
1.0	$12.10^3$	9.0	1.5	780	390	24	89	48
			2.1	350	320	14	114	38
			2.5	27	78	4.2	187	23
			3.0	1.3	9.0	1.8	238	18
			3.5	0.13	2.3	0.70	275	16
			4.0	0.023	1.0	0.25	295	14.5
2.0	$6.10^3$	9.5	1.5	780	200	24	89	48
			2.1	350	130	15	110	39
			2.5	27	33	5.4	165	26
			3.0	1.3	4.6	1.7	253	18
			3.5	0.13	1.0	0.7	275	16
			4.0	0.023	(0.5)	(0.25)	(300)	(14)
5.0	$24.10^2$	12.0	1.5	780	16.5	114	42	102
			2.1	350	11.5	73	52	82
			2.5	27	3.4	19	98	44
			3.0	1.3	0.5	6.0	154	28
			3.5	0.13	(0.12)	(2.4)	(200)	(21)
			4.0	0.023	(0.04)	(1.4)	(224)	(19)
10	$12.10^2$	35.0	1.5	780	(1.0)	(930)	(15)	(285)
			2.1	350	(0.7)	(600)	(18)	(232)
			2.5	27	(0.14)	(240)	(28)	(154)
			3.0	1.3	(0.025)	(60)	(38)	(89)

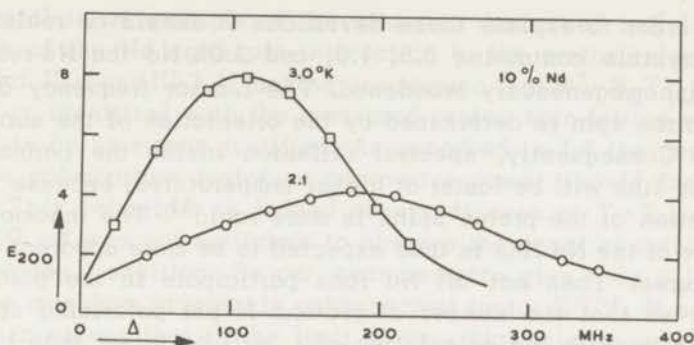


Fig. IV.11. Proton polarization factor for  $P=200$  mW in a 10% Nd crystal as a function of the irradiation frequency for two temperatures.

#### IV-2. Discussion of the experimental results

In order to compare the experimental results with the predictions on the basis of (I.65)-(I.70), both the time-dependent and the steady state solutions of these equations have been computed numerically. The calculations have been carried out on the TR-4 computer of the Wiskundige Dienst of the Technische Hogeschool in Delft. The values of the various parameters used in these computations are listed in table IV.1. The numbers in brackets are estimated by extrapolation. The last two columns in table IV.1 represent the values of  $E^{\max}$  and  $\Delta^{\max}$  calculated from (IV.1).

In the discussion of the results for all crystals the most important features of the polarization factor and the polarization time will be considered separately.

##### a. $E^{\max}$ as a function of temperature

The values of  $E^{\max}$ , extrapolated from the measurements, are plotted in fig.IV.12 as a function of temperature. The solid curves represent  $E^{\max}$  calculated from (IV.1) given in table IV.I. For all crystals the observed temperature dependence of  $E^{\max}$  agrees quite well with the theoretical predictions. Only the absolute values of the observed polarization factors are smaller than the calculated ones; this discrepancy is small for small Nd concentrations, but increases to a factor three in the 10% Nd crystal.

In order to explain these deviations it should be realized that in the crystals containing 0.5, 1.0, and 2.0% Nd the Nd resonance line is inhomogeneously broadened. The Larmor frequency of a certain electron spin is determined by the orientation of the surrounding protons. Consequently, spectral diffusion inside the paramagnetic resonance line will be faster at higher temperatures, because then the reorientation of the proton spins is more rapid<sup>5)</sup>. The inhomogeneous character of the Nd line is thus expected to be more apparent at lower temperatures. Then not all Nd ions participate in the polarization process, so that the number of protons  $N$  per polarizing spin, that should be used in the calculation of  $f$ , will be larger than the value given in table IV.I. As a result the calculated values of  $E^{\max}$  will be smaller than those given in the table. This explains the fact that the deviations between the experimental data and the predictions from (IV.1) are larger at the lower temperatures.

The deviations in the 10% Nd crystal have a different origin. Here the Nd resonance line is homogeneously broadened ( $\omega_L = 35$  MHz), so it should be expected that the values of  $E^{\max}$  calculated from (IV.1) with the  $f$ -values of table IV.I would be in agreement with the experimental data. However, the behaviour of the polarization factor

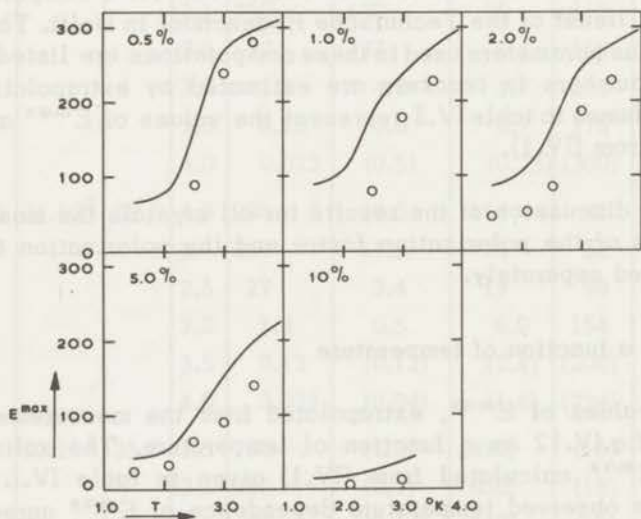


Fig. IV.12. Proton polarization factor for all measured crystals as a function of temperature. The circles represent the values extrapolated from the measurements. The solid lines are the enhancements calculated from (IV.1).

in this crystal is an example of the situation discussed in I-4. The contribution of the Nd spin-spin interaction to the proton relaxation is so large (cf. III-1 and III-3.1), that the assumption that  $W^{\pm} = W_0 T_{1e} / T_{1n}$ , where  $T_{1n}$  is identified with the measured proton spin-lattice relaxation time, is by no means justified. As remarked in I-4 the dependence of the polarization factor on microwave power should then be weakened. This behaviour is indeed observed: even at  $T = 2.1$  °K a power of 200 mW was not sufficient to observe the onset of saturation of the forbidden transition. So our measurements give only a lower limit for the maximum obtainable enhancement factor  $E^{\max}$ . It seems reasonable to expect that in the limit of very high microwave power levels the enhancement factor will be given by (IV.1), but this limit cannot be obtained experimentally.

b.  $\Delta_{200}^{\max}$  as a function of temperature

The values of the irradiation frequencies  $\Delta_{200}^{\max}$  for which the maximum polarization factors  $E_{200}^{\max}$  were obtained are given in fig. IV.13. The drawn curves represent the calculated values of  $\Delta^{\max}$  given in table IV.1. For all crystals a good agreement between theory and experiment is observed over the whole temperature region. The increase of the factor  $f$  as proposed in the preceding paragraph causes a small increase of the calculated values of  $\Delta^{\max}$ . On the other hand the experiments show that a further increase of the microwave power above 200 mW would also result in a small increase of the experimental values of fig. IV.13.

c.  $E$  as a function of microwave power

Figs. IV.4a and b show an example of the calculated and the observed behaviour of  $E$  for various microwave power levels. A good agreement is found, just as in the crystals with other Nd concentrations at temperatures above  $T = 2.5$  °K. Only for large values of  $\Delta$  a serious discrepancy between figs. IV.4a and b is observed. This deviation is simply a consequence of the assumption made in the calculations that the forbidden transitions have a Lorentzian lineshape.

At temperatures below  $T = 2.5$  °K the increase of  $E$  with increasing microwave power is too weak in all crystals. This may be due to the presence of unknown impurities in the crystals as discussed in I-3.2b. However, it is more probable that the inhomogeneous broadening of the Nd resonance line as mentioned in IV-2.a is the cause of these deviations: at lower temperatures, where the spectral diffusion

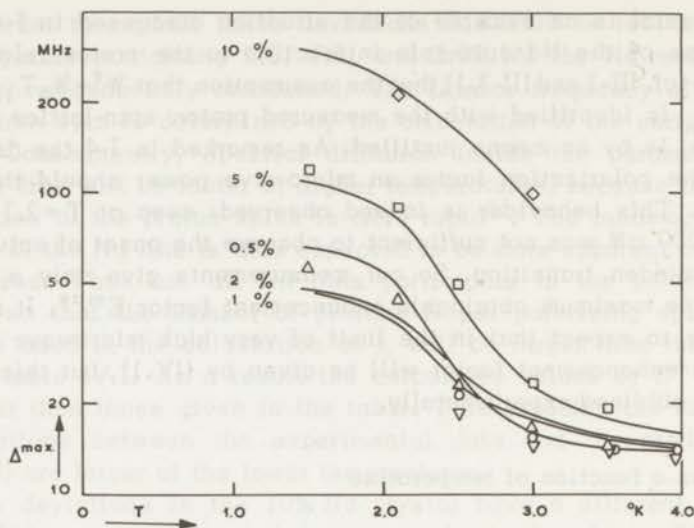


Fig. IV.13. Microwave irradiation frequencies for which the maximum polarization factor is obtained, plotted as a function of temperature. The solid lines are the values of  $\Delta^{\max}$  calculated from (IV.1).

- |                       |                     |
|-----------------------|---------------------|
| $\nabla$ - 0.5% Nd    | $\square$ - 5.0% Nd |
| $\circ$ - 1.0% Nd     | $\diamond$ - 10% Nd |
| $\triangle$ - 2.0% Nd |                     |

inside the electron resonance line is slow, not all Nd ions take part in the polarization process. Consequently the factor  $f$  is larger than the value given in table IV.I, so that the calculated polarization factor  $E^{\max}$  is too large at these low temperatures (cf. IV-2.a). Furthermore all remaining Nd spins will behave as paramagnetic impurities, which tend to relax the polarized protons. In I-3.2.b it was shown that the dependence of  $E$  on microwave power is weakened if such impurities are present in the crystal. This behaviour is indeed observed for temperatures below  $T = 2.5^\circ\text{K}$ .

d.  $\tau_3$  as a function of microwave power and frequency

The observed dependence of the polarization time  $\tau_3$  on microwave power and frequency at  $T = 2.8^\circ\text{K}$  is in good agreement with the calculations on the basis of (I.65) - (I.70), as shown in figs. IV.6 and 7.

At  $T = 2.1^\circ\text{K}$  these equations do not yield proper solutions for

the polarization time for  $15 \text{ MHz} < \Delta < 100 \text{ MHz}$ . This is due to the fact that it was assumed in the computations that  $W^{\pm} = W_0 T_{1e} / T_{1n}$ . In view of the arguments given in IV-2.a and c this value of  $W^{\pm}$  is too large, firstly because  $T_{1n}$  is also determined by Nd spin-spin interactions, secondly because at low temperatures not all Nd ions participate in the polarization, while they do contribute to the relaxation rate  $(T_{1n})^{-1}$ . If  $W^{\pm}$  would be calculated in the correct way, a smaller value would be found. If this smaller value is inserted in the equations (I.65) - (I.70) a polarization time can be calculated for all values of  $\Delta$ . The time constants  $\tau_3$  computed in this way increase, which is in better agreement with the experimental data.

e. The structure in the curves of E as a function of  $\Delta$

The curves of E versus  $\Delta$  show a pronounced structure especially at low temperatures, while at  $T = 4.0^\circ \text{K}$  in none of the crystals any structure is observed. According to the description given in I-3.2 for the case that the electron resonance linewidth is of the same order of magnitude as the nuclear Larmor frequency, the polarization should display a structure analogous to that of the derivative of the electron line for low rf power levels. At high power levels a smooth dispersion-like shape should be observed, because then all electron spins have the same temperature in the rotating frame. This predicted behaviour is indeed observed, but only at low temperatures.

As was already mentioned in IV-2.a and c, the reorientation of the protons surrounding an electron spin is more rapid at higher temperatures. The spectral diffusion inside the electron resonance line is then faster, so that saturation of one of the small satellites will only result in a small cooling factor of all electrons, and the nuclear polarization will be small. Only irradiation of the main resonance line results in an appreciable nuclear enhancement factor.

In the 10% Nd crystal no structure was observed in the E versus  $\Delta$  curves, although the Nd line itself showed a structure like that of the other crystals. This is due to the fact that in this crystal the microwave power necessary to obtain a certain nuclear polarization is much larger than that in other crystals. Because of the homogeneous broadening of the Nd line all electron spins will then have the same temperature in the rotating frame, so that a smooth dispersionlike shape is found.

#### IV-3. Concluding remarks

By varying the concentration of the Nd ions in LaMN single crystals a variation of the factor  $f = NT_{1e}/T_{1n}$  of two orders of magnitude can be obtained in the temperature region from 1.5°K to 4.0°K. The observed values of the polarization factors and the polarization times are compared with the predictions from the theory given in I-3. In most of the crystals a good agreement is found. The relatively small deviations can be explained by assuming that the inhomogeneous character of the Nd resonance line is more apparent at lower temperatures. The behaviour of the polarization time shows that Nd spin-spin interactions contribute to the nuclear relaxation rate.

The large deviations occurring in the 10% Nd crystal indicate however, that the dependence of the enhancement factor on microwave power predicted by the theory of I-3 is not correct. For this high concentration the treatment indicated in I-4 should be used.

The influence of the spin-spin interactions of the paramagnetic ions on the proton relaxation rate  $(T_{1n})^{-1}$  can be treated in exactly the same way as the influence of paramagnetic impurities. In I-3.2 we showed that if these impurities are present the transition probabilities  $W^{\pm}$  should be calculated from  $W^{\pm} = W_0 T_{1e}/T'_{1n}$ , where  $(T'_{1n})^{-1}$  is the part of the nuclear relaxation rate that is due to the polarizing spins only. Consequently more rf power will be required to saturate the forbidden transition, and the numerical solutions of (I.65)-(I.70) show that simultaneously the dependence of the polarization factor on the rf power is weakened. In order to simplify the discussion we will refer to this effect in the following as "extraneous relaxation". Its influence is apparent also in the Ce crystals that will be discussed in the next chapter. In the measurements given in chapter VI this extraneous relaxation is greatly enhanced by adding impurities to the crystals.

No comparison of the experimental data with the predictions from the theory of I-1 was given. However, if fig.IV.4a is compared with fig.I.4 which shows the calculated behaviour of E for different microwave power levels, enormous discrepancies are observed. In none of the crystals a decrease of the polarization factor with increasing power, as expected from fig.I.4, was found. Also the behaviour of  $\tau_3$  as a function of microwave power is in contradiction with that expected from I-1 (cf. fig.I.6).

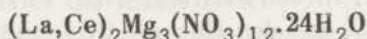
As a conclusion it may be stated that the theory given in I-3 and I-4 is in much better agreement with the experiments performed in these crystals, than the theory based on the rate equations for the populations of the Zeeman levels.

## References

1. Ruby, R.H., Benoit, H. and Jeffries, C.D., Phys.Rev. **127**, 51 (1962).
2. Swanenburg, T.J.B., van den Heuvel, G.M. and Poulis, N.J., Commun. Kamerlingh Onnes Lab. No 355c.; Physica **34**, (1967).
3. Cf. references 5 and 6 of chapter II.
4. Leifson, O.S. and Jeffries, C.D., Phys.Rev. **122**, 1781 (1961).
5. Abragam, A. and Borghini, M., Prog. in Low Temp. Phys. Vol. IV. Ed. C.J. Gorter (North Holland Publ. Co., A'dam 1964).

## Chapter V

## DYNAMIC POLARIZATION OF PROTONS IN

*Introduction*

The polarization process of protons in  $\text{La}_2\text{Mg}_3(\text{NO}_3)_{12}\cdot 24\text{H}_2\text{O}$  containing various amounts of Ce is more complicated than that in the case of  $(\text{La,Nd})\text{MN}$ . Again one single paramagnetic spin species is present, but now the spin-lattice relaxation of this ion is limited by a phonon bottleneck at temperatures below  $T = 2.0$  °K, as was mentioned in III - 2.2<sup>1)</sup>.

For temperatures above 2.0 °K the proton polarization can be described, just as in the case of the Nd salt, by the equations (I.65) - (I.70). At  $T = 1.5$  °K however the existence of a phonon bottleneck should be taken into account, so that also equation (I.81) is necessary for the calculation of the polarization factor. As discussed in I - 3.4 the maximum obtainable enhancement factor is then given by

$$E = \frac{\omega_e \Delta}{\Delta^2 + 2(1 + \sigma)\omega_L^2 + f(1 + \sigma)\omega_n^2} \quad (\text{V.1})$$

where  $\sigma$  is the bottleneck factor. Equation (V.1) shows that the irradiation frequency  $\Delta^{\text{max}}$  for which this expression obtains its maximum value has increased by a factor  $\sqrt{1 + \sigma}$  compared with the case that  $\sigma = 0$  (cf. chapter IV). The maximum value of  $E$  is reduced by the same factor  $\sqrt{1 + \sigma^2}$ .

In order to determine experimentally the influence of the phonon bottleneck on the polarization, measurements have been carried out both at  $T = 2.1$  °K and  $T = 1.5$  °K in single crystals of  $\text{LaMN}$  with 0, 1, 0.2, 0.5, 1.0, 2.0 and 5.0 % Ce<sup>3,4)</sup>. The steady state solutions of (I.65) - (I.70) and (I.81) have been computed numerically, with the bottleneck factor  $\sigma$  as a parameter. The results of these calculations will be compared with the experimental data. Also the polarization time  $\tau_3$  has been calculated for some of the crystals (cf. fig. I.15).

As was shown in chapter III - 3.2 the proton spin-lattice relaxation times are influenced by the Ce spin-spin interaction for Ce concentrations which are larger than 0.5%. Because of this extraneous relaxation the observed dependence of the polarization factor on micro-

wave power will be weaker than that predicted from (I.65) – (I.70) and (I.81). In solving these equations no account was taken of the influence of this spin-spin interaction.

As in the preceding chapter we will give a summary of the measurements of  $E$  and  $\tau_3$  for all crystals, which is followed by a discussion of the most important features.

### V - 1. Experimental results

The relaxation time of the Ce spin which enters into the expression (I.71) for the magnitude of the forbidden transition probability is not equal to the measured spin-bath relaxation time, because of the presence of a phonon bottleneck. In the calculation of the transition probabilities  $W^\pm$  and of the factor  $f$  the spin-phonon relaxation time  $T_{1e}$  should be used. Because this time constant is about two orders of magnitude shorter than that of the Nd ion, while the proton spin-lattice relaxation times are of the same order of magnitude as in the Nd crystals, the factor  $f$  is smaller than unity for the Ce concentrations under consideration, both at  $T=1.5$  °K and at  $T=2.1$  °K.

Another consequence of the fact that for the Ce crystals the ratio  $T_{1e}/T_{1n}$  is much smaller than in the case of Nd is, that at the same microwave power level the saturation factor  $W^\pm T_{1n}$  of the forbidden transition is smaller. Indeed in performing the experiments it turned out to be impossible to obtain the maximum enhancement with the available microwave power of 200 mW. However, at 1.5 °K the onset of saturation could be observed.

#### a. 0.1% Ce

In this crystal the polarization factors were only determined at  $T=2.1$  °K because at lower temperatures the proton spin-lattice relaxation times were too long. In fig. V.1 the polarization factors are plotted as a function of  $\Delta = \omega_e - \omega$  for three values of the microwave power in the cavity. The maximum enhancement factor  $E_{200}^{max} = 66$  is obtained for  $\Delta = 16$  MHz which is close to the forbidden transition ( $\omega_n \approx 15$  MHz in the external field  $H_0 \approx 3600$  Oe).

#### b. 0.2% Ce

For the same reasons as in the preceding crystal the measurements could only be performed at  $T=2.1$  °K. The results are shown in fig. V.2. The factor  $f$  and the Ce resonance linewidth are the same

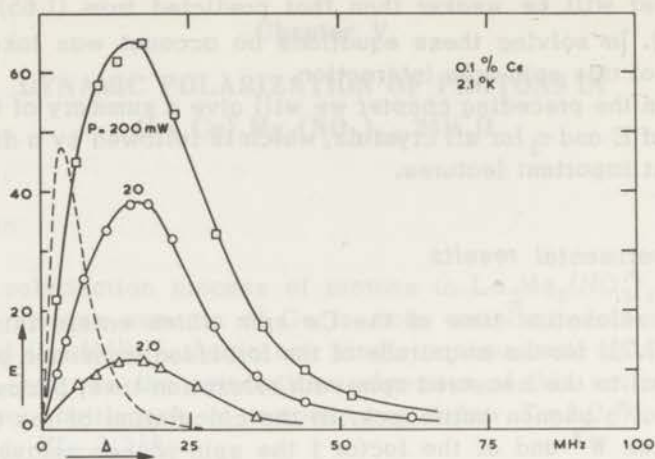


Fig. V.1. Proton polarization factor at  $T=2.1^{\circ}\text{K}$  in a 0.1% Ce crystal as a function of the irradiation frequency for different values of the microwave power in the cavity. The dotted curve is the derivative of the electron resonance line.

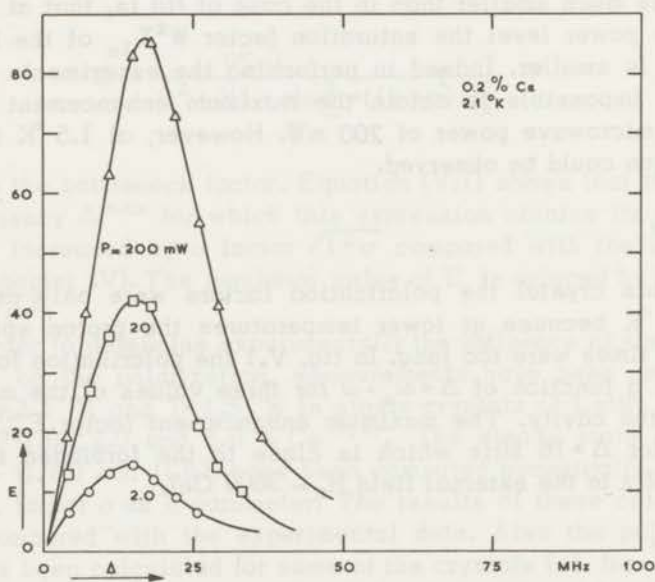


Fig. V.2. Proton polarization factor at  $T=2.1^{\circ}\text{K}$  in a 0.2% Ce crystal as a function of the irradiation frequency for different values of the microwave power in the cavity.

as in the 0.1% crystal, so the polarization factors at corresponding power levels are expected to be equal in the two crystals. However, in the 0.2% Ce crystal the polarization is  $\sim 25\%$  larger than in the 0.1% crystal. This is due to the fact that both will contain approximately the same amount of impurities, which has a relatively larger influence in the 0.1% crystal. The dependence of  $E$  on microwave power will thus be weaker in the most dilute crystal, because of the larger extraneous relaxation.

The proton polarization time  $\tau_3$  was also measured in this crystal, at  $2.1^\circ\text{K}$  for three values of  $\Delta$ . The curves shown in fig. V.3 have been drawn through many experimental points. The average scatter of these data is indicated by the error bar.

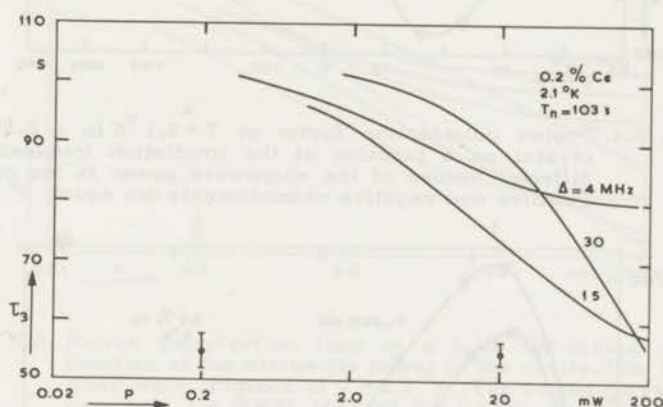


Fig. V.3. Proton polarization time at  $T = 2.1^\circ\text{K}$  in a 0.2% Ce crystal as a function of the microwave power in the cavity for three values of the irradiation frequency. The accuracy is shown by the error bar.

#### c. 0.5% Ce

The proton polarization factors could be measured in this crystal both at  $T = 2.1^\circ\text{K}$  and at  $T = 1.5^\circ\text{K}$ . In fig. V.4 the results obtained at  $2.1^\circ\text{K}$  are plotted versus  $\Delta$  for four values of the microwave power in the cavity. This figure clearly shows the symmetry in the behaviour of the polarization factor for positive and negative values of  $\Delta$ . This symmetry has also been observed in the other Ce crystals, and in those with Nd as polarizing spin (chapter IV).

In fig. V.5 the enhancement factors measured at  $1.5^\circ\text{K}$  are

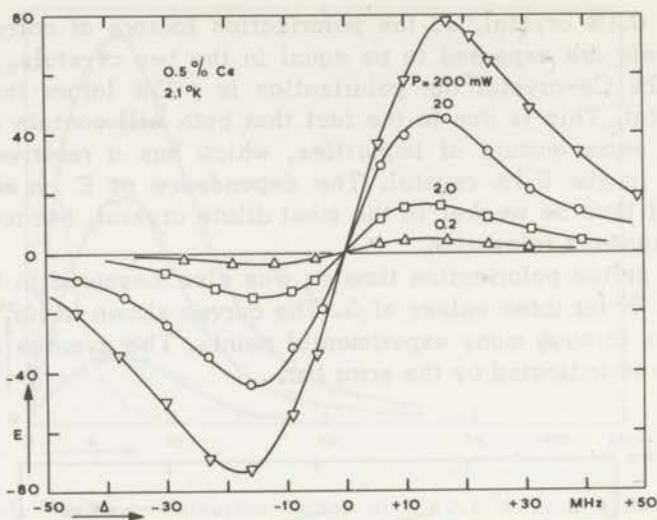


Fig. V.4. Proton polarization factor at  $T=2.1^{\circ}\text{K}$  in a 0.5% Ce crystal as a function of the irradiation frequency for different values of the microwave power in the cavity. Positive and negative enhancements are equal.

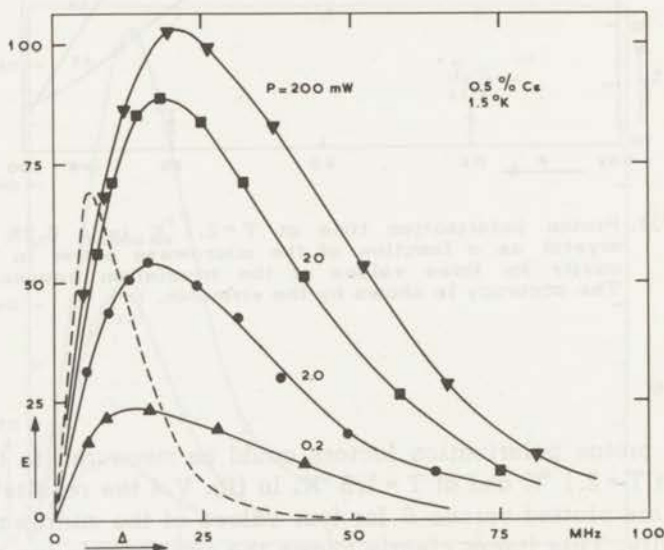


Fig. V.5. Proton polarization factor at  $T=1.5^{\circ}\text{K}$  in a 0.5% Ce crystal as a function of the irradiation frequency for different values of the microwave power in the cavity. The dotted curve is the derivative of the electron resonance line.

plotted versus  $\Delta$ . For a cavity power  $P = 200$  mW the maximum value  $E_{200}^{\max} = 103$  is obtained for  $\Delta_{200}^{\max} = 21$  MHz while the corresponding value at  $2.1^\circ\text{K}$  was  $\Delta_{200}^{\max} = 17$  MHz.

At  $T = 2.1^\circ\text{K}$  the proton polarization time  $\tau_3$  was measured for six different values of the irradiation frequency  $\Delta$  as a function of the microwave power in the cavity. The results are shown in fig. V.6. The decrease of  $\tau_3$  with increasing  $\Delta$  at high power levels is in good agreement with the numerical calculations, an example of which was shown in fig. I.15. However, the absolute values of  $\tau_3$  are too large, while the dependence of  $\tau_3$  on  $P$  is too weak.

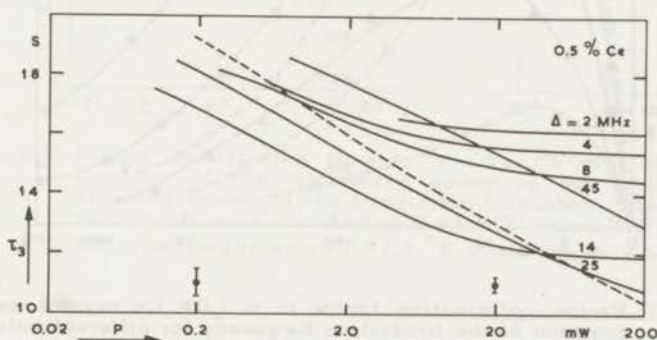


Fig. V.6. Proton polarization time in a 0.5% Ce crystal as a function of the microwave power in the cavity. The solid lines were obtained at  $T = 2.1^\circ\text{K}$ . The dotted curve was measured for  $\Delta = 25$  MHz at  $T = 1.5^\circ\text{K}$ . For this curve the vertical scale is multiplied by a factor 10.

#### d. 1.0% Ce

The measured polarization factors are shown in fig. V.7 for  $T = 2.1^\circ\text{K}$  and  $T = 1.5^\circ\text{K}$ . According to (V.1) the irradiation frequency for which the maximum enhancement is obtained  $\Delta_{200}^{\max}$  should increase when the bottleneck factor  $\sigma$  increases. This is clearly demonstrated by a comparison of figs. V.5 and V.7;  $\Delta_{200}^{\max}$  is shifted from 21 MHz to 31 MHz at  $1.5^\circ\text{K}$ . At  $2.1^\circ\text{K}$  the difference is much smaller:  $\Delta_{200}^{\max} = 17$  MHz and 20 MHz respectively. At this temperature  $\sigma \approx 0$ , and the increase of  $\Delta_{200}^{\max}$  can be attributed to the increase of the Ce resonance linewidth from 10 MHz in the 0.5% Ce crystal to 12 MHz in the crystal with 1.0% Ce (cf. table V.I.). The increasing influence of the bottleneck with increasing Ce concentration is also responsible for the

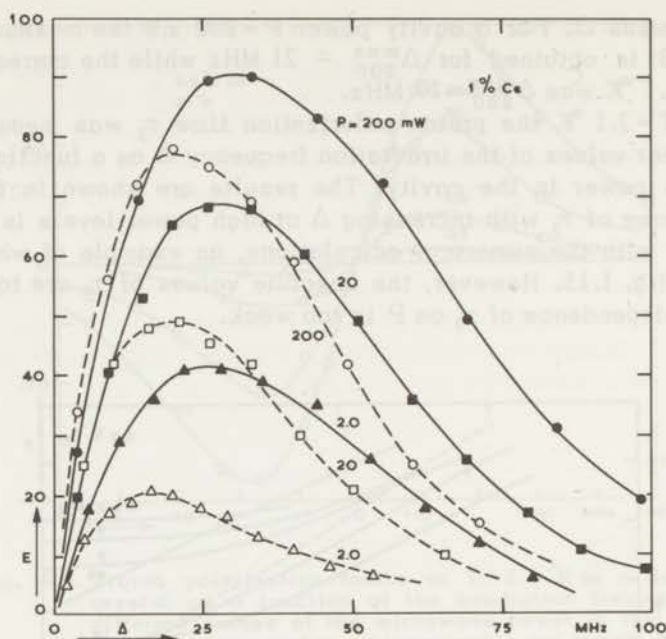


Fig. V.7. Proton polarization factor in a 1.0% Ce crystal as a function of the irradiation frequency for different values of the microwave power in the cavity. The dotted curves were measured at  $T = 2.1$  °K, the solid lines at  $T = 1.5$  °K.

larger polarizations at large values of  $\Delta$ . In the 0.5% crystal  $E_{200} = 5$  for  $\Delta = 100$  MHz, while  $E_{200} = 18$  for  $\Delta = 100$  MHz in the 1.0% Ce crystal.

The polarization times  $\tau_3'$  were determined at  $T = 1.5$  °K and at  $T = 1.8$  °K. The results are shown in fig. V.8. Just as in figure V.6 the dependence of  $\tau_3$  on  $\Delta$  is in agreement with the numerical calculations, but also in this crystal the decrease of  $\tau_3$  with increasing microwave power is too weak.

#### e. 2.0% Ce

The proton polarization factors obtained for this Ce concentration are shown in fig. V.9, both for 1.5 °K and for 2.1 °K. The values of  $E_{200}^{\max}$  are smaller than those for the 1.0% Ce crystal, namely 83 and 48 respectively. The corresponding values of  $\Delta_{200}^{\max}$  are 32 MHz and 26 MHz. Because of the increase of the bottleneck factor,  $E_{200}$  at  $\Delta = 100$  MHz has now increased to 30, although  $E_{200}^{\max}$  is smaller than in the preceding crystal.

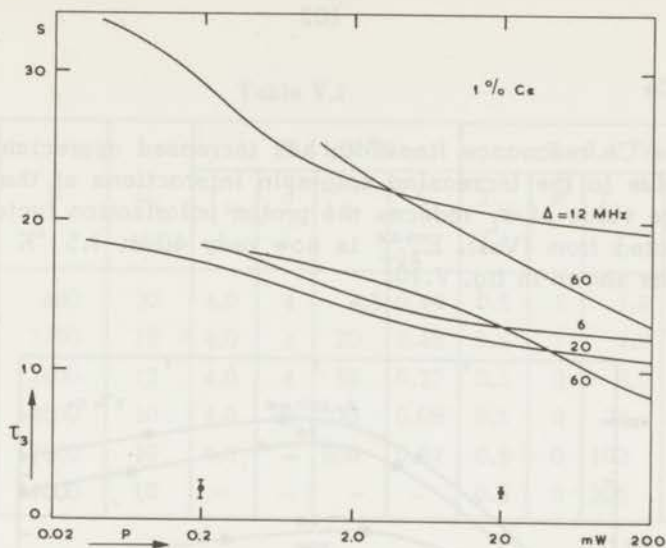


Fig. V.8. Proton polarization time in a 1.0% Ce crystal as a function of the microwave power in the cavity for different values of the irradiation frequency. The upper two curves were obtained at  $T = 1.5^\circ\text{K}$  where  $T_{1n} = 35$  s, the remaining three at  $T = 1.8^\circ\text{K}$  where  $T_{1n} = 19.5$  s.

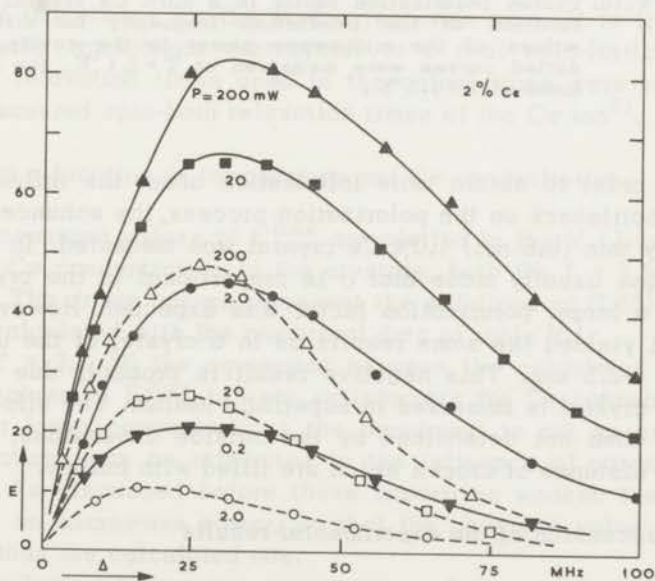


Fig. V.9. Proton polarization factor in a 2.0% Ce crystal as a function of the irradiation frequency for different values of the microwave power in the cavity. The dotted curves were measured at  $T = 2.1^\circ\text{K}$ , the solid lines at  $T = 1.5^\circ\text{K}$ .

f. 5.0% Ce

The Ce resonance linewidth has increased appreciably in this crystal due to the increasing spin-spin interactions of the Ce ions. The large value of  $\omega_L$  reduces the proton polarization factor, as can be expected from (V.1).  $E_{200}^{\max}$  is now only 40 at 1.5 °K and 16 at 2.1 °K, as shown in fig. V.10.

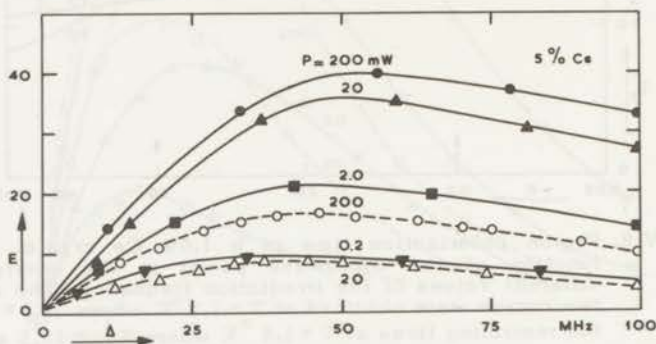


Fig. V.10. Proton polarization factor in a 5.0% Ce crystal as a function of the irradiation frequency for different values of the microwave power in the cavity. The dotted curves were measured at  $T = 2.1$  °K, the solid lines at  $T = 1.5$  °K.

In order to obtain more information about the influence of the phonon bottleneck on the polarization process, the enhancement factor in a very thin (0.6 mm) 1.0% Ce crystal was measured. In view of the assumption usually made that  $\sigma$  is proportional to the crystal thickness  $l$ , a larger polarization factor was expected. However, the experiment yielded the same results as in a crystal of the usual thickness of  $\sim 2.5$  mm. This negative result is probably due to the fact that the crystal is immersed in superfluid helium. The effective thickness is then not determined by the outside dimensions, but by the average distance of cracks which are filled with helium.

#### V - 2. Discussion of the experimental results

The values of the various parameters used in the numerical calculation of the steady state values of the polarization factors from (I.65) – (I.70) and (I.81) are listed in table V.I. In the computations the bottleneck factor was varied between 0 and 20 at  $T = 1.5$

Table V.I

% Ce	N	$\omega_L$ MHz	T = 1.5 °K				T = 2.1 °K			
			$T_{le}$ ms	$\sigma$	$T_{ln}$ s	f	$T_{le}$ ms	$\sigma$	$T_{ln}$ s	f
5.0	480	30	4.0	4	4.5	0.44	0.5	1	1.0	0.25
2.0	1200	16	4.0	4	20	0.48	0.5	1	4.0	0.15
1.0	2400	12	4.0	4	55	0.27	0.5	0	8.0	0.15
0.5	4800	10	4.0	2	220	0.09	0.5	0	24	0.10
0.2	12000	10	4.0	-	660	0.07	0.5	0	103	0.06
0.1	24000	10	-	-	-	-	0.5	0	205	0.06

°K, and between 0 and 4 at T = 2.1 °K. Those values of  $\sigma$  which gave the best fit with the experimental data are given in the table.

The calculations of the polarization time  $\tau_3$  were performed without taking the bottleneck influence into account. This is no serious limitation because only the transition rate of the electron spins is of importance for the proton response time. It is irrelevant whether these transitions correspond to a real spin-lattice relaxation. The relaxation times used in the calculations were estimated from the measured spin-bath relaxation times of the Ce ion<sup>5)</sup>.

a.  $E_{200}^{\max}$  as a function of temperature and Ce concentration

The measured values of  $E_{200}^{\max}$  are plotted in fig. V.11 as a function of the Ce concentration in the crystals, both for T = 1.5 °K and for 2.1 °K. The drawn curves represent the solutions of (I.65) - (I.70) and (I.81) calculated with the numerical data of table V.I.

For T = 2.1 °K the agreement between the calculated and the measured values of  $E_{200}^{\max}$  is very satisfactory for Ce concentrations  $c \geq 1\%$ . For lower concentrations the agreement is not so good, but these deviations can be attributed to the influence of paramagnetic impurities. As discussed before these impurities weaken the dependence of E on microwave power, so that the observed value of  $E_{200}^{\max}$  is smaller than the calculated one.

At the lowest temperatures again a good agreement is found for the largest Ce concentrations. It is to be noted that the concept of a phonon bottleneck is necessary for obtaining this agreement : if  $\sigma$

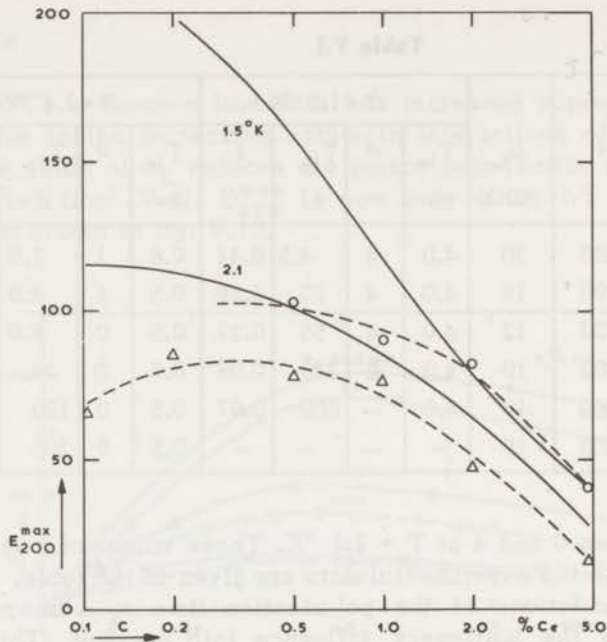


Fig. V.11. Measured values of the polarization factor at  $T=1.5^{\circ}\text{K}$  and  $T=2.1^{\circ}\text{K}$  as a function of the Ce concentration. The solid lines are calculated from (I.65) - (I.70) and (I.81). The dotted curves give the observed values of E.

o -  $T=1.5^{\circ}\text{K}$        $\Delta$  -  $T=2.1^{\circ}\text{K}$

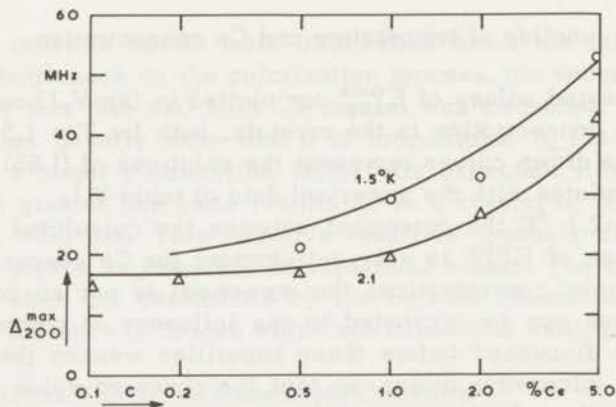


Fig. V.12. Microwave irradiation frequency for which the maximum polarization factor is obtained as a function of the Ce concentration.

o -  $T=1.5^{\circ}\text{K}$        $\Delta$  -  $T=2.1^{\circ}\text{K}$ .

is taken equal to zero, the calculated polarization factor is larger by a factor of about two. The measured value of  $E_{200}^{\max}$  in the 0.5% Ce crystal is too small. Just as at  $T=2.1$  °K this is attributed to the influence of impurities.

b.  $\Delta_{200}^{\max}$  as a function of temperature and Ce concentration

The observed values of  $\Delta_{200}^{\max}$  are shown in fig. V.12 together with the calculated curves. The agreement is very good at both temperatures. Again attention is drawn to the fact that these experimental data cannot be explained from the factor  $f$  alone, without taking account of a phonon bottleneck. The increase of  $\Delta_{200}^{\max}$  with decreasing temperature is due to the increasing bottleneck factor  $\sigma$ ;  $f$  is practically constant between 2.1 °K and 1.5 °K (cf. table V.I).

c.  $E$  as a function of microwave power

An example of the calculated behaviour of the polarization factor  $E$  for various microwave power levels is shown in fig. V.13 for a 1.0% Ce crystal at  $T=1.5$  °K. The curve for  $P=200$  mW is in good agreement with the experimental curve of fig. V.7. According to fig. V.13 the same polarization factor should be obtained for  $P=20$  mW, which is however certainly not observed in the experiment. The measured increase of  $E$  with increasing microwave power is thus

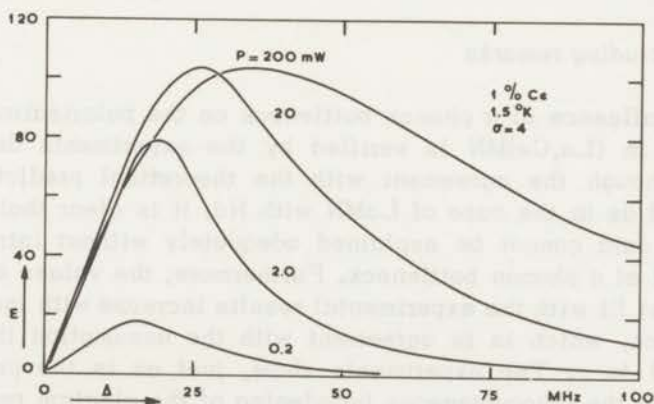


Fig. V.13. Proton polarization factor at  $T=1.5$  °K in a 1.0% Ce crystal as a function of the irradiation frequency, calculated from (I.65) - (I.70) and (I.81), assuming that  $\sigma=4$ .

slower than that predicted by the theory. For all crystals qualitatively the same behaviour is found, both at  $T = 1.5$  °K and at  $T = 2.1$  °K.

Just as in the crystals containing Nd (cf. chapter IV) this is due to the inhomogeneous broadening of the Ce resonance line. At intermediate microwave power levels not all Ce spins will take part in the polarization process, while all spins are equivalent for the proton relaxation. In the Nd crystals this phenomenon also influenced the maximum obtainable polarization factor  $E^{\max}$ , because the factor  $f$  is larger than for the crystals discussed in this chapter. In these Ce crystals  $f$  will also be larger than the calculated values of table V.I, but here the effect of the same relative variation of  $f$  on  $E^{\max}$  can be neglected.

#### d. $\tau_3$ as a function of microwave power

The proton polarization time  $\tau_3$  shows approximately the behaviour that is expected from the calculations: for small values of  $\Delta$   $\tau_3$  becomes constant at a relatively low microwave power, while for large  $\Delta$  more power is necessary to obtain a constant value, which decreases with decreasing  $\Delta$ .

The predicted dependence of  $\tau_3$  on  $\Delta$  is well verified experimentally (cf. fig. I.15), but the decrease of  $\tau_3$  with increasing microwave power is too weak. As discussed before, the Ce spin-spin interactions are responsible for a too large value of  $W^\pm$  which was used in the calculations. If this value is reduced, the calculated dependence of  $\tau_3$  on  $P$  becomes weaker, in better agreement with the observations.

### V - 3. Concluding remarks

The influence of a phonon bottleneck on the polarization factor of protons in (La,Ce)MN is verified by the experiments described above. Although the agreement with the theoretical predictions is not so good as in the case of LaMN with Nd, it is clear that the experimental data cannot be explained adequately without introducing the concept of a phonon bottleneck. Furthermore, the values of  $\sigma$  that give the best fit with the experimental results increase with increasing concentration, which is in agreement with the assumption that  $\sigma$  is proportional to  $c$ . The experiments show, just as in the preceding chapter, that the inhomogeneous broadening of the electron resonance line has to be taken into account in order to explain the observed power dependence of the polarization factor.

A detailed comparison of the proton polarization observed in a

number of these crystals with the theoretical description given in I - 1 was made a few years ago by Leifson and Jeffries<sup>6</sup>). Their experimental values of  $E_{200}^{\max}$  and  $\Delta_{200}^{\max}$  are approximately the same as those given in this chapter. However, a quantitative agreement with the theoretical data could by no means be obtained. This can be attributed to the failure of the description based on the rate equations, and to the fact that no account was taken of the phonon bottleneck.

### References

1. Ruby, R.H., Benoit, H. and Jeffries, C.D., Phys. Rev. **127**, 51 (1962).
2. Borghini, M., Phys. Letters **20**, 228 (1966).
3. Swanenburg, T.J.B., Poulis, N.J. and Ancher, L.J., Phys. Letters **15**, 12 (1965).
4. Swanenburg, T.J.B., van den Heuvel, G.M. and Poulis, N.J., Commun. Kamerlingh Onnes Lab. no. 354 a, Leiden; Physica **33**, 707 (1967).
5. Scott, P.L. and Jeffries, C.D., Phys. Rev. **127**, 32 (1962).
6. Leifson, O.S. and Jeffries, C.D., Phys. Rev. **122**, 1781 (1961).

## Chapter VI

THE INFLUENCE OF PARAMAGNETIC IMPURITIES  
ON THE DYNAMIC POLARIZATION OF PROTONS*Introduction*

The measurements discussed in the preceding chapters were performed in crystals in which only two spin species were of importance: the electron spins  $S$  and the nuclear spins  $I$ . Because both the relaxation and the polarization of the protons are due to the same matrix elements of the dipolar interaction between  $S$  and  $I$ , the steady state saturation factor  $W^{\pm}T_{1n}$  will be the same for all protons. If there are no paramagnetic impurities  $S'$  present in the crystal, there is no "leakage" of polarization. It is then not important whether the proton relaxation is limited by nuclear spin diffusion or not.

However, if such impurities  $S'$  with a  $g$ -value different from that of the spins  $S$  are present, the influence of spin diffusion may no longer be neglected in general<sup>1)</sup>. The proton polarization is then transported to the impurities, which try to maintain the proton spin temperature equal to that of the lattice. A continuous flow of polarization from the protons surrounding the spins  $S$  in the direction of the spins  $S'$  will thus exist, even under steady state conditions. The observed enhancement factor will depend on the average polarization and relaxation rates due to the polarizing spins, on the relaxation rate caused by the impurities, and finally on the rate at which the proton polarization can be transported from the polarizing spin to the impurity.

As discussed in detail in chapter I - 3.3, two extreme situations should be distinguished:

a. If the relaxation rate due to the impurities is smaller than the diffusion rate, the main part of the proton spin system will be in internal equilibrium. The problem can then be treated as if all protons have the same relaxation rate  $(T_{1n})^{-1} = (T'_{1n})^{-1} + (T''_{1n})^{-1}$ , where  $T'_{1n}$  and  $T''_{1n}$  are the relaxation times due to the polarizing spins and to the impurities respectively. Because the factor  $f$  is increased by the presence of these impurities, the maximum obtainable polarization factor

$$E = \frac{\omega_e \Delta}{\Delta^2 + 2\omega_L^2 + f\omega_n^2} \quad (\text{VI.1})$$

is reduced. The forbidden transition probabilities  $W^\pm$  however remain the same when impurities are added, because their magnitude only depends on the interaction between the spins  $S$  and the protons. Consequently, the microwave power which is necessary to obtain the maximum polarization will be larger when impurities are present; it is more difficult to satisfy the condition  $W^\pm T_{1n} \gg 1$ , because  $T_{1n}$  is shortened.

b. If the relaxation rate due to the spins  $S'$  is larger than the spin diffusion rate, the dependence of the polarization factor on microwave power will be different, although the maximum obtainable polarization remains the same. If the nuclear relaxation is limited by spin diffusion,  $T_{1n}$  is proportional to  $T_{1e}^{1/2}$ , as was outlined in I - 1.3 and I - 3.3. Because of the equivalence of nuclear polarization and relaxation, the average value of  $W^\pm$  is then proportional to  $W_0^{1/2}$ , while in a.  $W^\pm$  was proportional to  $W_0^{1,2}$ . As a result more microwave power will be needed to satisfy the saturation condition  $W^\pm T_{1n} \gg 1$ ; at a given power level the polarization factor will be smaller than in the case that spin diffusion is fast enough to maintain internal equilibrium in the proton spin system.

The measurements to be discussed in this chapter were performed single crystals of LaMN all containing 2.0% Nd and various amounts of Ce or Pr. The Nd spins were used as polarizing spins, the Ce or the Pr ions as impurities. The choice of LaMN with 2.0% Nd as a host crystal was based on the following considerations:

1. The polarization factor is large over the whole temperature region (cf. chapter IV), so that an appreciable reduction of the polarization by the impurities is possible without making the proton polarization too small for accurate measurements.
2. The proton spin-lattice relaxation times are long. They can be reduced by the addition of impurities by one or two orders of magnitude, without becoming too short to be determined experimentally. On the other hand, the proton relaxation times in the pure Nd crystal are probably only determined by the Nd ions, and not by unknown impurities.

It is well known from detailed studies of proton relaxation in LaMN with 1.0% Nd, that nuclear spin diffusion is fast enough to maintain internal equilibrium in the proton spin system<sup>3)</sup>. This will also be the case in a 2.0% Nd crystal, so that we may expect that the experimental data can be explained from (I.65) - (I.70), assuming that spin diffusion is very fast. Therefore we will compare our measurements with the solutions of these equations. If the impurity con-

centration increases, the leakage of polarization becomes more and more important. Then the observed enhancement factor will be smaller than the calculated one.

## VI - 1. Experimental results

### VI - 1.1. LaMN containing 2.0% Nd and various amounts of Ce

The proton polarization factors in crystals of LaMN containing 2.0% Nd and 0.02, 0.10, 0.20, and 0.50% Ce have been measured in the liquid helium temperature range. In one of the crystals also the polarization time  $\tau_3$  was measured<sup>4)</sup>.

#### a. The leakage factor $f$

The factor  $f = NT_{1e}/T_{1n}$  was calculated from the proton relaxation times given in III-3.3. The Nd spin-lattice relaxation time was

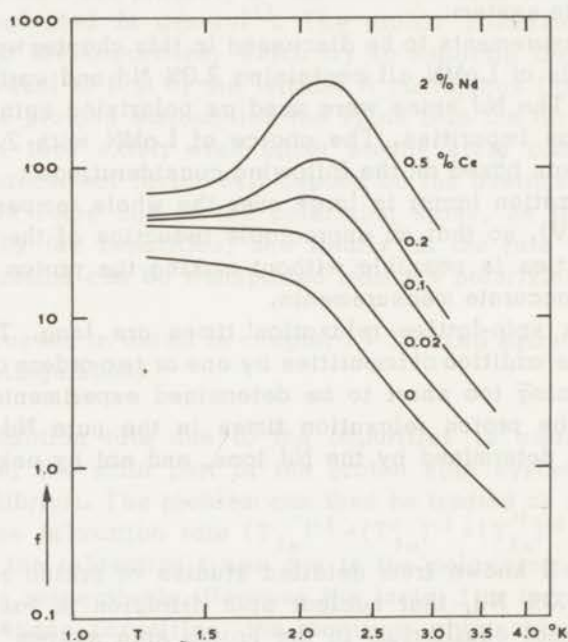


Fig. VI.1. Factor  $f = NT_{1e}/T_{1n}$  as a function of temperature in crystals containing 2.0% Nd and different amounts of Ce.

assumed to be the same as that in a pure Nd crystal. Although the Ce relaxation time is much shorter than that of Nd, cross relaxation is quite improbable because of the difference of the  $g$ -factors. The number of protons  $N$  per polarizing spin is the same for all crystals.

Fig. VI.1 shows the factor  $f$  as a function of temperature for the various crystals. For those with the smallest Ce concentration  $f$  increases with decreasing temperature, but for the highest Ce concentrations a maximum is found at a temperature of about 2.2 °K. The maximum obtainable polarization factor is thus expected to decrease continuously with decreasing temperature for the smallest Ce concentration, while in the crystals with higher Ce contents  $E^{\max}_{200}$  will show a minimum at 2.2 °K, and increase again at lower temperatures.

#### b. 2.0% Nd; 0.02% Ce

The proton polarization factors at the largest microwave power available are plotted in fig. VI.2 as a function of the irradiation frequency  $\Delta$ . The temperatures at which the measurements were performed are indicated in the figure. For  $T < 3.5$  °K the polarization factor  $E^{\max}_{200}$  decreases with decreasing temperature, and becomes constant at 2.1 °K, as expected from the value of  $f$  from fig. VI.1. At  $T = 4.0$  °K  $E^{\max}_{200}$  is much smaller than  $E^{\max}$ , because the maximum available microwave power of 200 mW is insufficient.

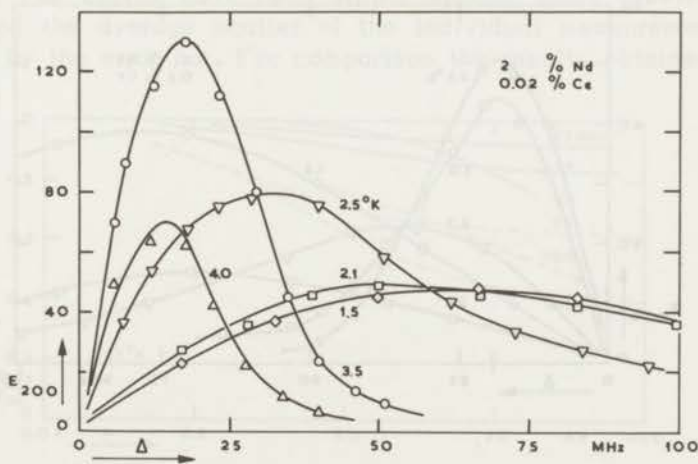


Fig. VI.2. Proton polarization factor for  $P = 200$  mW in a 2.0% Nd, 0.02% Ce crystal as a function of the irradiation frequency for different temperatures.

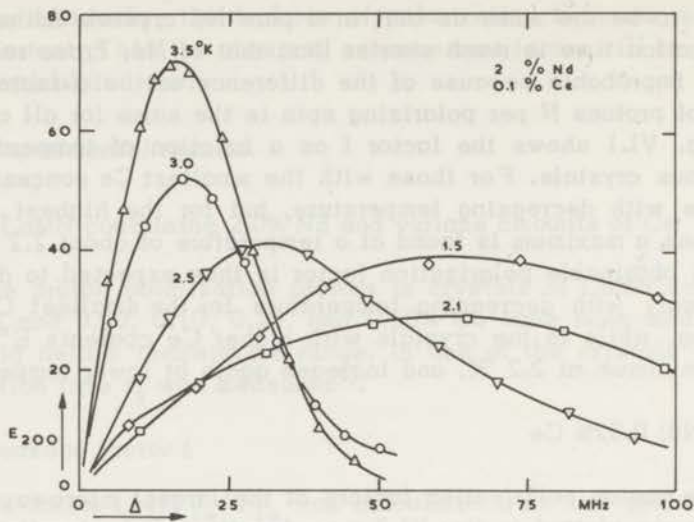


Fig. VI.3. Proton polarization factor for  $P = 200$  mW in a 2.0% Nd, 0.10% Ce crystal as a function of the irradiation frequency for different temperatures.

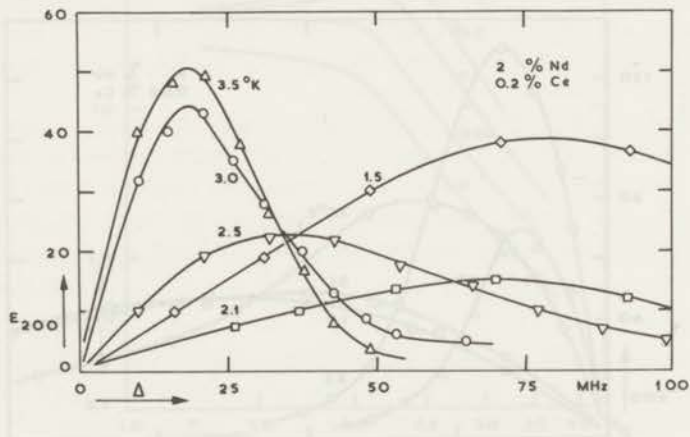


Fig. VI.4. Proton polarization factor for  $P = 200$  mW in a 2.0% Nd, 0.20% Ce crystal as a function of the irradiation frequency for different temperatures.

The maximum values of  $E_{200}$  are, even with this small amount of Ce in the crystal, considerably smaller than those for a pure 2.0% Nd crystal at corresponding temperatures. Comparison with fig. IV.5 shows that at the lowest temperature the Ce influence is relatively small.

c. 2.0% Nd; 0.10% Ce

Fig. VI.3 shows the polarization factors  $E_{200}$  as a function of  $\Delta$ . Just as in the preceding crystal the enhancement decreases with decreasing temperature, but now a minimum is found for  $T = 2.1$  °K. The curve for  $T = 1.5$  °K shows that for this temperature approximately the same value of  $E_{200}^{\max}$  is obtained as at 2.5 °K. This behaviour is expected from the values of  $f$  in this crystal.

d. 2.0% Nd; 0.20% Ce

As for the preceding crystals,  $E_{200}$  is shown as a function of the irradiation frequency  $\Delta$  at different temperatures (fig. VI.4). The minimum of the polarization factor  $E_{200}^{\max}$  at 2.1 °K has become more pronounced, as could be expected from the behaviour of  $f$  as a function of temperature.  $E_{200}^{\max}$  at 1.5 °K is now even larger than at 2.5 °K.

In this crystal the polarization times  $\tau_3$  have also been measured, at  $T = 2.1$  °K for three values of  $\Delta$ . The results are shown in fig. VI.5. The curves have been drawn through many experimental points, and the average scatter of the individual measurements is indicated by the error bar. For comparison the results obtained in a

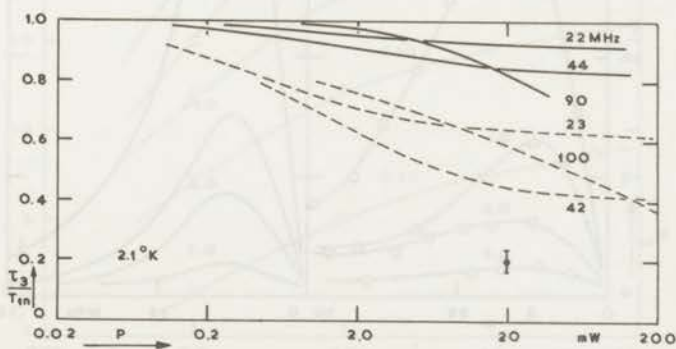


Fig. VI.5. Proton polarization time at  $T = 2.1$  °K as a function of the microwave power in the cavity. The dotted curves were measured in a pure 2.0% Nd crystal, the drawn curves in a 2.0% Nd, 0.20% Ce crystal.

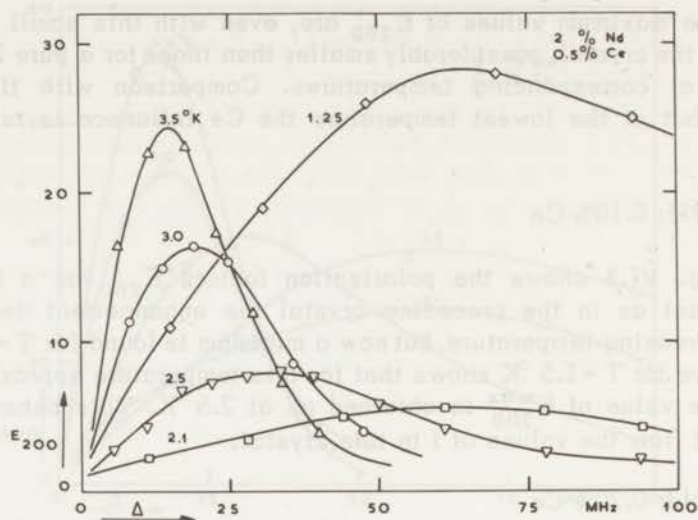


Fig. VI.6. Proton polarization factor for  $P=200$  mW in a 2.0% Nd, 0.50% Ce crystal as a function of the irradiation frequency for different temperatures.

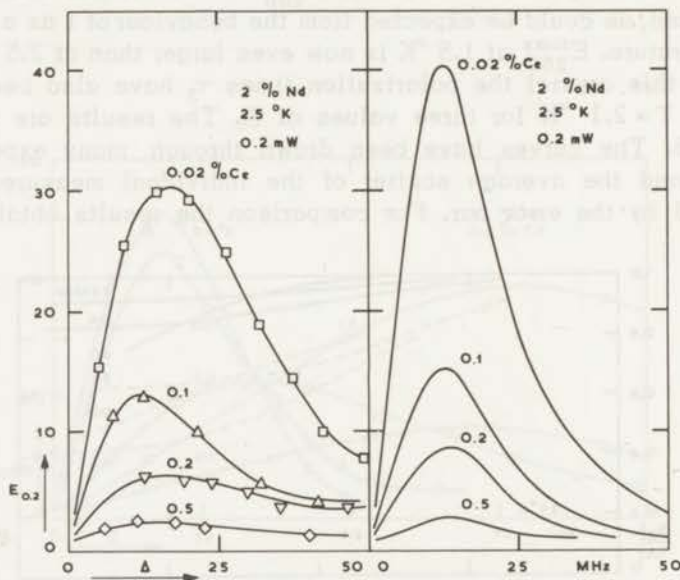


Fig. VI.7. a. Proton polarization factor for  $P=0.2$  mW in crystals containing 2.0% Nd and different amounts of  $Ce_8$  as a function of the irradiation frequency at  $T=2.5$  K.  
b. The figure on the right hand side shows the values calculated from (1.65) - (1.70).

pure 2.0% Nd crystal (see chapter IV) at the same temperature are also given in the figure. The values of  $\tau_3/T_{1n}$  for corresponding curves are larger if Ce impurities are present. This is a consequence of the fact, that the impurities shorten the proton relaxation time  $T_{1n}$ , while the forbidden transition probabilities  $W^\pm$  are not influenced by the Ce ions. A more extensive discussion of this phenomenon was given in I - 3.2.c.

e. 2.0% Nd; 0.50% Ce

In this crystal the factor  $f$  is very large in the temperature region between 2.0 °K and 3.0 °K. The observed enhancement factors, as shown in fig VI.6, are indeed very small. The decrease of  $f$  from 360 at 2.1 °K to 67 at 1.25 °K is reflected in the increase of  $E_{200}^{max}$  from 5.5 to 28.

In all crystals the polarization factors  $E$  were also measured at lower microwave power levels as a function of  $\Delta$ . Fig. VI.7a shows the enhancements observed with a cavity power of 0.2 mW for the various crystals at  $T = 2.5$  °K. In fig. VI.7b the values of  $E_{0.2}$  calculated from (I.65) - (I.70) are given.

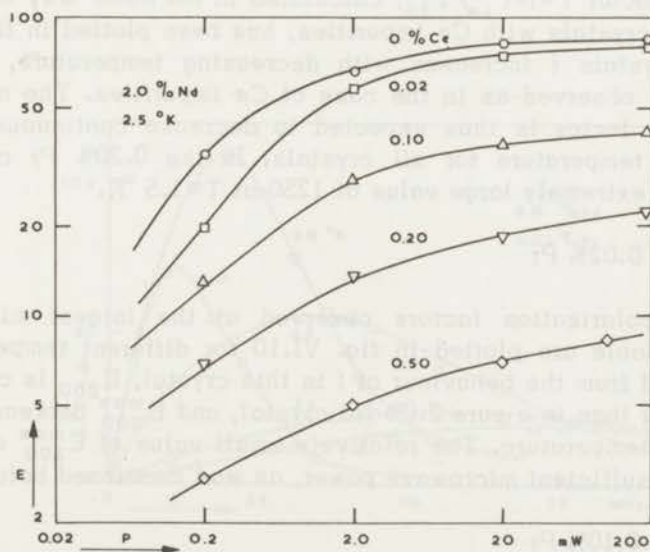


Fig. VI.8. Proton polarization factor at  $T = 2.5$  °K in crystals containing 2.0% Nd and different amounts of Ce as a function of the microwave power in the cavity.

In fig. VI.8 the maxima of the  $E$  -versus-  $\Delta$  curves are plotted as a function of the applied microwave power on a logarithmic scale. The curves for the crystals containing 0% and 0.02% Ce appear to be well saturated at  $P=200$  mW. For the crystals with a larger amount of Ce however, the slope of the curves at the highest power level of 200 mW increases with increasing Ce concentration, indicating that nuclear spin diffusion and the large leakage factor slow down the polarization process. Furthermore, fig. VI.8 clearly shows that for higher Ce concentrations more microwave power is necessary to obtain the maximum polarization. The power for which half the maximum value is obtained, increases by at least 10 db from the pure Nd crystal to the crystal with 0.50% Ce.

#### VI - 1.2. LaMN containing 2.0% Nd and various amounts of Pr

The proton polarization factors in crystals of LaMN containing 2.0% Nd and 0.02, 0.10 and 0.20% Pr have been measured in the liquid helium temperature range.

##### a. The leakage factor $f$

The factor  $f = NT_{1e}/T_{1n}$ , calculated in the same way as in the (La,Nd)MN crystals with Ce impurities, has been plotted in fig. VI.9. For all crystals  $f$  increases with decreasing temperature, and no maximum is observed as in the case of Ce impurities. The maximum polarization factor is thus expected to decrease continuously with decreasing temperature for all crystals. In the 0.20% Pr crystal  $f$  obtains the extremely large value of 1250 at  $T=1.5$  °K.

##### b. 2.0% Nd; 0.02% Pr

The polarization factors observed at the largest microwave power available are plotted in fig. VI.10 for different temperatures. As expected from the behaviour of  $f$  in this crystal,  $E_{200}$  is considerably smaller than in a pure 2.0% Nd crystal, and  $E_{200}^{\max}$  decreases with decreasing temperature. The relatively small value of  $E_{200}^{\max}$  at 4.0 °K is due to insufficient microwave power, as was mentioned before.

##### c. 2.0% Nd; 0.10% Pr

For all temperatures the polarization factors are slightly smaller than those observed in the 0.02% Pr crystal, as shown in fig. VI.11.

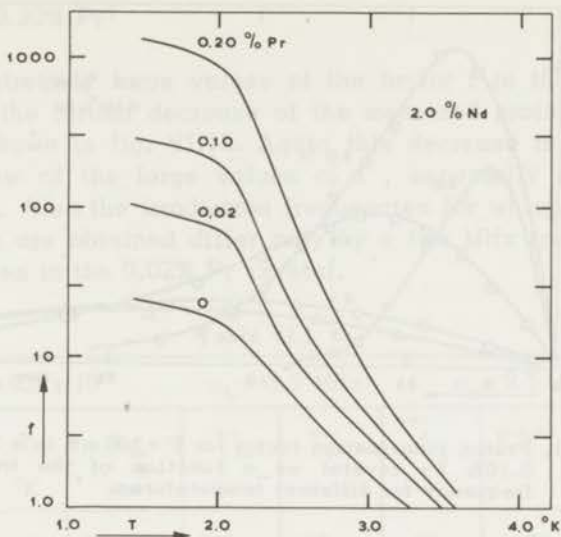


Fig. VI.9. Factor  $f = NT_{le}/T_{ln}$  as a function of temperature in crystals containing 2.0% Nd and various amounts of Pr.

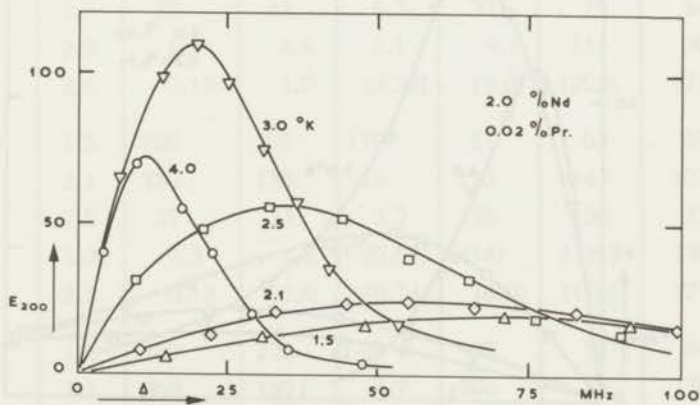


Fig. VI.10. Proton polarization factor for  $P = 200$  mW in a 2.0% Nd, 0.02% Pr crystal as a function of the irradiation frequency for different temperatures.

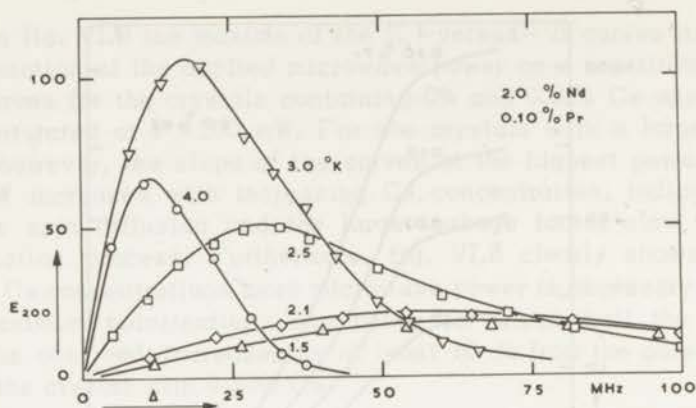


Fig. VI.11. Proton polarization factor for  $P=200$  mW in a 2.0% Nd, 0.10% Pr crystal as a function of the irradiation frequency for different temperatures.

However, the increase of  $f$  from 100 at 1.5 °K in the 0.02% Pr crystal to 300 in this crystal has a remarkably small influence on the values of  $E_{200}^{\max}$ , which are given by 20 and 18 respectively. In the crystals with 2.0% Nd and 0.2% or 0.5% Ce approximately the same increase of  $f$  reduces the polarization factor from 15 to 5.5 (cf. figs. VI.4 and 6).

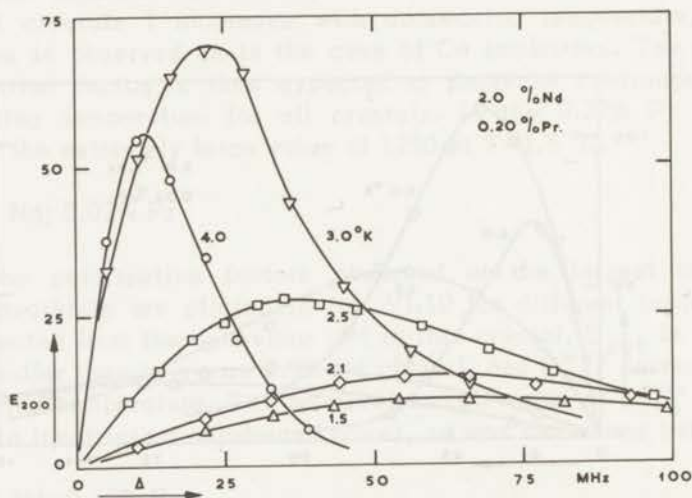


Fig. VI.12. Proton polarization factor for  $P=200$  mW in a 2.0% Nd, 0.20% Pr crystal as a function of the irradiation frequency for different temperatures.

d. 2.0% Nd; 0.20% Pr

The extremely large values of the factor  $f$  in this crystal are reflected in the further decrease of the measured proton polarization factors as shown in fig. VI.12. Again this decrease is unexpectedly small in view of the large values of  $f$ , especially at the lowest temperatures. Also the irradiation frequencies for which the maximum polarizations are obtained differ only by a few MHz from the corresponding values in the 0.02% Pr crystal.

Table VI.1

		$N = 6.0 \times 10^3$			$\omega_L = 9.5 \text{ MHz}$	$\omega_n = 9.5 \text{ MHz}$		
% Ce	T °K	$T_{1e}$ ms	$T'_{in}$ s	$T''_{in}$ s	$f$	$E^{\max}$	$\Delta^{\max}$ MHz	
0.02	1.5	780	200	230	39	71	61	
	2.1	350	130	99	31	79	55	
	2.5	27	33	26	11	124	34	
	3.0	1.3	4.6	3.8	3.2	194	22	
	3.5	0.13	1.0	1.0	0.77	240	16	
0.10	1.5	780	200	200	47	65	66	
	2.1	350	130	34	61	57	75	
	2.5	27	33	6.2	30	79	54	
	3.0	1.3	4.6	1.1	8.1	141	30	
	3.5	0.13	1.0	(0.33)	(3.0)	(202)	(21)	
0.20	1.5	780	200	170	51	63	69	
	2.1	350	130	16	110	43	101	
	2.5	27	33	3.2	58	59	73	
	3.0	1.3	4.6	(0.61)	(14)	(121)	(38)	
	3.5	0.13	1.0	(0.14)	(6.0)	(160)	(27)	
0.50	1.5	780	200	96	76	52	84	
	2.1	350	130	4.7	360	24	170	
	2.5	27	33	0.92	180	34	128	
	3.0	1.3	4.6	(0.16)	(44)	(67)	(65)	
	3.5	0.13	1.0	(0.03)	(25)	(87)	(49)	

## VI- 2. Discussion of the experimental results

## VI - 2.1. LaMN containing 2.0% Nd and various amounts of Ce

As discussed in the introduction to this chapter, the steady state solutions of (I.65)– (I.70) have been computed numerically, assuming that spin diffusion is very fast. The values of the parameters used in these calculations are listed in table VI.I. The numbers in brackets are estimated by extrapolation. The last two columns of table VI.I represent the maximum values of  $E$  and the corresponding values of  $\Delta$ , calculated from (VI.1). The total proton relaxation rate is given by  $(T_{1n})^{-1} = (T'_{1n})^{-1} + (T''_{1n})^{-1}$ .

A detailed comparison between the experimental data and the theoretical predictions will be made below for the different aspects of the polarization process.

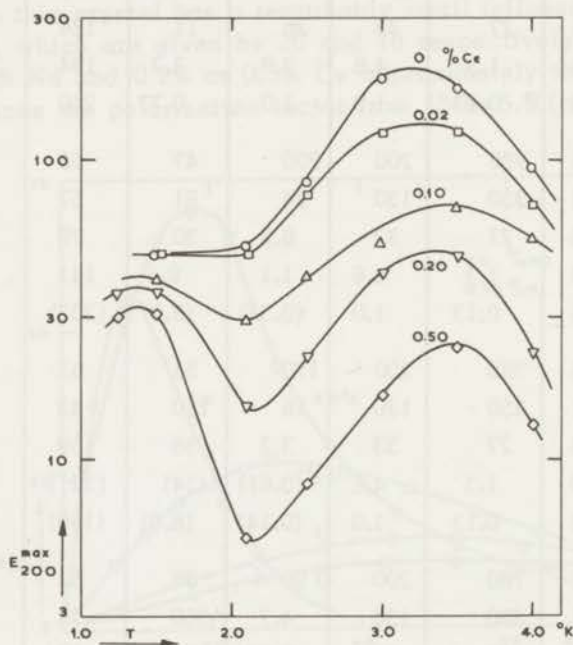


Fig. VI.13. Measured values of  $E_{200}^{\max}$  as a function of temperature for crystals containing 2.0% Nd and different amounts of Ce.

a.  $E_{200}^{\max}$  as a function of temperature

The measured values of  $E_{200}^{\max}$  are shown in fig. VI.13 as a function of temperature for all crystals. These data should be compared with those given in fig. VI.14, which represent the polarization factors calculated from (I.65) - (I.70). The measured values of  $E_{200}^{\max}$  are smaller than the theoretical ones by a factor of about 1.5. This discrepancy is of the same order of magnitude as that observed in the pure Nd crystal (cf. chapter IV).

For a closer examination the ratio of the calculated and the observed values of  $E_{200}^{\max}$  has been plotted in fig. VI.15. This figure clearly shows, that for all temperatures and in all crystals  $E_{\text{calc}}/E_{\text{meas}}$  is about 1.5, except for the crystals with 0.20% and 0.50% Ce at 2.1 °K, where a much larger discrepancy is observed. At this temperature the influence of the Ce ions on the proton relaxation is very large (cf. fig. III.11), while  $f$  obtains its maximum value (110 and 360 respectively). As was discussed in I - 3.2.b and in the introduction to

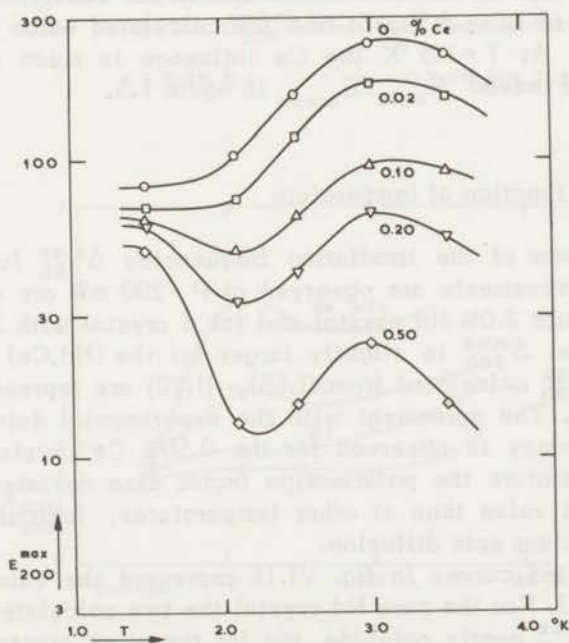


Fig. VI.14. Calculated values of  $E_{200}^{\max}$  as a function of temperature for crystals containing 2.0% Nd and different amounts of Ce.

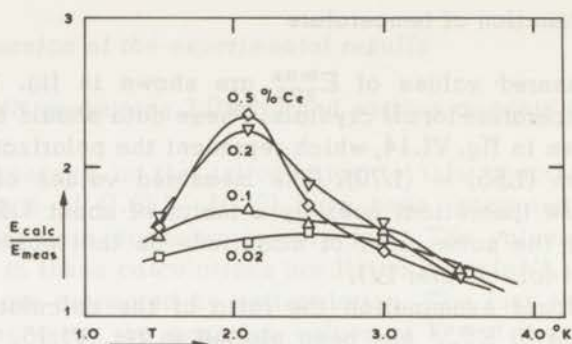


Fig. VI.15. Ratio of the calculated and the observed values of  $E_{200}^{max}$  as a function of temperature for crystals containing 2.0% Nd and different amounts of Ce.

this chapter, the equations (I.65) - (I.70) will fail in the description of the polarization process under these conditions, because nuclear spin diffusion has to be taken into account. The observed polarization factor is indeed more different from the calculated value than at other temperatures. At  $T = 1.5$  °K the Ce influence is much smaller than at 2.1 °K, and indeed  $E_{calc}/E_{meas}$  is again 1.5.

b.  $\Delta_{200}^{max}$  as a function of temperature

The values of the irradiation frequencies  $\Delta_{200}^{max}$  for which the maximum enhancements are observed at  $P = 200$  mW are given in fig. VI.16 for a pure 2.0% Nd crystal and for a crystal with 2.0% Nd and 0.50% Ce.  $\Delta_{200}^{max}$  is slightly larger for the (Nd,Ce) crystal. The values of  $\Delta_{200}^{max}$  calculated from (I.65) - (I.70) are represented by the drawn curves. The agreement with the experimental data is good; a minor discrepancy is observed for the 0.50% Ce crystal at 2.1 °K. At this temperature the polarization factor also deviated more from its calculated value than at other temperatures, indicating the influence of nuclear spin diffusion.

The dotted curves in fig. VI.16 represent the values of  $\Delta^{max}$  from table VI.I. For the pure Nd crystal the two calculated curves for  $\Delta^{max}$  and  $\Delta_{200}^{max}$  nearly coincide, but for the other crystal there is a large discrepancy above 1.8 °K. This deviation clearly demonstrates, that the forbidden transition is far from saturation in this crystal.

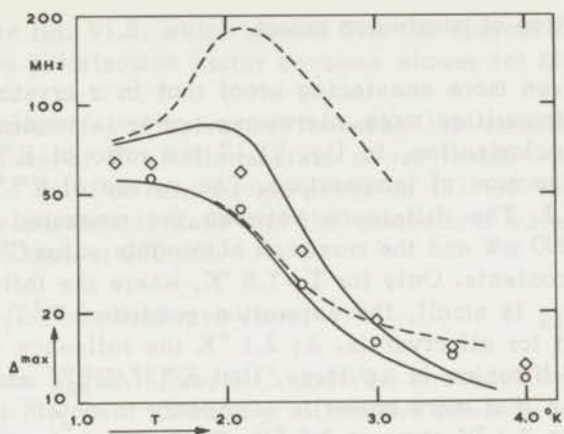


Fig. VI.16. Comparison of the calculated and the observed values of  $\Delta_{200}^{\max}$  and the calculated values of  $\Delta^{\max}$ . The dotted curves represent  $\Delta^{\max}$ , and the drawn curves the values of  $\Delta_{200}^{\max}$  calculated from (I.65) - (I.70).

o - 2.0% Nd

◇ 2.0% Nd, 0.50% Ce.

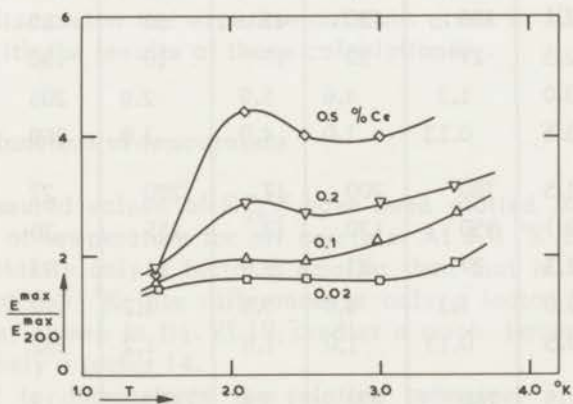


Fig. VI.17. Ratio of the calculated values of  $E^{\max}$  and the observed values of  $E_{200}^{\max}$  as a function of temperature for crystals containing 2.0% Nd and different amounts of Ce.

## c. E as a function of microwave power

As an even more convincing proof that in a crystal containing paramagnetic impurities more microwave power is required to obtain the maximum polarization, in fig. VI.17 the ratio of  $E^{\max}/E_{200}^{\max}$  is plotted as a function of temperature. The values of  $E^{\max}$  are taken from table VI.I. The difference between the measured polarization factor for  $P = 200$  mW and the maximum obtainable value  $E^{\max}$  is larger for larger Ce contents. Only for  $T = 1.5$  °K, where the influence of the Ce ions on  $T_{1n}$  is small, the saturation condition  $W^{\pm}T_{1n} \gg 1$  seems to be satisfied for all crystals. At 2.1 °K the influence of the factor  $f$  and of spin diffusion is so large, that  $E^{\max}/E_{200}^{\max}$  shows a maximum, indicating that more power is necessary to obtain the maximum enhancement at 2.1 °K than at 2.5 °K. The same behaviour can also

Table VI.II

% Pr	$N = 6.0 \times 10^3$		$\omega_L = 9.5$ MHz		$\omega_n = 9.5$ MHz		
	T °K	$T_{1e}$ ms	$T'_{1n}$ s	$T''_{1n}$ s	f	$E^{\max}$	$\Delta^{\max}$ MHz
0.02	1.5	780	200	67	100	46	96
	2.1	350	130	43	58	59	73
	2.5	27	33	17	10	130	33
	3.0	1.3	4.6	5.9	2.9	205	21
	3.5	0.13	1.0	4.0	1.0	269	16
0.10	1.5	780	200	17	280	27	160
	2.1	350	130	12	155	36	119
	2.5	27	33	8.9	21	93	46
	3.0	1.3	4.6	3.8	4.2	179	24
	3.5	0.13	1.0	1.6	1.2	252	17
0.20	1.5	780	200	3.4	1250	13	335
	2.1	350	130	2.6	700	17	250
	2.5	27	33	1.9	80	50	86
	3.0	1.3	4.6	1.4	7.5	148	29
	3.5	0.13	1.0	(0.7)	(1.6)	(238)	(18)

be observed in fig. VI.8, which shows that the approach to the maximum obtainable polarization factor becomes slower for higher Ce concentrations.

An example of the agreement between the measured and the calculated values of  $E$  at intermediate power levels was shown in figs. VI.7a and 7b. For this cavity power of 0.2 mW the difference between the experimental data and the theoretical values of  $E_{0.2}^{\max}$  is even smaller than at 200 mW.

d.  $\tau_3$  as a function of microwave power

Comparison of the figures I.15 and VI.5 shows that the observed behaviour of  $\tau_3/T_{1n}$  as a function of microwave power is in qualitative agreement with the theoretical predictions. The curves of these two figures do not represent exactly identical situations, but nevertheless the increase of the factor  $f$  due to the impurities causes larger values of  $\tau_3/T_{1n}$ , both theoretically and in the experiment.

VI-2.2. LaMN containing 2.0% Nd and various amounts of Pr

The steady state solutions of (I.65) - (I.70) have been computed numerically; the values of the parameters used, are listed in table VI.II. In the discussion the experimental data given in VI - 1.2 will be compared with the results of these calculations.

a.  $E_{200}^{\max}$  as a function of temperature

The measured values of  $E_{200}^{\max}$  have been plotted in fig. VI.18 as a function of temperature for all crystals. At 3.0 °K  $E_{200}^{\max}$  in the 0.20% Pr crystal is only a factor 3 smaller than that in the pure Nd crystal, and at 1.5 °K this difference is only a factor 5. The calculated curves, shown in fig. VI.19, predict a much larger difference at 1.5 °K, namely a factor 14.

In order to demonstrate the relative behaviour of  $E_{\text{calc}}$  and  $E_{\text{meas}}$  more clearly, the ratio  $E_{\text{calc}}/E_{\text{meas}}$  is plotted in fig. VI.20 just as in the case of Ce. At temperatures above  $T=2.5$  °K this ratio is again of the order of 1.5 for all Pr concentrations. For the crystal containing 0.02% Pr  $E_{\text{calc}}/E_{\text{meas}}$  increases to 2.3 at 2.1 °K. and 1.5 °K. This indicates that nuclear spin diffusion should be taken into account, just as in the crystals with 2.0% Nd and 0.20% or 0.50%

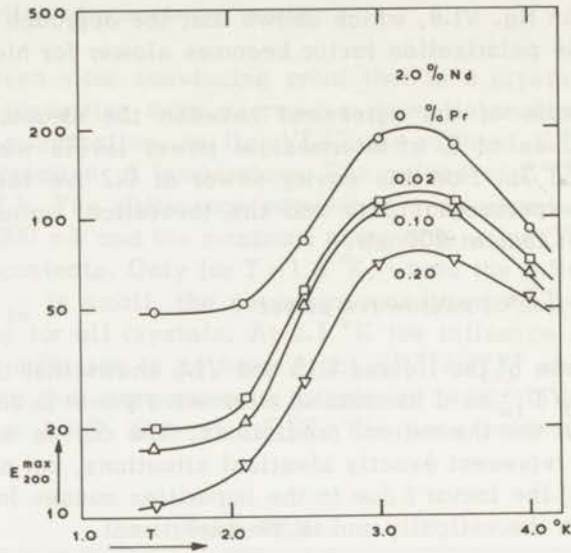


Fig. VI.18. Measured values of  $E_{200}^{\max}$  as a function of temperature for crystals containing 2.0% Nd and different amounts of Pr.

Ce at 2.1 °K. Likewise, one would expect a further increase of  $E_{\text{calc}}/E_{\text{meas}}$  for higher Pr concentrations, but the reverse is true: for larger Pr contents  $E_{\text{calc}}/E_{\text{meas}}$  decreases. In the 0.20% Pr crystal the calculated value of  $E_{200}^{\max}$  is even a factor two smaller than the observed one.

These results can be explained by assuming that the Nd spin-lattice relaxation time  $T_{1e}$  is shortened considerably by cross relaxation with the Pr ions, which are known to have a very fast relaxation rate (cf. III-2.3). Then the factor  $f$  becomes smaller than the values of table VI.II that were used in the calculations. This results in a larger calculated polarization factor, which is in better agreement with the experimental results.

#### b. $\Delta_{200}^{\max}$ as a function of temperature

In fig. VI.21 the measured values of  $\Delta_{200}^{\max}$  have been plotted, both for the pure 2.0% Nd crystal and for the crystal containing also 0.20% Pr. For the latter  $\Delta_{200}^{\max}$  is only slightly larger. Comparison with the drawn curves which represent the calculated values of  $\Delta_{200}^{\max}$  shows, that especially at the lowest temperatures the experimental

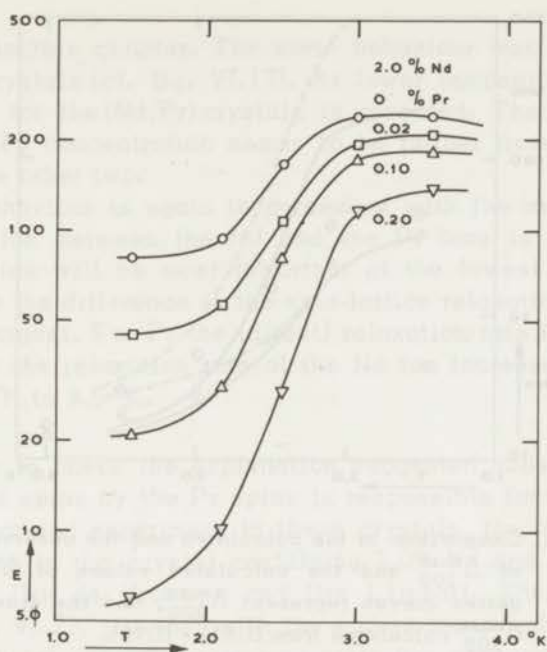


Fig. VI.19. Calculated values of  $E_{200}^{\max}$  as a function of temperature for crystals containing 2.0% Nd and different amounts of Pr.

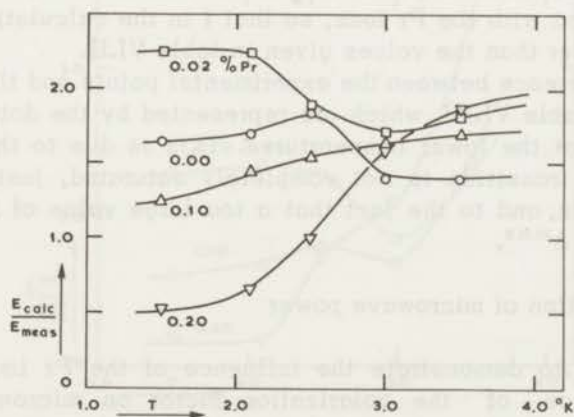


Fig. VI.20. Ratio of the calculated and the observed values of  $E_{200}^{\max}$  as a function of temperature for crystals containing 2.0% Nd and different amounts of Pr.

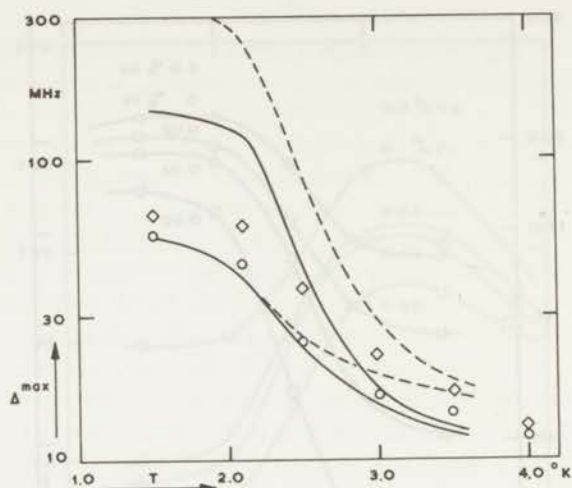


Fig. VI.21. Comparison of the calculated and the observed values of  $\Delta_{200}^{\max}$  and the calculated values of  $\Delta^{\max}$ . The dotted curves represent  $\Delta_{200}^{\max}$ , and the drawn curves  $\Delta_{200}^{\max}$  calculated from (I.65) - (I.70).

○ - 2.0% Nd

◇ 2.0% Nd, 0.20% Pr.

data do not agree with the computations. Again these deviations can be explained by assuming that  $T_{1e}$  is shorter than expected due to cross relaxation with the Pr ions, so that  $f$  in the calculations should be taken smaller than the values given in table VI.II.

The difference between the experimental points and the maximum values of  $\Delta$  (table VI.II), which are represented by the dotted curves, is a factor 5 at the lower temperatures. This is due to the fact that the forbidden transition is not completely saturated, just as in the (Nd,Ce) crystals, and to the fact that a too large value of  $f$  was used in calculating  $\Delta^{\max}$ .

### c. E as a function of microwave power

In order to demonstrate the influence of the Pr impurities on the dependence of the polarization factor on microwave power, the ratio  $E^{\max}/E_{200}^{\max}$  is plotted in fig. VI.22 for the three crystals;  $E^{\max}$  is the maximum obtainable polarization factor, taken from table VI.II. At  $T = 3.5$  °K the curve for the crystal with the highest Pr contents lies highest, which is expected from the discussion given in the

introduction to this chapter. The same behaviour was also found in the (Nd,Ce) crystals (cf. fig. VI.17). At lower temperatures however, the situation for the (Nd,Pr) crystals is reversed. The crystal with the smallest Pr concentration seems to be further from its saturated value than the other two.

This behaviour is again in agreement with the assumption that cross relaxation between the Nd and the Pr ions is present. This cross relaxation will be most important at the lowest temperatures, because there the difference in the spin-lattice relaxation rates of the two ions is largest. For Pr the (direct) relaxation rate is proportional to  $T^{-1}$ , while the relaxation rate of the Nd ion increases by a factor  $10^4$  from 1.5 °K to 3.5 °K.

In order to check the explanation suggested above that relaxation of the Nd spins by the Pr spins is responsible for the deviations between theory and experiment in these crystals, the Nd spin-lattice relaxation time in the crystal containing 2.0% Nd and 0.20% Pr was measured by Drs de Vroomen and Drs Lijphart. Their results are shown in fig. VI.23, together with the values measured previously in a pure Nd crystal. The decay curves were non-exponential, and both the starting and the final slopes are given in fig. VI.23. Especially at the lowest temperatures, where the difference between the two slopes is a factor of about 4, the influence of the Pr ions is evident.

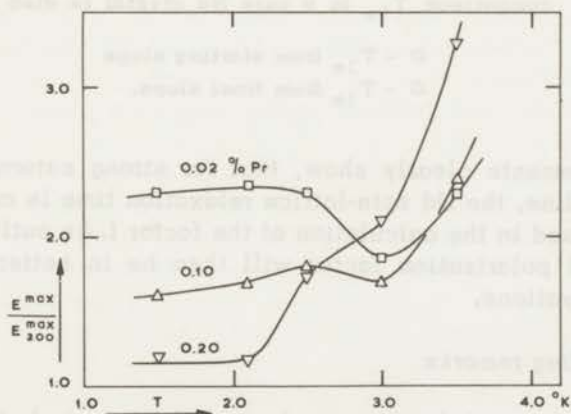


Fig. VI.22. Ratio of the calculated values of  $E^{\max}$  and the observed values of  $E_{200}^{\max}$  as a function of temperature for crystals containing 2.0% Nd and different amounts of Pr.

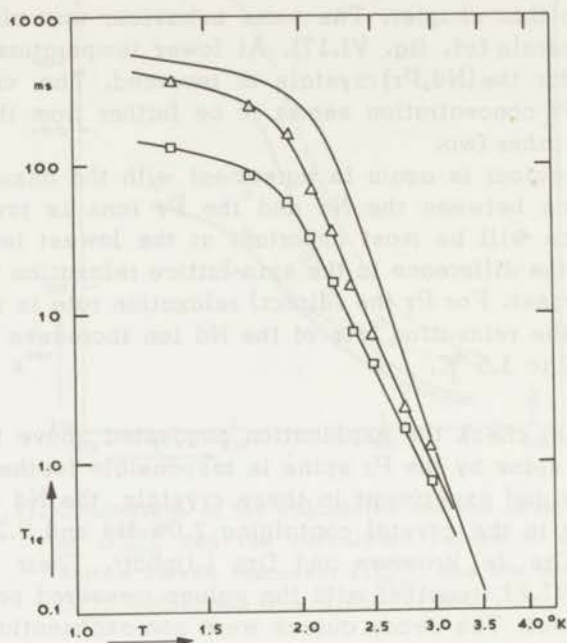


Fig. VI.23. Nd spin-lattice relaxation time  $T_{1e}$  as a function of temperature in a 2.0% Nd, 0.20% Pr crystal. For comparison  $T_{1e}$  in a pure Nd crystal is also shown.

- -  $T_{1e}$  from starting slope  
 Δ -  $T_{1e}$  from final slope.

These measurements clearly show, that for strong saturation of the Nd resonance line, the Nd spin-lattice relaxation time is much shorter than the one used in the calculation of the factor  $f$ . As outlined above, the calculated polarization factor will then be in better agreement with the observations.

### VI - 3 Concluding remarks

The behaviour of the proton polarization factor in LaMN crystals with 2.0% Nd and various amounts of Ce can be explained in all its aspects from the theoretical description given in I-3. For the lowest Ce concentrations the steady state solutions of (I.65) - (I.70) are in good agreement with the experimental data, for larger Ce contents the influence of nuclear spin diffusion is apparent, so that  $E_{200}^{max}$  is smaller

than the calculated value. The same conclusion can be drawn from a comparison of the observed and the calculated values of  $\Delta_{200}^{\max}$ . The fact that for higher impurity contents the approach of the polarization factor to its maximum value  $E^{\max}$  is slower, is strongly confirmed by the experiments.

In the crystals containing Pr as impurity, spin diffusion also plays a part, but its effect is obscured by the fact that the Nd relaxation time is shortened by cross relaxation with the Pr ions. Because the spin-lattice relaxation of Nd can no longer be described by one single  $T_{1e}$ , a numerical comparison between the calculated and the observed enhancement factors is impossible. Nevertheless it may be stated that the effect of cross relaxation shows the correct temperature dependence, and has about the expected magnitude.

### References

1. Abragam, A. and Borghini, M., Progr. in Low Temp. Phys. Vol. IV. Ed. C.J. Gorter (North Holland Publ. Co., A'dam 1964).
2. Leifson, O.S. and Jeffries, C.D., Phys. Rev. **122**, 1781 (1961).
3. Schmutge, T.J. and Jeffries, C.D., Phys. Rev. **138**, A 1785 (1965).
4. Swanenburg, T.J.B., Booy, R. and Poulis, N.J., Commun. Kamerlingh Onnes Lab., Leiden, No. 358b; Physica, to be published.

### Samenvatting

De onderzoeken die in dit proefschrift beschreven worden, zijn uitgevoerd met het doel het verschijnsel van dynamische polarisatie van protonen in verdunde paramagnetische kristallen te bestuderen. In het bijzonder waren de experimenten gericht op het bepalen van de polarisatiefactor in die gevallen, waarin de breedte van de paramagnetische resonantielijnen van dezelfde orde van grootte was als de splitsing tussen de verboden overgangen, die de polarisatie veroorzaken. De relatief eenvoudige benadering, op grond waarvan de eerste polarisatie experimenten verklaard werden, en waarbij de bezettingen van de verschillende energieniveaux worden berekend, is in deze gevallen niet meer geldig. Het gedrag van de spinsystemen als geheel moet dan beschreven worden met behulp van een quantumstatistische theorie, die ontwikkeld is door Borghini. Een overzicht van deze twee theorieën wordt gegeven in hoofdstuk I. Het blijkt, dat de spin-roosterrelaxatietijden zowel van de paramagnetische ionen als die van de protonen een fundamentele rol vervullen in het polarisatieproces.

In hoofdstuk II volgt een beschrijving van de gebruikte apparatuur en een bespreking van de meetmethoden.

De metingen, die in de daarna volgende hoofdstukken besproken worden, zijn alle uitgevoerd aan éénkristallen van  $\text{La}_2\text{Mg}_3(\text{NO}_3)_{12} \cdot 24\text{H}_2\text{O}$  (LaMN), waarin een klein percentage van de La ionen vervangen is door paramagnetische ionen uit de groep der zeldzame aarden. Deze kristallen werden gekozen, omdat het bekend is dat een grote polarisatiefactor bereikt kan worden, en omdat het zeer gemakkelijk is om verschillende paramagnetische ionen in het kristal op te nemen.

In hoofdstuk III wordt aan de hand van een eenvoudig model een beschrijving gegeven van de kernspin-roosterrelaxatietijd. Deze blijkt in een groot concentratiegebied van de paramagnetische ionen evenredig te zijn met de relaxatietijd van deze ionen. Maar, in tegenstelling tot vroegere beschrijvingen, is nu de kernspinrelaxatietijd omgekeerd evenredig met de derde macht van de concentratie, indien deze groter is dan 1%. Dit is een gevolg van het feit, dat de energie van het kernspinsysteem afgevoerd wordt via de dipool-dipool wisselwerking van de electronspins. De relaxatietijdmetingen die in de verschillende kristallen uitgevoerd zijn worden besproken op basis van dit model.

In hoofdstuk IV worden de resultaten van de polarisatiemetingen aan  $(\text{La},\text{Nd})\text{MN}$  gegeven. Zij kunnen over het gehele temperatuurgebied

goed verklaard worden met de genoemde theorie van Borghini. Alleen voor het kristal met 10% Nd worden grote afwijkingen gevonden. De oorzaak van deze discrepanties kan verklaard worden uit de beschrijving van de kernspinrelaxatie, zoals die gegeven is in hoofdstuk III.

Op grond van Borghini's theorie kan men verwachten, dat het optreden van een fonon-bottleneck in de spin-roosterrelaxatie van het Ce ion in LaMN van invloed is op de polarisatie in dit kristal. De metingen die besproken worden in hoofdstuk V vormen hiervan een duidelijk bewijs.

De invloed van paramagnetische verontreinigingen wordt onderzocht aan LaMN kristallen met 2% Nd, waaraan bekende hoeveelheden Ce of Pr zijn toegevoegd. Bij verontreiniging met Ce zijn de resultaten in goede overeenstemming met de theoretische voorspellingen. De toevoeging van Pr heeft minder invloed dan men op grond van de gemeten protonrelaxatietijden zou verwachten. Dit vindt zijn oorzaak in het feit, dat de Nd spin-roosterrelaxatietijd zelf ook verkort wordt door de aanwezigheid van Pr.

Teneinde te voldoen aan de wens van de faculteit der Wiskunde en Natuurwetenschappen volgt hier een kort overzicht van mijn academische studie.

Na het behalen van het eindexamen Gymnasium  $\beta$  aan het Gymnasium Haganum te 's Gravenhage begon ik in september 1956 mijn studie aan de Rijksuniversiteit te Leiden. Het kandidaatsexamen in de Natuur- en Wiskunde met bijvak Scheikunde legde ik in 1959 af. Bij mijn intrede in het Kamerlingh Onnes Laboratorium werd ik ingedeeld bij de werkgroep voor magnetische kernresonantie, die onder leiding staat van Prof. Dr N.J. Poulis. Aanvankelijk assisteerde ik bij protonresonantiemetingen aan magnetische éénkristallen. Na enige tijd werd een begin gemaakt met de opbouw van een apparatuur voor het bestuderen van kern-electron-dubbelresonantie. De adviezen die ik hierbij van Dr G.W.J. Drewes kreeg, zijn zeer waardevol geweest.

In 1962 legde ik het doctoraalexamen in de experimentele natuurkunde af. Met de inmiddels gereedgekomen dubbelresonantie-apparatuur werd een onderzoek ingesteld naar het gedrag van paramagnetische ionen in magnetisch geconcentreerde kristallen onder invloed van een sterk hoogfrequent wisselveld. Met het werk waarop dit proefschrift gebaseerd is werd een begin gemaakt in 1964. Bij de voorbereiding en de uitvoering van de metingen heb ik achtereenvolgens samengewerkt met Drs L.J. Ancher en de Heren van den Heuvel, Booy en Heyning. De dagelijkse gedachtenwisselingen met Dr S. Wittekoek leverden een belangrijke bijdrage aan de totstandkoming van dit proefschrift.

Sinds 1961 ben ik in dienst van de werkgemeenschap Vaste Stof van de Stichting voor Fundamenteel Onderzoek der Materie, aanvankelijk als wetenschappelijk assistent, na het doctoraal examen als wetenschappelijk medewerker. Deze werkgroep staat onder leiding van Prof. Dr C.J. Gorter, wiens belangstelling voor mijn werk altijd leidde tot stimulerende discussies.

Gedurende de zomermaanden in 1965 heb ik aan het onderzoek van muonische röntgenstralen, dat bij CERN in Genève onder leiding van Prof. Dr J.C. Sens verricht werd, meegewerkt.

Behalve van de wetenschappelijke staf ondervond ik veel steun van het technisch en administratief personeel van het Kamerlingh Onnes Laboratorium. Vooral de medewerking van de Heer J. Hoogwerf bij het construeren van de vaak gecompliceerde trilholtjes was van groot belang. Ook de zorg van de Heer D. de Jong voor het cryogene

gedeelte van de opstelling heeft veel bijgedragen tot het slagen van de metingen.

De stimulerende discussies met Ir. P.A. Tas, tot voor kort adjunct directeur van de Wiskundige Dienst van de Technische Hogeschool in Delft, en de prettige samenwerking met de Heer J.C. Poll bij het behandelen van numerieke problemen, zijn door mij bijzonder op prijs gesteld.

De Heer W.F. Tegelaar verzorgde de tekeningen voor dit proefschrift.

De afzender van de postkaart heeft vastgesteld dat het slagen van de postkaart is.

De afzender van de postkaart heeft vastgesteld dat het slagen van de postkaart is.

De afzender van de postkaart heeft vastgesteld dat het slagen van de postkaart is.

**INSTITUUT-LORENTZ**  
**voor theoretische natuurkunde**  
**Nieuwsteeg 18-Leiden-Nederland**

De afzender van de postkaart heeft vastgesteld dat het slagen van de postkaart is.

De afzender van de postkaart heeft vastgesteld dat het slagen van de postkaart is.

De afzender van de postkaart heeft vastgesteld dat het slagen van de postkaart is.

De afzender van de postkaart heeft vastgesteld dat het slagen van de postkaart is.

De afzender van de postkaart heeft vastgesteld dat het slagen van de postkaart is.

De afzender van de postkaart heeft vastgesteld dat het slagen van de postkaart is.

